DIVERSITY OF STRESS RANGES IN CABLES OF CABLE-STAYED BRIDGE DUE TO TRAFFIC LOADS AND FAR-FIELD SEISMIC EXCITATION

LEE CHONG HOE

B. ENG (HONS.) CIVIL ENGINEERING

UNIVERSITI MALAYSIA PAHANG

UNIVERSITI MALAYSIA PAHANG

DECLARATION OF THESIS AND COPYRIGHT

Author's Full Name   : _____

Date of Birth   : _____

Title   : _____

                         _____

                         _____

Academic Session   : _____

I declare that this thesis is classified as:

    ☐ CONFIDENTIAL   (Contains confidential information under the Official
                                 Secret Act 1997)*

    ☐ RESTRICTED   (Contains restricted information as specified by the
                                 organization where research was done)*

    ☑ OPEN ACCESS   I agree that my thesis to be published as online open access
                                 (Full Text)

I acknowledge that Universiti Malaysia Pahang reserves the following rights:

1. The Thesis is the Property of Universiti Malaysia Pahang
2. The Library of Universiti Malaysia Pahang has the right to make copies of the thesis for the purpose of research only.
3. The Library has the right to make copies of the thesis for academic exchange.

Certified by:

_____
    (Student's Signature)   (Supervisor's Signature)

_____
New IC/Passport Number   Name of Supervisor
Date: Date:

NOTE : * If the thesis is CONFIDENTIAL or RESTRICTED, please attach a thesis declaration letter.

THESIS DECLARATION LETTER

Librarian,
Perpustakaan Universiti Malaysia Pahang,
Universiti Malaysia Pahang,
Lebuhraya Tun Razak,
26300, Gambang, Kuantan.

Dear Sir,

CLASSIFICATION OF THESIS AS RESTRICTED

Please be informed that the following thesis is classified as RESTRICTED for a period of three (3) years from the date of this letter. The reasons for this classification are as listed below.

Author's Name	LEE CHONG HOE
Thesis Title	DIVERSITY OF STRESS RANGES IN CABLES OF CABLE-STAYED BRIDGE DUE TO TRAFFIC LOADS AND FAR-FIELD SEISMIC EXCITATION
Reasons	(i)
	(ii)
	(iii)

Thank you.

Yours faithfully,

_____
     (Supervisor's Signature)

Date:

Stamp:

Note: This letter should be written by the supervisor, addressed to the Librarian, *Perpustakaan*

STUDENT'S DECLARATION

I hereby declare that the work in this thesis is based on my original work except for quotations and citations which have been duly acknowledged. I also declare that it has not been previously or concurrently submitted for any other degree at Universiti Malaysia Pahang or any other institutions.

_____

(Student's Signature)

Full Name   : LEE CHONG HOE

ID Number   : AA15290

Date   : 30 May 2019

DIVERSITY OF STRESS RANGES IN CABLES OF CABLE-STAYED BRIDGE
DUE TO TRAFFIC LOADS AND FAR-FIELD SEISMIC EXCITATION

LEE CHONG HOE

Thesis submitted in fulfilment of the requirements
for the award of the
B. Eng (Hons.) Civil Engineering

Faculty of Civil Engineering and Earth Resources

UNIVERSITI MALAYSIA PAHANG

MAY 2019

ACKNOWLEDGEMENTS

ABSTRAK

Secara amnya, analisis kelesuan di jambatan memberikan penekanan yang besar kepada beban hidup kitaran dalam bentuk beban lalu lintas dan angin yang bergerak. Walau bagaimanapun, peningkatan aktiviti seismik di rantau ini menyebabkan struktur keluli lebih terdedah kepada fenomena kelesuan di mana ianya menambahkan beban kitaran yang mana dapat mengurangkan jangka hidup kelesuan mereka. Dalam kajian ini, analisis kelesuan terhadap jambatan kabel dengan mengambilkira bebanan secara statik dan dinamik dilakukan dengan memberi tumpuan kepada variasi tekanan dalam kabel kerana kesan beban lalu lintas yang bergerak dan galakan gerak tanah. Reaksi dinamik jambatan tertakluk kepada beban lalu lintas dan pergerakan bawah tanah yang secara mendatar dan menegak. Beban trafik yang digunakan adalah berdasarkan Fatigue Load Model (FLM) yang mana digunakan untuk menghasilkan beban kelesuan yang setara dengan trafik sebenar. Dalam kajian ini, Fatigue Load Model 4 (FLM4) telah digunakan sebagai bentuk beban trafik yang digunakan kerana kemampuannya menghasilkan pelbagai hasil dengan ketepatan yang mencukupi. Dua bentuk konfigurasi trafik akan digunakan; beban lalu lintas dalam konfigurasi Tunggal Lori dan konfigurasi Konvoi Lori. Tiga set usul tanah menegak jauh dari pelbagai magnitud juga telah digunakan dalam analisis terhadap jambatan kabel ini. Keputusan kajian ini menunjukkan pengaruh ketara beban trafik terhadap variasi tekanan jambatan kabel yang mempunyai kesan yang ketara disebabkan oleh pergerakan tanah dalam tempoh '*return period*' yang dijangkakan. Dalam kajian ini didapati bahawa kabel yang lebih hampir dengan tiang jambatan dan kabel di hujung rentang sisi jambatan mengalami perubahan yang ketara dari segi perbezaan tekanan apabila terdedah kepada beban lalu lintas dalam konfigurasi Tunggal Lori akibat interaksi setempat antara kabel dan penyebaran beban yang lebih kecil. Walau bagaimanapon, kombinasi beban yang melibatkan beban lalu lintas dalam konfigurasi Konvoi Lori menghasilkan peningkatan yang ketara dalam julat tekanan maksimum yang dialami oleh kabel yang disambungkan kepada rentang utama dan juga '*backstays*' yang disambungkan kepada tiang dan '*anchorange*' berhampiran dengan hujung rentang sisi jambatan. Berdasarkan keputusan analisis yang dilakukan, penempatan beban bergerak dalam konfigurasi ini mempunyai spektrum yang lebih luas dari segi kesannya pada jambatan kabel. Selain itu, hasil analisa berdasarkan pergerakan tanah dari magnitud yang berbeza telah menunjukkan bahawa peningkatan kepada kekuatan gempa bumi yang mana secara langsung akan meningkatkan peningkatan tekanan maksimum yang dialami oleh kabel di sepanjang jambatan.

ABSTRACT

Generally, the analysis of fatigue in bridges places a large emphasis on cyclic live loads in the form of moving traffic and wind loads. However, the rise in seismic activities in the region increases the exposure of steel structures towards additional cyclic loads that could reduce their fatigue life. In this study, the static and dynamic behaviour of a cable-stayed bridge in terms of fatigue of steel elements are addressed by focusing on the stress variation in stay cables due to the effects of moving traffic loads and ground motion excitations. Dynamic responses of the bridge are subjected to moving traffic loads and ground motions considering horizontal and vertical motions from far-field faults. The applied traffic loads are based on Fatigue Load Model (FLM) to produce fatigue damage equivalent to actual traffic. In this study, Fatigue Load Model 4 (FLM4) have adopted as a form of applied traffic load due to its ability to produce a wider range of results with sufficient accuracy. Two forms of traffic configuration will be used: traffic loads in Single Lorry configuration and Convoy Lorry configuration. A suite of three far-field vertical ground motions of varying magnitude has been used. Effects of traffic loads and ground motion on variations of nominal stress in stay cables are presented. The results of this study revealed the notable influence of traffic loads on stress variations of cable-stayed bridges with significant effects due to ground motions scaled to the expected return period. It has been found that stay cables closer to the pylons and side span supports experienced a significantly large stress range when exposed towards traffic loads in Single Lorry configuration due to the localized interaction between the stay cables and narrower load distribution. In contrast, load combinations involving traffic loads in Convoy Lorry configuration resulted in a substantial increase in the maximum stress ranges experienced by stay cables connected to the main span as well as backstays connecting the pylon head to the anchorages near the side span supports. Based on the results, the placement of moving loads in this configuration has a wider spectrum in terms of its effect on the cable-stayed bridge. Moreover, analysis results based on the application of ground motions of different magnitudes have shown that increments to the strength of an earthquake would tend to increase the maximum stress ranges experienced by stay cables throughout the cable-stayed bridge.

TABLE OF CONTENT

LIST OF TABLES

LIST OF FIGURES

xi

LIST OF SYMBOLS

MPa	Mega Pascal
GPa	Giga Pascal
m	metre
mm	millimetre
mm²	area
km	kilometre
s	seconds
ms^{-1}	velocity
w_p	weight per unit length
ρ_s	density
g	gravitational acceleration ($9.81ms^{-1}$)
A_T	cross-sectional area
$F_{p,o}$	Initial post-tension force
γ_{eq}	Equivalent Tangential Modulus of Elasticity
N	Newton
N/mm²	Pressure/Stress
kN	Kilo Newton
$\sigma_m \, \sigma_\alpha$	Stress
M_w	Moment Magnitude Scale
%	Percent
C	Carbon
Si	Silicon
Mn	Manganese
Cu	Copper
Ni	Nickel
Cr	Chromium
P	Phosphorus
S	Sulphur
E	Modulus of Elasticity
R_{epi}	Epicentral Distance

LIST OF ABBREVIATIONS

ASTM	American Society for Testing and Materials
BA	Button Anchorage
HDPE	High Density Polyethylene
UTS	Ultimate Tensile Strength
Y_s	Yield Strength
MBP	Minimum Breaking Point
E	East
N	North
S	South
PGA	Peak Ground Acceleration
GMPE	Ground Motion Prediction Equations
PSHA	Probabilistic Seismic Hazard Maps
PE	Probabilities of Exceedance
RP	Return Period
Nos.	Numbers
BS	British Standard
EN	Eurocode
FLM	Fatigue Load Model
N_{obs}	Number of estimated heavy vehicles per year per slow lane
PEER	Pacific Earthquake Engineering Reseach
NGA	Next Generation Attenuation
USGS	United States Geological Survey
CESMD	Center for Engineering Strong Motion Data
H	Horizontal Axis
V	Vertical Axis
2D	Two-dimension
3D	Three-dimension
LHS	Left Hand Side
RHS	Right Hand Side
DL	Dead Loads
PS	Post-tension

SL	Single Lorry
CL	Convoy Lorry
KCL	Koceali Bornova
DNL	Denali
SSN	San Simeon
EQ	Earthquake
MET	Malaysia Meteorological Department

CHAPTER 1

INTRODUCTION

1.1   Preamble

Since the early 1940s, longer bridges became very important due to the requirement of a large amount of traffic use daily from one place to another place. The long–span bridges not only to enhance the efficiency of the entire transportation system globally but also to reduce the travel time that could take hours to arrive. There are three types of long-span bridges based on the main span length which are:

1.   Arch Bridge (max span of 552m)
2.   Cable-Stayed Bridge (max span of 1104m)
3.   Suspension Bridge (max span of 3911m)

Arch bridges are known by their arch or curved structure that provides structural support to the entire structure. Due to the nature of the curved shape, vertical loads that comes from both the structural self-weight and imposed loads such as traffic loads are transferred along the arch to both ends of the abutments. The result of such structure allows the vertical loads to be distributed uniformly along the entire span of the bridge, ensuring mutual support among all parts of the structure. In conventional thrust arches, this would result in greater reliance on horizontal restraint of the supports, therefore imposing a significant magnitude along the horizontal component. This in return requires the support of the arch to be anchored into foundation material that is competent in bearing the loads such as rocks. However, rocks are not always available for the use of foundations in such a way that there exists a requirement for significant engineering that is un-economic towards the foundation as compensation. In response to such limitations, tied-arch bridges introduce the deck as a tie member that takes the forces along the horizontal component and reducing the forces that have to be resisted by the supports to

predominantly vertical loads (Ayres C., 2015). Consequently, the application of a tie enables arch bridges to achieve longer spans as they are no longer limited by the supports but rather on the properties of the materials used. Holding the current record for the world's longest arch bridge, is the Chaotianmen Bridge that spans 552 meters across the Yangtze River in Chongqing, China as presented in Figure 1.1.

Figure 1.1: Chaotianmen Bridge (China Communications Construction Company Ltd., 2010)

Meanwhile, suspension bridges utilize large cables that pass over the cable saddles on the towers and are anchored on both ends of the bridge to suspend the bridge deck. The main cables sustain tensile forces that transfer from the deck through hanger cables and transfers them into both the towers and the anchorages where the towers are designed to sustain forces that are dominant along the direction of gravity and the anchors resist a larger magnitude of horizontal forces. In contrast, allowable stress of materials is one of the limitations when it comes to the maximum span length of bridges. Till this day, steel and concrete remain as the predominant material in terms of the construction of long-span bridges due to their availability and continuous improvement. To date, the Akashi Kaikyō Bridge in Kobe shown in Figure 1.2 holds the title for the world's longest suspension bridge at a span of 1991 meters.

Figure 1.2: Akashi Kaikyō Bridge, Kobe. (Rötzel K., 2005)

In the case of the cable-stayed bridge, the maximum span is limited by the compressive stress in the bridge deck with the deck, pylons and stay cables being the main load carrying members. Stress components in bridge decks are comprised of axial stress and flexural stress due to the bending moment induced by the vertical and lateral loadings. The arrangement of stay cables consequently results in the increase of axial forces in the deck with a relative decrease in the distance with the towers (Gimsing, N. J. & Georgakis, C. T., 2012).

In addition, torsional stiffness is crucial in resisting torsional oscillations that originates from eccentric loadings and aerodynamic actions. Conventional box girders present in most cable-stayed bridges are capable of providing sufficient resistance to massive forces. Furthermore, increments to the torsional rigidity of girders can be achieved by spacing out the distance between two cable planes. This ties in directly to the option of increasing the cross-sectional size of the girders to increase its allowable stress and effectively enhances the spanning ability of cable-stayed bridges (Gimsing, N. J. & Georgakis, C. T., 2012).

Cable-stayed bridges are comprised of cables that connect the bridge girder to the pylons to form a series of overlapping triangles as depicted in Figure 1.3. All of the members are under compressive forces with the exception of the cables that are in tension. For a typical cable-stayed bridge, the occurrence of high local flexural stresses is mainly

concentrated in the pylons and deck areas due to the anchorage locations of the cables (Muhamad Khairussaleh, N. A. B., 2016). Moreover, cables that span symmetrically along the longitudinal axis of the bridge are anchored on two ends; the pylon and the bridge deck. In standard load cases, the deck element is locked in position by the stay cables and pylons, inducing tensile forces in the cables that are subsequently decomposed into axial compression in the pylons. Therefore, the load path of the cable-stayed bridge starts from the deck loads that transfer up into the pylon and down towards the foundation, effectively balancing both ends of the horizontal girders as illustrated in Figure 1.3.
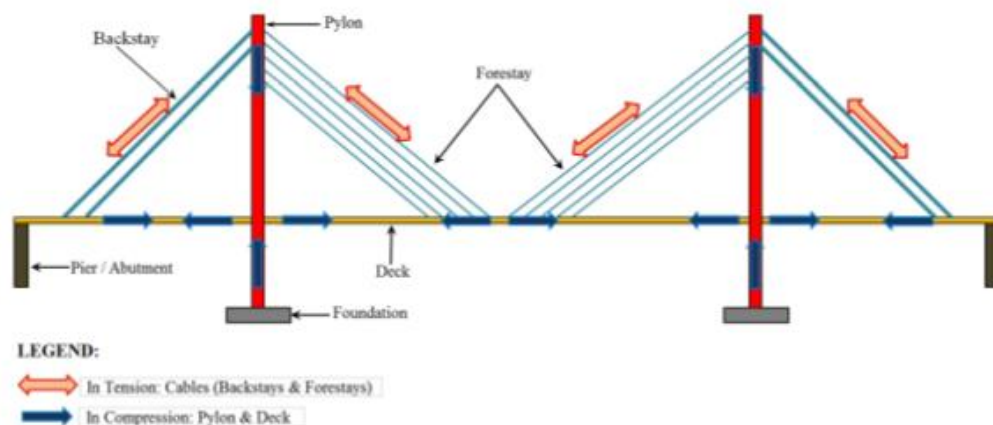
Figure 1.3: Load Path of a Typical Cable-Stayed Bridge. (Muhamad Khairussaleh, N. A. B., 2016)

One of the earliest modern cable-stayed bridges were the Tampul Aquaduct and Donzere Canal Bridge built by Eduardo Torroja in 1920 and Albert Caquot in 1952 respectively (Virlogeux, M., 1999). Further developments began in Germany with the proposal of having a suspension system in the central span whereas the side spans to be supported by stay cables to achieve efficient structural system by Dischinger, leading to the completion of the Stromsund Bridge in Sweden 1956, which has a clear main span of 183m (Gimsing, N. J. & Georgakis, C. T., 2012). Its success would then become a catalyst for the developments of future long-spanned cable-stayed bridges. With a central span of 1104m, the Russky Bridge that was opened to the public in Vladivostok, Russia in the year 2012 is the world's longest cable-stayed bridge. Therefore, with the achievement highlighted by the possibilities and capabilities of the Russky Bridge shows

that cable-stayed bridges are an upcoming contender in the realm of long spanned bridges.

Despite the recent achievements, the fatigue of steel structures remains a potential threat to the premature reduction of the service life of cable-stayed bridges. This is because cables play a fundamental role in cable-stay bridges. According to a research by Hobbs and Ghavami (1982), fatigue failures of socketed strands generally occur close to the strand/socket interface (Hobbs, R. E. & Ghavami, K., 1982). By anchoring into the girders and towers, cables are subjected to static and dynamic loadings from the girders and towers (Nakamura, S. and Hosokawa, H., 1989). Thereby sustaining a constant barrage of load cycles that affects their fatigue strength. Over the past 30 years, the assessment of fatigue life of cables and anchorage has become a crucial issue in order to maintain the integrity of cable-stayed bridges (Muhamad Khairussaleh, N. A. B., 2016). A majority of fatigue damages found in bridges are a direct result of the passages of individual trucks that could exceed 100 million in a 50 to 100-year of design life. Even though the stress ranges from 5 to 20 MPa they are sufficient to cause fatigue fracture in steel elements due to the cumulative damage (Morales, M. and Bauer, D., 2006). An example can be seen by the collapse of the bridge over the Firth of Tay Island in Scotland that had a mortality of approximately 75 people. The occurrence fatigue failure takes place in four phases which occur in the consequtive order of: crack initiation at ares of high stress concentration, progression of crack, crack propagation and the final rupture. Due to its momentous failure characteristics, they have the tendency of failing at an instant without any warnings (Boardman, B. & Deer and Company, 1990). Furthermore, Nakamura & Hosokawa (1989) thoroughly discussed that stays on cable-stayed bridges will oscillate due to winds and resulting in fluctuations in cable stresses with addition to moving traffic loads (Nakamura, S. & Hosokawa, H., 1989). Moreover, Muhamad Khairussaleh (2016) implied that the large stress variations in stay cables are produced due to the loading and off-loading of live loads along with their susceptibility to vibrations has the potential to accelerate fatigue failure (Muhamad Khairussaleh N. A. B., 2016).

Concerns about the safety of infrastructure networks under the earthquake strike have been historically a matter of great concern, especially towards infrastructure. Along with major road networks, bridges are of the great component as their failure bears the

capability of disrupting infrastructure that prevents emergency access as well as evacuation (Casado, A. C. 2011). With the ever-increasing frequency of seismic activities over the past decade, events such as the recent Magnitude 7.8 quake hit Palu of the Central Sulawesi Region of Indonesia caused major destruction and casualties. This event increases the tremor pulse to the area nearby. Since seismic activities transmit forces in via wave propagation, they also carry the same characteristics in pulsating loads as the amplitudes represent loading and off-loading scenarios. Consequently, it would contribute to fatigue for metallic structures. An exemplary case would be the case of Canada's Shipshaw Bridge that saw damages to the anchorage plate during the 1988 Saguenay earthquake that released a moment magnitude scale of 6.0 (Filliatrault *et al.*, 1993). Even though Malaysia is considered as a seismically inactive nation, but with a recent earthquake swarm (Kundu *et al.*, 2012) in 1983, 1994 and 2004 near northern Sumatra have been felt and caused some cracking in buildings in Malaysia. This raises concerns regarding the effects of seismic activities on fatigue stresses on metallic structures especially for bridges in this region.

1.2   Problem Statement

Cracks found in steel components of bridges are normally a result of fatigue. Fatigue in metals is the process where cracks initiate and propagate under the repetitive loading and off-loading action. Fatigue cracks may lead to catastrophic failures if the remaining un-cracked section no longer possess the ability to sustain the loads that have been exerted on the structure. Existent studies on the fatigue of cable-stayed bridges generally only consider traffic or wind load action respectively (Yan Li *et al.*, 2011). With the increased frequency of seismic activities around the region, it poses a threat to the fatigue strength of cable-stayed bridges as their attributes in pulsating loads will cause variations in the stress range of the cable connections. Therefore, these stress patterns have the capability to not only accelerate the fatigue failure in cables, but also increase the chances of cable corrosion due to infiltration of corrosive elements through the fatigue cracks. With such events, the designed service life of cable-stayed bridges will be consequently affected to an extent.

1.3   Objectives

The main purpose of this research is to study the fatigue behaviour of cable-stayed bridges that emphasizes the action that causes vibration and consequently increases the stresses in the cables due to traffic loads and seismic activities. Therefore, the aims of this research are as follows:

i.   To analyse the cable-stayed bridge with the suitable Fatigue Load Model (FLM) based on Eurocode.

ii.   To analyse the cable-stayed bridge with the effect of selected ground motion due to seismic excitation.

iii. To analyse the behaviour of the cable-stayed bridge due to moving loads and seismic excitation.

iv.   To determine the obtained stresses occurring in the stay cables of the cable-stayed bridge due to moving loads, seismic effect, and the combination of both loadings.

v.   To determine the stress ranges occurring in the stay cables of the cable-stayed bridge due to moving loads, seismic effect, and the combination of both loadings.

1.4   Scope of Research

The possible elements of cable-stayed bridges are diverse in order to obtain an accurate study on its fatigue behaviour. Therefore, the scope of this thesis is limited to:

i.   The simulation of the Second Penang Bridge in 2-Dimensional and 3-Dimensional form to attain accurate values for the stress range.

ii.   The analysis of the bridge model with SAP 2000 version 20/21 to determine global response.

iii. The stress analysis will be particularly at the cable connection with regards to its significant vulnerability in a cable-stayed bridge.

The aim of this research is to determine the diversity of stress range that could affect the fatigue performance of the cable-stayed bridge with respect to the point of connection between the stay cables and the anchorage blocks by analysing the variation of stress ranges in the cables due to its response towards movements of traffic loads (lorries) along the bridge as well as seismic excitations.

1.5 Significance of Research

Despite the major milestones achieved by cable-stayed bridges, major emphasis was placed on bridges that are structurally sound to withstand the forces of nature while being aesthetically pleasing. On the other hand, fatigue remains as a problematic phenomenon that occurs in steel bridges, especially in the vicinity of the connections. This is a result of bridges being subjected to cyclic loadings that arises from moving traffic, in-sync with the vibrations that are caused by wind loads on the main girder as well as the cables. Vehicles such as trucks that travels across a bridge will induce dynamic effects that includes global vibrations and local hammer effects.

While the current trend is to achieve longer bridge spans, their light-weight and low-damping properties hold responsibilities for the high amplitude oscillations when to subject to dynamic excitations. Consequently, the resulting stress fluctuations will have an impact on the fatigue life of bridges and its damage upon it. If neglected, prolonged fatigue damage could result in catastrophic failures of high-level structures such as bridges that will involve the loss of property and lives.

Apart from wind loads and moving traffic, the occurrence of earthquakes will also induce cyclic loadings via seismic waves. Although there is no evidence of catastrophic collapses in cable-stayed bridges under seismic actions, notable damages have been found on several cable-stayed bridges after strong earthquakes in the 80s and 90s, namely the Shipshaw Bridge and Higashi-Kobe Bridge (Camara A., 2018). Moreover, recent studies have indicated an increase in seismic activities around the region of Peninsular Malaysia subsequent to the 2004 Mega Quake of 9.1 M_w. (Yunus *et al*., 2014); (Nabilah, A. B. & Belendra, T., 2012); (Shoushtari *et al.*, 2017). In addition, the activation of ancient inactive faults in Malaysia has resulted in more frequent far-field earthquakes within Peninsular Malaysia (Yunus *et al*., 2014).

The combination of the above events have the potential to increase the stress range on stay cables and will result in a decrease in the fatigue life-cycle of steel elements on bridges. Therefore, this study is significant in terms of determining the life-span of stay cables in terms of fatigue strength. Moreover, this study could be used to schedule the maintenance checking for the purpose of stay cable replacement before they eventually fail due to the effects of fatigue.

CHAPTER 2

LITERATURE REVIEW

2.1   Introduction

This chapter reviews the history of cable-stayed bridges and their evolution throughout the years which includes various successes, technological advancements and complications. Further investigation eventually leads to the in-depth discussion on the theories behind fatigue phenomenon and the investigation on how the performance of cable-stayed bridge with the inclusion of forces that originates from seismic activities around the region on top of existing traffic loads.

2.2   History of Cable-Stayed Bridges

Dating back to 1784, it has been known that a German carpenter named C. T. Loescher took the first endeavour in designing a cable-stayed bridge strictly out of timber (Walther *et al.*, 1999). Prior to the early 19th century, none of such bridges was built until a self-taught French engineer named Marc Seguin constructed the first permanent cable-supported bridge that featured cables that are made of drawn iron wires in 1823 (Gimsing, N. J. & Georgakis, C. T., 2012). Contrary to popular belief, Virlogeoux, M. (1999) pointed out that the first "modern" cable-stayed bridge was actually the Tampul Aqueduct by Eduardo Torroja and Donzere Canal Bridge by Albert Caquot that were constructed of concrete (Gimsing, N. J. & Georgakis, C. T., 2012). Around the same timeline, a study conducted by French engineer and scientist Claude-Loius Navier has shown that his idea of bridges with the stiffened deck by wrought iron chains was closely related to fan-shaped and harp-shaped systems shown in Figure 2.1 but contrary to current day practices, the back-stays were earth-anchored (Gimsing, N. J. & Georgakis, C. T., 2012).
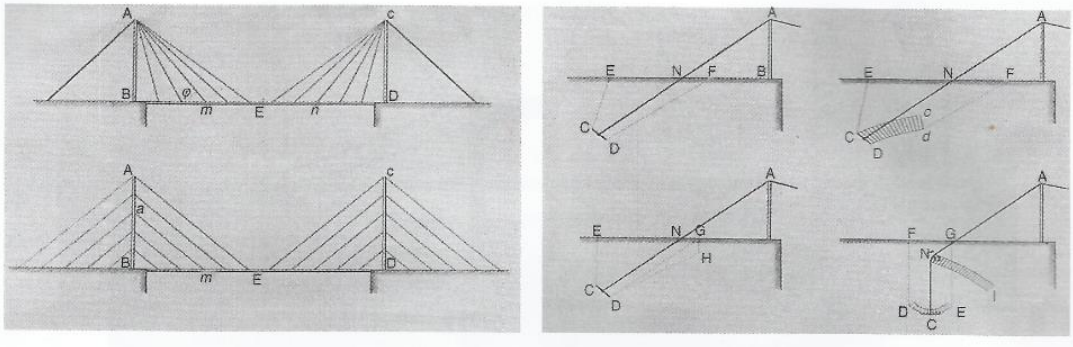
Figure 2.1: Bridge systems investigated by Claude Navier in 1823. (Gimsing, N. J. & Georgakis, C. T., 2012)

Nonetheless, Seguin's structure has been long preceded by its hybrid counterparts that were a part suspension and part stayed. This type of design was implemented in the 124 m catenary over the Schuylkill, Philadelphia and the Galashiels wire-stayed bridge in Scotland at the end of the 18th century (Walther *et al.*, 1999). Even though the application of thin wires as main cables resulted in various issues regarding their durability against corrosion but still it gave rise to the prospect of utilizing pin-connected eye-bars that merges into a chain-like configuration (Gimsing, N. J. & Georgakis, C. T., 2012). Such principles were adopted by British engineer, Thomas Telford in the Menai Bridge (opened 1826) that used chains made of wrought iron eye-bars to supports it's 176 m long span (Walther *et al.*, 1999). Since then, cable-supported bridges grew in terms of their popularity and the previous development laid a roadmap for its future development.

Despite the rapid development of the cable-stayed bridge, the Dryburgh Abbey Bridge shown in Figure 2.2 that collapsed in 1818 highlighted the weaknesses of structures that primarily supports inclined rods. The failure of this type of structure resulted in the decline in their popularity. According to Walther *et al.* (1999), Navier attributed such failures with the lack of fixity and poor production quality of inclined chains, leading to their inability to attain aerodynamic stability and structural integrity (Walther *et al.*, 1999). This is because aerodynamic stability is a crucial factor to windstand the effects of oscilation and vibration either from wind or moving load (Walther *et al.*, 1999). Such failures were even prominent with the collapse of the Tacoma Narrows Bridge in 1940 after four months open to the public use due to its susceptibility towards wind loads.

Figure 2.2: The Dryburgh Abbey Bridge. (Föhl, K., 2005)
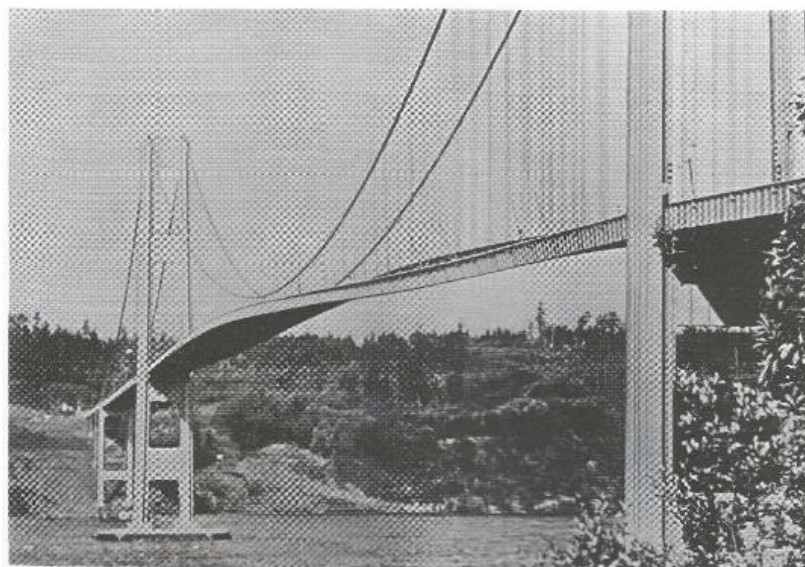
Figure 2.3: The fatal twisting oscillation of the First Tacoma Bridge. (Gimsing, N. J. & Georgakis, C. T., 2012)

The Tacoma Narrows Bridge shown in Figure 2.3 offered little torsional stiffness due to its slender deck profile that attributed to vortex shedding and torsional flutter. This phenomenon leading to its failure as it exceeded its natural ability to dampen the motion (Walther *et al.*, 1999). Because of this catastrophic event, it raised the awareness of bridge engineers towards the significance of aerodynamic stability and dynamic behaviour in long-span bridges. At the time of when the Dryburgh Abbey Bridge

collapsed, J. Roebling implemented steel wires on a test bridge, Niagra Bridge, as a substitute for suspension chains that features a double deck arrangement on the top and bottom. Although it carried significant loads, the arrangement resulted in significant increase in local stiffness that reduces the amount of deflection (Walther *et al*., 1999).

Despite the development incurred by Roebling and Navier in the 19th century, only a substantial growth in cable-stayed bridge was seen after the Second World War with the achievement of Franz Dischinger (Walther *et al*., 1999). In 1938, he implemented inclined, pre-stressed stays for the design of a suspension bridge in Hamburg that utilized high strength steel cables with the aims of reducing the deck's deformation by increasing the capacity of cables working under high stress (Walther *et al*., (1999). Following his victory in an international design-construction competition organized by the Swedish government in 1953, the renowned Strömsund Bridge was constructed based on his concept of a modern cable-stayed bridge (Walther *et al*., (1999). In comparison with a part-suspension and part-cable-stayed system, it was found to achieve greater economic viability due to the reduction in materials without giving up in its load-bearing capacity (Billington, D. P. & Nazmy, A., 1991). Upon the completion of the Strömsund Bridge, it was opened for public use in 1956 and therefore was generalized as the first modern cable-stayed bridge. His winning proposal featured a cable-stayed bridge that is supported by two sets of cables that radiates from the two main towers of portal type, such that resembles a pure fan-type arrangement. Completion of the Strömsund Bridge marks an evolutionary milestone for the development of cable-stayed bridge which is primarily due to its refined structural analysis approach that allowed for the calculation of cable forces during the construction period to account for the cable efficiency for once the structure has been finalized (Gimsing, N. J. & Georgakis, C. T., 2012).

Figure 2.4: The Strömsund Bridge. (Gimsing, N. J. & Georgakis, C. T., 2012)

Following the success of the Strömsund Bridge shown in Figure 2.4 , engineers around the world have recognized the potentials of the cable-stayed bridge as a long-span bridge and have taken advantage of the resources to construct multitudes of such structures (Walther *et al*., 1999). Over the next several decades, continuous developments in their design and materials allowed the spans of cable-stayed bridges to exceed well over 1000m such as the Sutong Yangtze Bridge at 1088m and the Russky Bridge at 1104m.

2.3   Present-Day Cable-Stayed Bridges

In contrast to the early 19th century, cable-stayed bridges underwent massive breakthroughs in terms of their design choices and structural components to achieve longer spans while maintaining an adequate amount of structural integrity. For the past two decades, over 50 prominent long-span cable-stayed bridges have been constructed across the globe. Notably, China in particular, the country has contributed to the rapid growth of long-span bridges due to the vast amount of rivers that impeded the efficiency of local transportations. For instance, the Yang-Tze River. For the purpose of catering different stay arrangement, pylons of varying geometry have been developed to allow the provision for sufficient stability and structural performance. Advancing from the preliminary form of H-shaped pylons, the 20th century has seen a rise in popularity among A-frames, inverted Y-frames, diamond frames as well as free-standing pylons. The inherent stiffness of bridges caused by the use of different cable-plane arrangement in conjunction with varying pylon shapes allows modern cable-stayed bridges to span longer distances without suffering from the loss of structural instability. The additional torsional

stiffness induced by cable planes helped reduced the requirement of stiff bridge decks and in return, allowed for slender and lighter steel decks for the purpose of weight reduction. Consequently, the development of single, dual and triple cable planes led to the application of different materials for bridge decks; concrete girders, orthotropic steel decks, steel box girders, and composite decks.

2.3.1 Cable Arrangement in Cable-Stayed Bridges

Cable-stayed bridges are none of the same with the varying configuration of the cable arrangements. Each arrangement bears distinct characteristics and affects both the structural and aesthetics performance of each bridge. The basic form of cable-stayed systems is comprised of straight cables that radiate from the sides of the pylons and connecting with the deck, portraying a triangular pattern.
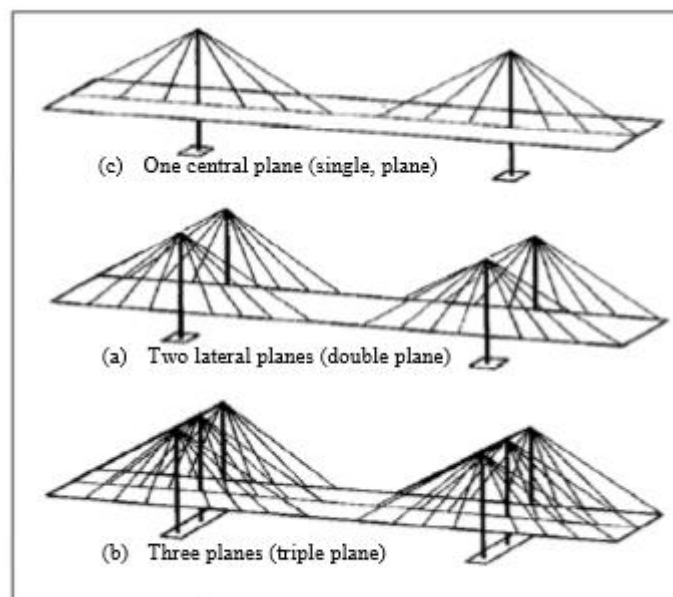
Figure 2.5: Layout of stays in a planar system. (Walther *et al.*, 1999)

Generally, there are two types of cable planes that exist in cable-stayed bridges, two planed cables and single planed cables. However in some cases, triple planed cables are present as shown in Figure 2.5. The two planed arrangements are found in most conventional cable-stayed bridges that are erected along the longitudinal direction of the bridge and is normally located at the sides of the structure (Walther *et al.*, 1999). Single-planed arrangement only differs in terms of the location in which the cables are erected from the bridge centerline. Regardless of the number of cable planes, the cables can be

arranged in several configurations, namely the harp, fan and semi-fan pattern as shown in Figure 2.6 (Walther *et al.*, 1999).
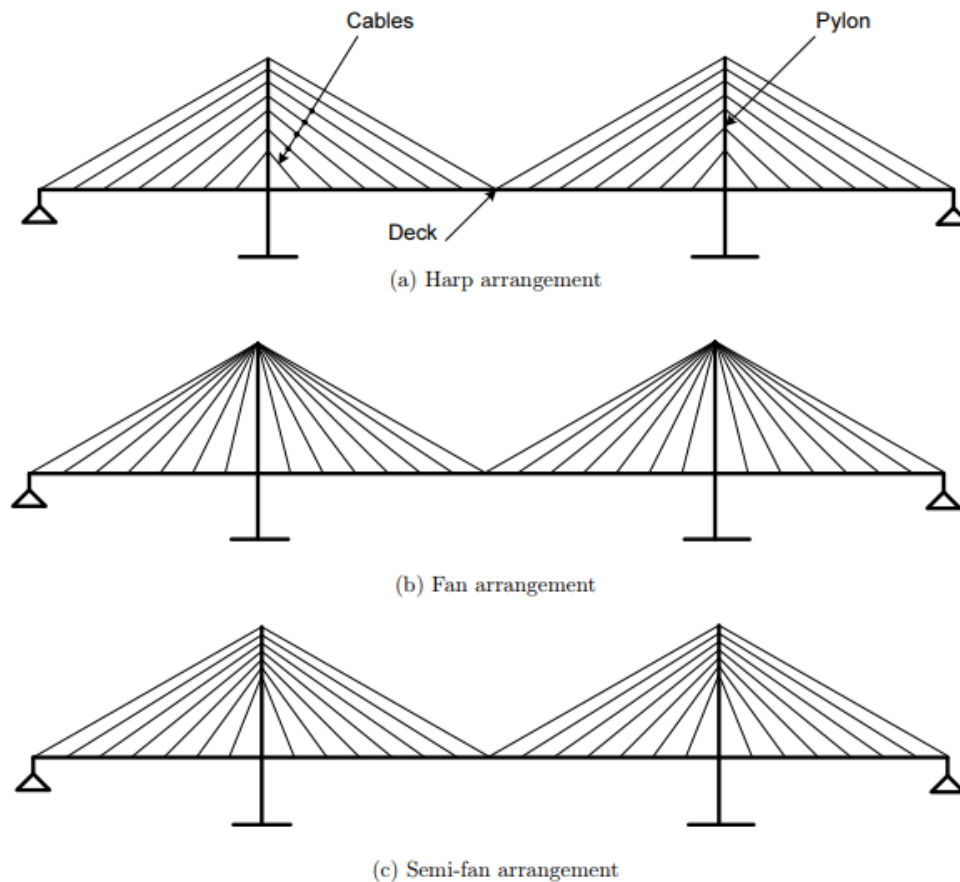
Figure 2.6: Different arrangement of stay cables. (Walther *et al.*, 1999)

Harp patterns consist of parallel cables that are erected along the length of the towers, uniform angles which they span over each other provides an aesthetically pleasing structure. However, they are not the best selection in terms of structural performance as the overall stiffness of the system will be reduced (Gimsing, N. J. & Georgakis, C. T., 2012). Fan pattern features cables that radiate from the top of the pylons which reduces the total weight of cables in contrast to the harp arrangement. As the horizontal forces induced by the cables are reduced, deck movements caused by expansion and contraction of members can be absorbed by expansion joints. However, exact convergence at the pylon heads is impossible thus it is required to spread out the anchorages (Walther *et al.*, 1999). On the other hand, a semi-fan pattern is an intermediate solution between harp and fan patterns that attributes to the best of both worlds whilst discarding their drawbacks. Instead of converging at the pylon head, semi-harp arrangements allows the

cable anchorages or saddles to be spread sufficiently, simplifying both the detailing process as well as its construction. Since the cable anchorages are placed close to the pylon tops, it performs almost identically to the pure fan arrangement (Walther *et al.*, 1999).

2.3.2 Structural Elements of Cable-Stayed Bridges

Cable-stayed bridges are comprised of 3 main elements; bridge deck, stay cables and pylons/towers. Careful selection of the aforementioned elements is critical for the design of the cable-stayed bridge as they pose a significant impact on its structural performance in both static and dynamic conditions. Depending on the purpose, location and environmental impacts on the bridge, both the type and materials used for each element may differ drastically for each distinct bridge.

2.3.2.1 Bridge Deck

Bridge decks are constantly subjected to a considerable amount of external loads for cable-stayed bridges due to the absolute traffic loads that are applied directly on the deck surface. The torsional resistance required in bridge decks is reliant on the degree of torsional support provided by the cable systems. A single planed cable system would tend to offer less torsional stiffness in comparison to multi-planed systems (Gimsing, N. J. & Georgakis, C. T., 2012). Therefore, the stability of a bridge would heavily rely on the torsional stiffness of the deck when a single-planed system is being utilized in conjunction with eliminating the effects of aeroelastic flutter that is induced by wind loads whilst being subjected to eccentric traffic loads (Walther *et al.*, 1999). Thus, decks that are made of box sections or enclosed spaced frames as shown in Figure 2.7 have high torsional stiffness are required instead of slender decks. Moreover, it has also been specified that the longitudinal moments is proportional with the deck stiffness, where the greater the deck stiffness, the greater the bending moment. With the growth of multi-stayed bridges, the provisions for stiff girders are relatively non-existent. Hence, flexible decks are much preferred in contrast to decks that have a reasonable amount of torsional stiffness and reduced longitudinal bending (Walther *et al.*, 1999).
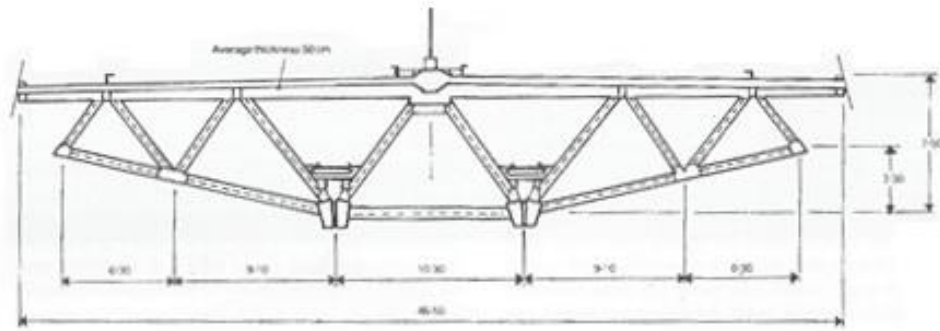
Figure 2.7: Example of a deck formed by a space frame for a proposed cable-stayed bridge in Abidjan, Ivory Coast. (Walther *et al*., 1999)

Due to the limitations of construction cost and the impact of self-weight of the deck on the selection of stay cables, pylons' and foundation's design, the materials for deck construction are bound to steel, concrete and steel/concrete composites. The significant difference in density between steel and concrete that portrays a ratio of 1-to-5 resulted in steel as a preferred choice for deck construction during the past century (Walther *et al*., 1999). Application of steel as the bridge deck were a common sight among suspension bridges until the completion of the Stromsund Bridge which makes use of I-shaped plate as its stiffening girders. Within the first two decade since the completion of the Stromsund Bridge, developments of cable-stayed bridges were exclusive to steel bridges that featured cross sections of orthotropic steel floors connected to steel plates or box girders for its main span, notably the Theodor Heuss Bridge in Düsseldorf, Severins Bridge in Cologne, Knie Bridge in Düsseldorf and Papineau Bridge in Canada that completed in 1957, 1959, 1969 and 1969 respectively (Gimsing, N. J. & Georgakis, C. T., 2012).

However, the application of steel decks in modern days proved to be less economical due to the rising cost for the fabrication of structural members and the long-term serviceability cost that is two to four times more than concrete. Therefore, the adoption of steel decks should be justified by the cost reduction in other structural elements due to its equivalent weight reduction in order to maintain a competitive standing (Gimsing, N. J. & Georgakis, C. T., 2012). The Maracaibo Bridge (1962) in Venuezela that was designed by R. Morandi was known to become the first multi stayed bridge constructed entirely out of concrete (Billington, D. P. & Nazmy, A., 1991).

Developments featuring concrete decks were still scarce until the late 1970's where the Brotonne Bridge, Pasco-Kennewock Bridge and Barrios de Luna Bridge exploited the prospects of using pre-stressed and/or pre-fabricated concrete.
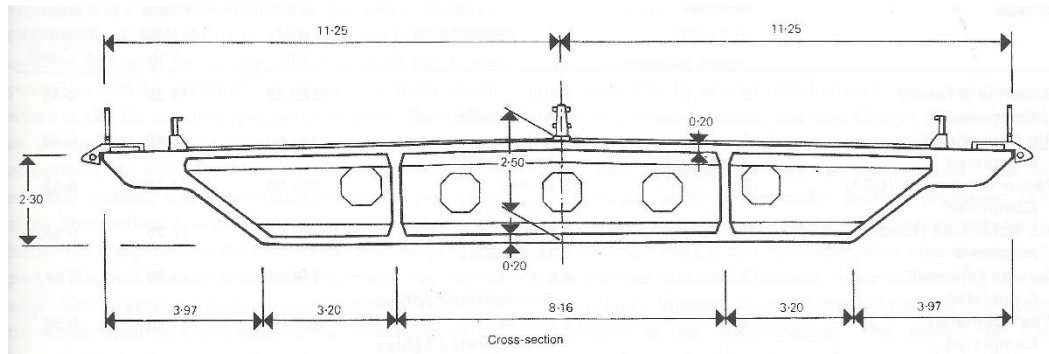
Figure 2.8: Prestressed Concrete Deck of the Barrios de Luna Bridge, Spain. (Walther *et al.*, 1999)

The preference in composite decks over conventional orthotropic steel slabs such as the one shown in Figure 2.8 for long spanning bridges are profound with the reduction in self-weight of concrete and cost while maintaining sufficient rigidity but also facilitating the erection process with steel elements. According to Mendes (2010), the number of bridges constructed of steel – concrete composite decks is experiencing an upward trend in several countries. Regardless of the additional dead load attributed to composite decks due to the implementation of concrete slab and steel structure as the running surface and supporting structure respectively. Walther *et al.* (1999) stated that the deck is able to exploit the high compressive strength of concrete and tensile performance of steel with the only exception for long-span bridges. One of the first pioneers in the application of composite decks was the Hooghly Bridge in Calcutta that required a lightweight superstructure to compensate for the lack of geotechnical bearing capacity and make use of the booming local steel manufacturers. However, certain issues relative to the elements' serviceability limit state are of concern when steel structures are required to sustain high compressive stress that originates from the stay cables along with the shrinkage and creep that is experienced in the curing of the concrete deck (Walther *et al.*, (1999). Therefore, bridge engineers were required to conduct an extensive structural analysis to optimize the use of different materials with regards to load bearing states, such as using concrete and steel respectively for members that are loaded in compression and tension (Walther *et al.*, 1999).

19

As the span of cable–stayed bridges become longer, the structures become more susceptible to dynamic instability. According to Virlogeux (1999), aerodynamic behaviour can be controlled if the effects of vortex shedding, aerodynamic stability and dynamic excitation can be carefully understood (Virlogeux, M., 1999). This is because the geographical location of the bridge and the geometrical layout of the bridge may expose the structure to crosswind flows which will excite these long span bridges (Walther *et al*., 1999). Basically, in controlling aerodynamic instability, three actions should be monitored; horizontal load, vertical load and torsional moment (Walther *et al*., 1999). Vertical load is mostly controlled by the axial stiffness of the cables which is very critical during bridge construction. The inertia of the deck with the aid of the connection to the pylon can prevent the bridge from swaying excessively in the transverse direction. Clearly, the torsional moment can be controlled with the rigidity of the box girder deck. A streamlined box girder section can help eliminate vortex shedding (the formation of oscillating flow that past un-streamlined body which cause the flow to separate from the structure rather than follow the body contour) and aerodynamic instability which has been shown by the aerodynamic profile of the Normandie Bridge (Virlogeux, M., 1999). However, the width of this type of box girder must be large as the ratio of the width to the span must not be less than 1/40 (Virlogeux, M., 1999).

2.3.2.2 Pylons

The selection of pylons as shown in Figure 2.9 and 2.10 is generally governed by the arrangement of stay cables and the suspension methods. In typical fashion, the longitudinal configuration of pylons must provide sufficient stability and satisfactory performance during its operation. Depending on the types of stay arrangement (harp, fan, semi-harp), the longitudinal bending moments in pylons may vary due to the eccentric traffic loadings in order to maintain equilibrium. Thus, the selected pylons should provide enough bending resistance and local stiffness to reduce the degree of deck deformation (Walther *et al*., 1999). A definitive solution to improving the structural stability and stiffness would be the application of A-frame pylons that allows for the deck and two inclined cable planes to act as an enclosed section that has sufficient torsional rigidity. It is directly applicable to long-span cable-stayed bridges that have a general preference to flexible deck solution where the pylon stiffness carries a significant impact on the global structural behaviour.
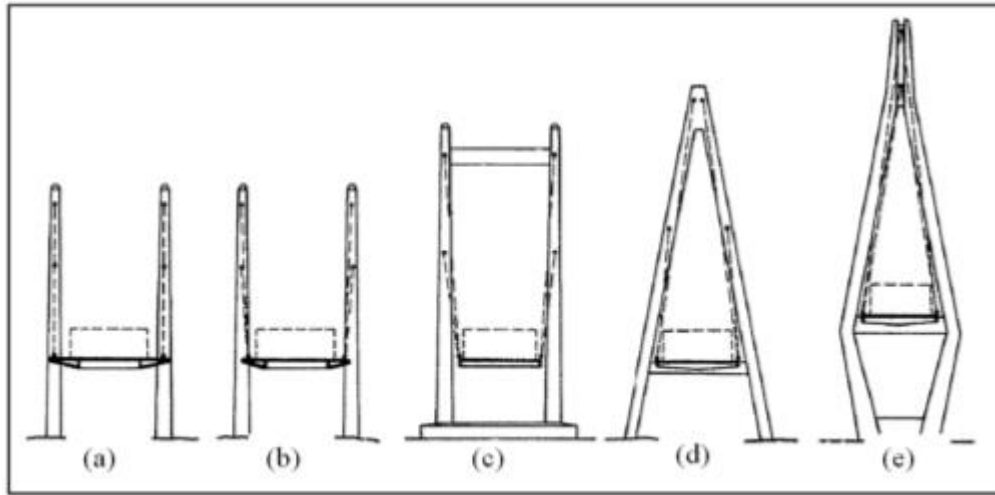
Figure 2.9: Pylons for two cable planes. (Walther *et al*., 1999)
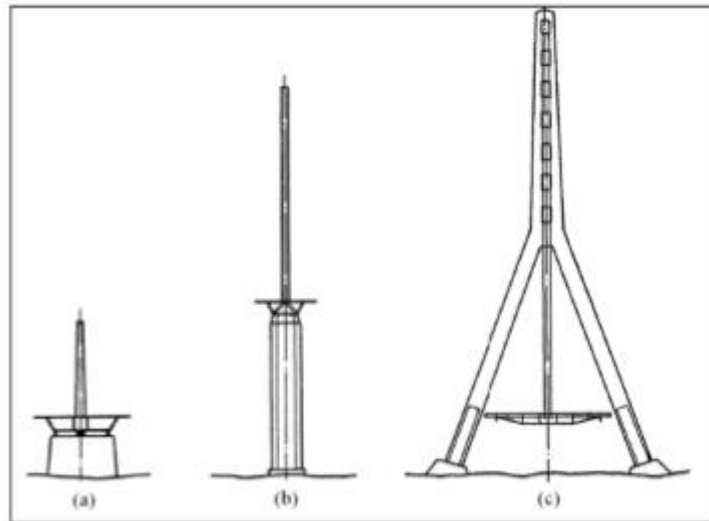
Figure 2.10: Pylons for single cable plane. (Walther *et al*., (1999)

2.3.2.3 Cables

The mechanical properties of galvanized wires in cables can be depicted by a typical stress-stain curve as shown in Figure 2.11. In comparison to structural steel, cable steel does not indicate a plastic plateau and the elongation at rupture is smaller than structural steel. The reduced plastic strains of cable steel would be insufficient to allow the plastic design of the entire structure assuming a profound redistribution of loads between the cable system and deck. Its high carbon content which is approximately four time that of structural steel, results in a significant increase in strength. Consequently, the additional carbon content results in steel cables being unsuitable in welding and has

a lower degree of ductility in contrast to structural steel. The comparison of mechanical properties between cable steel and structural steel can be seen in Table 2.1.
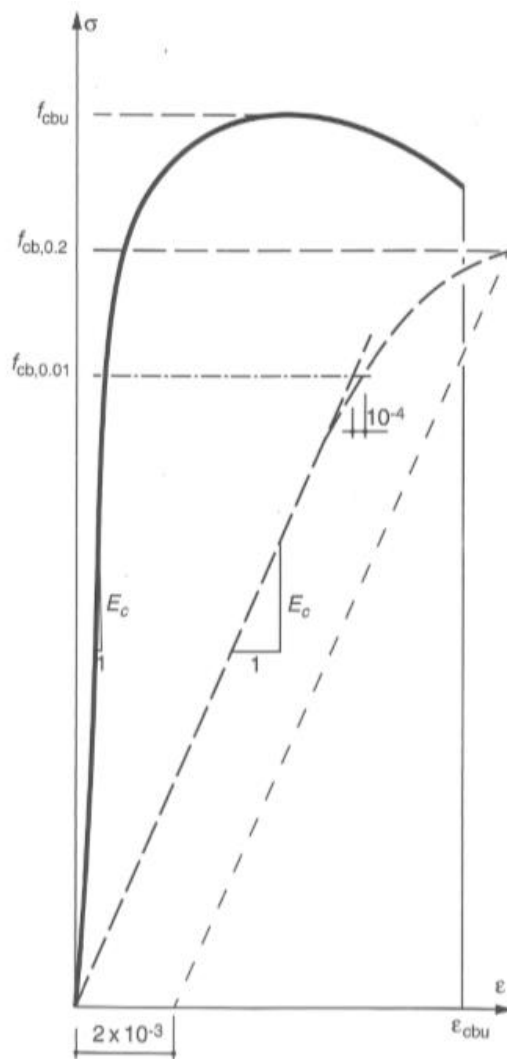
Figure 2.11: Typical Stress-strain curve of galvanized wires in cables (Gimsing, N. J. & Georgakis, C. T., 2012).

Table 2.1: Comparison between cable steel and structural steel based on typical values.

	Units	Conventional Cable Steel (5 or 7mm wires)	Structural Steel	
			Mild	High Strength
Yield Stress (=2% proof stress)	MPa	1180	240	690
Tensile Strength	MPa	1570	370	792
Strain at breaking	%	4	24	
Modulus of Elasticity	GPa	205	210	210
Typical Chemical Composition	C	0.80%	0.20%	0.15%
	Si	0.30%	0.30%	0.25%
	Mn	0.60%		0.80%
	Cu	0.05%	0.20%	0.30%
	Ni	0.05%		0.80%
	Cr	0.05%	0.30%	0.50%
	P	0.03%	0.04%	0.03%
	S	0.02%	0.04%	0.03%

Source: Gimsing, N. J. & Georgakis, C. T., (2012)

The fundamental elements for the cables found in modern cable supported bridges are comprised of steel wire which attributes to greater tensile strength in comparison to typical structural steel. Typically, steel wires with a diameter between 3 to 7mm, where diameters up to 7mm are adopted for parallel wire strands in cable-stayed bridges. Generally, the six types of cables used in cable-supported bridges are helical bridge

strands (spiral strands), locked-coil strand, parallel-wire, new parallel-wire strand, parallel-strand and bars. Helical cable strands are manufactured by spinning layers of cables that twists around a central core. The action results in a reduction of strength in comparison to straight wires but allows for a self-compacting action that eliminates the need to wrap the wires together (Gimsing, N. J. & Georgakis, C. T., 2012). Locked-coil strands consists of cables that are arranged in successive layers, wounding around a central core of circular parallel wires. The overlapping exterior sections form an envelope attributes to a self-compacting effect that ensures tight and watertight surface. Such effects are more pronounced during the tensioning stage of cables, (Walther *et al.*, 1999). Parallel-wire cables are made up of large amount of wires than those in suspension bridges. The cables used in cable-stayed bridges conforms to ASTM A421, Type BA, low-relaxation and are typically stress-relieved wires that are commonly used in the manufacturing of prestressed concrete (Ohio Department of Transportation, 2009). New Parallel-wire cables is a variation of parallel-wire cables but with straight wires. The bundle of wires have been slightly twisted with a long-lay to ease reeling and unreeling to produce a self-compacting strand when subjected to axial tension. Parallel-strand cables have identical properties with that of parallel-wire cables, but with the individual 7mm wires that are replaced by seven-wire strands. The strands are made of galvanized wires wrapped underneath several layers of extruded high-density polyethylene (HDPE) sheath to protect them against corrossion. Individual protection of each strand allows them to be bundled together as a parallel-strand without additional protection. Bar stay cables have the original 5-7mm wires replaced by high strength round bars. Due to its low fatigue resistance that resulted from discontinuities at the couplers, its use in cable-stayed bridges was limited in numbers. A summary of the attributes of different types of cables is shown in Table 2.2.

Table 2.2: Mechanical properties of different type of cables

Types of Cables	Mechanical Properties				
	Modulus of Elasticity, E Value (N/mm²)	Ultimate Tensile Strength, UTS Value (N/mm²)	Yield Strength, Y_s Value (kN/m²)	Equivalent Density, γ_{eq} Value (kN/m²)	Minimum Breaking Point (MBP) kN
Locked Coil Strand	160 000 – 165 000	1370 – 1570	865	88	367 – 31400 (BRIDON Structural System)
Helical or Spiral Strand	155 000 – 175 000	1570 – 1770	-	-	171 – 25200 (BRIDON Structural System)
Parallel Bar	210 000	Coupled (1030 – 1230) Uncoupled (1500)	Coupled (835 – 1080) Uncoupled (1350)	125	7339
Parallel Wire Strand	205 000	1570	1470	85 – 90	7487
New Parallel Wire Strand	205 000	1770	1470	82	-
Parallel Strand	190 000 – 200 000	1770 - 1879	1570 – 1670	130	265 per strand

Source: Muhamad Khairusaleh, N. A. B., (2016); Gimsing, N. J. & Georgakis, C. T., (2012)

2.4   Failure of Cable-Stayed Bridges

One of the more notable failures of cable-stayed bridges can be observed on the collapse of the Morandi Bridge in Genoa, Italy on August 14, 2018 that resulted in 43 casualties. Although the failure is still under investigation, the preliminary investigation pointed out that such failure was due to the combination of poor design that did not take into account of wind loads, questionable building practices and insufficient maintenance (Pollock, E., 2018). Instead of the conventional parallel stays, the Morandi Bridge adopted prestressed concrete around the tie-rods that prevented maintenance checks on the conditions of the prestressed cables. With the reliance on small number of stays for support, it is possible that failures could have occurred on the stay cables and resulted in the remaining stays to carry additional loads that is beyond their designed capacity. With only a pair of stays supporting the spans, failure of one of the stays could have resulted in the shift of additional loads that causes the presence of excessive forces that have to be supported by the remaining structural elements that are still intact (Pollock E., 2018). However, statements from event witnesses revealed that the bridge was struck by lightning before its failure. The significant amount of energy carried by the lightning increases the possibility of it contributing to critical fatigue of material as a result of the generation of excessive heat that vaporized infiltrated rainwater in the fatigue cracks, therefore increasing the crack size and led to a reduction in effective load bearing capacity (Griffin, A., 2018).

Figure 2.12: Collapse of Morandi Bridge, Italy (Griffin, A., 2018).

With regards to seismic activities, a pronounce example would be the damage of the Shipshaw Bridge in Canada during the 1988 Saguenay Earthquake ($M_w = 6.0$). A study by Filiatrault et al. (1993) has shown that the tie-rod assembly at one abutment of the Shipshaw Bridge was dealt with a significant amount of structural damage during the November 25, 1988, Saguenay earthquake (Filiatrault et al., 1993). According to Drysdale & Cajka (1989), the Saguenay earthquake was the largest seismic event recorded in eastern Canada where peak ground accelerations along the horizontal axis that are close to 0.15g have been recorded near the epicentral sector (Drysdale, J. & Cajka, M. 1989). The investigation on the available evidence has shown that the deck of the Shipshaw Bridge suffered from significant vibrations in the longitudinal direction during the quake. This resulted in the failure of one of the anchorage plates that connects the box girders to the abutment of the Shipshaw Bridge (Filiatrault et al., 1993). The failed plate of the Shipshaw abutment were subjected to high concentration of stresses under dead loads only. Although the effects of fatigue could not be directly linked to the failure of the anchorage plate, but it is clear that the 1988 Sanguenay earthquake can be directly attributed to the failure of an already locally yielded anchorage plate (Filiatrault et al., 1993).

Figure 2.13: Failed Anchorage Plate at Shipshaw Abutment. (Filliatrault et al., 1993)

A more recent event that occurred was the damage of the Chi-Lu Cable-Stayed Bridge in Taiwan on September 21, 1999. The magnitude of the Chi-Chu earthquake was determined to be $M_L = 7.3$ and 7.7 by the Seismology Center of the Central Weather Bureau and Harvard CMT respectively. The Chi-Lu bridge located 10-km southwest of the epicentre was under construction at the time when the earthquake occurred and it sustained notable damage to the decks and pylons. Since the deck of the bridge had not been completed near the pylons, the lack of closure joints at the ends of the deck resulted in the structure being susceptible to damage (Chang *et al.*, 2004). The shear keys at both ends of the stayed spans had translated laterally, gouging the supporting bent cap and inducing severe shear cracking. Referring to Figure 2.14, the pylon experienced concrete spalling and this has exposed two of the plastic hinge regions. It was clear that the splitting of concrete around the core occurred to nearly the height of the lowest cables. Furthermore, it has been found that one of the stay cables sustained failure at the cable anchorage and was found lying slack on the bridge deck (Chang *et al.,* 2004).

Figure 2.14: Concrete spalling at pylon base of Chi-Lu Cable-Stayed Bridge (Chang *et al.*, 2004).

2.5   Fatigue

Fatigue is a mechanism that is a result of cyclic loading that permits crack growth in a member, consequently leading to failure of the element. It is strongly influenced by the magnitude of applied stress range to which the element is subjected to in addition to the presence and acuity of stress concentrations occurring within the element (Parke, G. A. R., 2014). The pioneering investigation on fatigue was the work of August Wohler, a

German railroad system technologist due to his concern towards the failure of railroad axles after repetitions of significantly lower loads compared to the static strength of the structures. It resulted in the first systematic study of fatigue by conducting laboratory fatigue tests under cyclic stresses (X. W. Ye *et al.*, 2013).

In the middle of the 20th century, the problems regarding fatigue as a phenomenon that occurs in metallic elements have been reviewed by Peterson and Timoshenko in the 1950s and 1954s respectively. Peterson mentioned quoted ideas about fatigue as a material phenomenon and the microscopic studies carried out by Gough and co-workers and others around 1930. On the other hand, Timoshenko discussed the significance of stress distributions and emphasized stress concentrations around notches.

Cracks found in steel elements of bridges can usually be associated with fatigue. Fatigue is a progressive, localized and permanent alteration towards a structure that is subjected to repeated or fluctuating strains at nominal stresses that are well below the tensile strength of the materials. Fatigue may culminate into cracks and result in fracture after a sufficient number of fluctuations (W. Ye *et al.*, 2014). Fatigue cracks has the potential to result in structural failure when the remaining un-cracked areas no longer possess the ability to withstand the loads exerted on the structure. For bridges, fatigue failure tends to occurs due to the growth of fatigue crack that initiates from superficial discontinuities (Albrecht, P. & Wright, W., 2000).

According to a study by Roylance (2000), fatigue is a result of cumulative damage due to repetitive application of loads below the yield point of steel. However, the study stated that the effects will only be evident through prolonged experience of repetitive loads instead of a single application, thus, conventional stress analysis might lead to an assumption of false safety (Roylance, D., 2000). The process is strongly influenced by the magnitude of applied stress range to which the element is subject to and also by the presence and acuity of stress concentrations occurring within the element (Parke, G. A. R., 2014).

One of the more critical components that affect the fatigue life of an element is the applied stress range. With the applied loads fluctuating between a maximum and minimum value, the material will experience a corresponding fluctuation in the applied stress which will exceed the applied average stress and this may yield the material

(Kumar, S. R. S. & Kumar, A. R. S., 2012). Fatigue damage is a result of the simultaneous action of cyclic stress, tensile stress, and plastic strain. The lack thereof any of the above factors will not result in the initiation and propagation of fatigue cracks. The plastic strain that results from cyclic stress initiates the crack; whereas the tensile stress stimulates the propagation of cracks. Careful measurement of strain shows that microscopic plastic strain might otherwise appear to be totally elastic (Boardman, B. & Deer and Company., 1990).
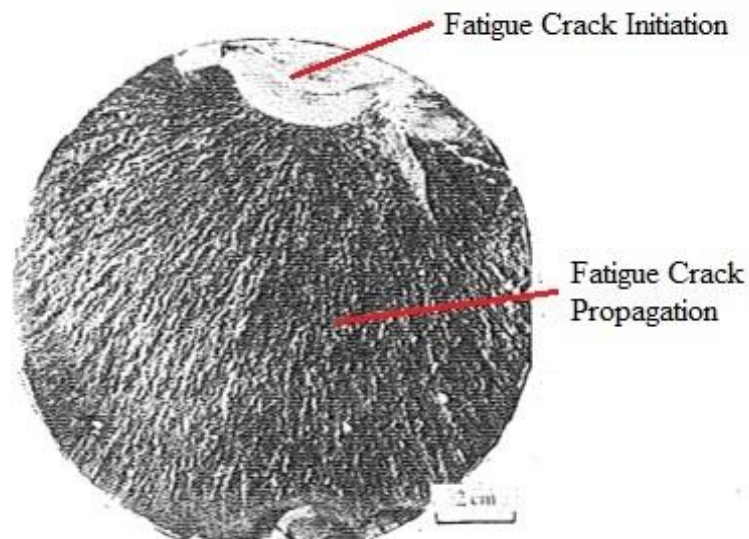
Figure 2.15: Typical fatigue failure in a steel component. (European Steel Design Education Programme, 1998)

As shown in Figure 2.15, mechanisms of fatigue failure can be separated into three stages: initial fatigue damage that leads to the initiation of cracks, crack propagation to a certain degree and abrupt fracture. Fatigue life is separated into crack initiation and crack growth period. Microcrack growth was not taken into account for the initiation period as the fatigue cracks are unnoticeable (Schijve, J., 2009). In the second stage, the crack will continue to propagate until absolute failure occurs. It is crucial to take account of the crack initiation period and crack growth period independentally because several practical conditions have a large influence on the crack initiation period. However, they have limited impact on the crack growth period (Schijve, J., 2009).

Research has found that there are two different forms of stress cycles that lead to fatigue failure. In light of the works of Coffin Jr. (1962) as well as Manson *et al.* (1964),

it has been determined that fatigue can occur due to plastic strain deformation resulting from cyclic loading (Schijve, J., 2009). As described by Imam & Chryssanthopoulos (2012), fatigue has two characteristic failure mechanisms namely; high-cycle fatigue and low-cycle fatigue. Both these failure mechanism have different characteristics from each other. High-cycle fatigue is stress driven with fatigue lives being more than 10^5 stress cycles while low-cycle fatigue is strain driven with fatigue lives limited to only a few hundred strain cycles (Imam, B. M. & Chryssanthopoulos, M. K., 2012). A study by Park & Lee (2017) has shown that a large degree of focus has been placed on components that were subjected to high-cycle fatigue, especially when the conditions require at least 10^4 number of cycles to result in failure. High-cycle fatigue is the condition where a metallic element experiences low cyclic stress that results in elastic deformation. In these cases, the material performance can be characterized by an S-N curve that is a graph which presents the magnitude of a cyclic stress against the logarithmic scale of the cycles to failure (Park S. H. & Lee C. S., 2017).

Most structural components are exposed to cyclic loading during its service life. These components have the tendency to produce fractures after a definite duration due to the repetitive experience of stress that are some times significantly lower than the stress required to cause critical fracture. Examples of fatigue failure can be seen in cases ranging from the breaking of train acles to the cracking of wings in aircrafts. Therefore, the determination of fatigue life of steel components is crucial to ensure the design of sufficient resistance towards fatigue failure (Park, S. H. & Lee, C. S., 2017). As mentioned in Section 2.3.2.3, stay cables have an unusually higher amount of carbon content in comparison to structural steel. With the increase in carbon content in steel, it has the potential to increase its tensile strength and rigidity. In contrast, little or no plastic deformation will be displayed if low ductility steel has been undergoing the process of fatigue. Thus, they have the tendency to fail without any prior indication. In addition, stay cables are more likely to fail at an earlier rate in comparison to other elements such as welds and anchorage due to their discontinuities.

According to Hobbs & Ghavami (1982), fatigue failure of the socketed strands in cable supported bridges occurred close to the strand/socket interface in all cases. Based on their observations, wire failure initiates from the outer layer that is follow by the failure of surrounding wires of the same layer with continuous load cycles being applied. The

subsequent layer will fail after the first layer and eventually, resulting to absolute failure of strand when the remaining wires are unable to sustain the maximum applied load (Hobbs R. E. & Ghavami K., 1982). From a practical standpoint, the large number of cycles required from first wire failure to reaching overall failure in a large strand implies that regular inspection will be able to detect damaged strands before its structural integrity becomes jeopardized. Referring back to the connection points of coupled bars, areas of high concentration occurs at the point of discontinuity; as with the connection areas between the cable anchorage and the stay cables (Hobbs R. E. & Ghavami K. 1982).

Bridges may be exposed to both types of fatigue; high-cycle fatigue and low-cycle fatigue but most of the vehicle bridges always experience high cycle fatigue as live traffic crossing the bridge throughout the design life produces millions of stress cycles (Imam, B. M. & Chryssanthopoulos, M. K., 2012). However, only some bridges will be exposed to low cycle fatigue. This is because not all bridges may encounter sudden high stresses for a very short period such as earthquake excitations (Mohamad Khairusalleh, N. A. B., 2016). Similarly with suspension bridges, cable-stayed bridges are also susceptible to vibrations. The main causes of vibration originates from rain-wind induced vibrations, sympathetic vibration of cables with other structural elements due to wind loads, galloping, and vortex shedding on a single or grouped cables. Moreover, the vibrations can affect the structural integrity of cables by potentially splitting the cable strands, therefore allowing the intrusion of corrosive chemicals that accelerates corrosion, consequently resulting in a reduced fatigue life (Ohio Department of Transportation, 2009).

2.6 Stress Ranges

It has been proven by investigations that the maximum tensile or compressive stress that is being subjected to a metallic element can be repeated without resulting in fractures relies on the applied stress range in comparison to the endurance limit. Stress range is defined as the maximum and minimum values of stresses that are applied in a repetitive cycle (Smith, J. O., 1942). In order to allow for the large repetitive cycles in terms of tensile stress application at its maximum value without resulting in fractures can be achieved by reducing the stress range. Most of the data upon which this conclusion is based were obtained from tests in which the stress varied from a small tensile stress to a larger tensile stress, the same applies to compressive stress (Smith, J. O., 1942).

Stress ranges can be partially designated by the magnitude of the change in stress in passing from the minimum stress to the maximum stress of a cycle, but either the maximum or minimum stress must be given in addition to the magnitude of the range (Smith, J. O., 1942). As illustrated in Figure 2.16, a range may be specified by stating the maximum stress or the minimum stress and stating the magnitude of the range of stress. The range could be described also by simply giving both the maximum and minimum stresses. Alternatively, it can be also thought of as being made up of a steady (mean) stress or and an alternating (completely reversed) stress superimposed upon it; the range of stress may then be expressed as $\sigma_m \pm \sigma_\alpha$ (Smith, J. O., 1942).
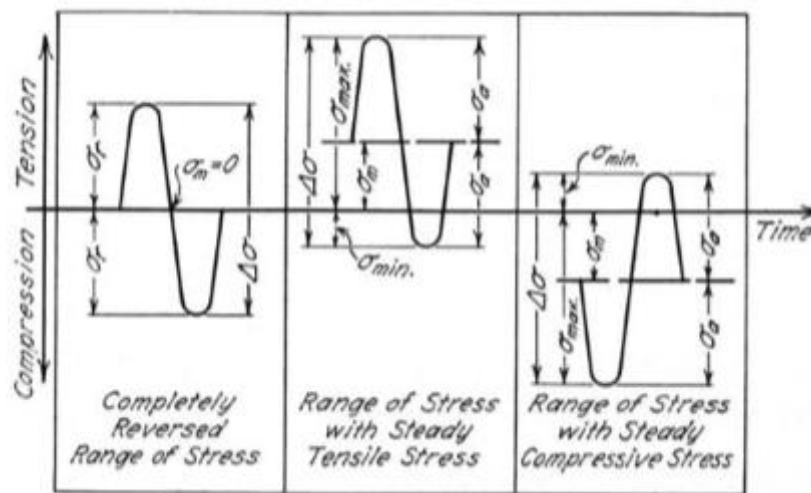
Figure 2.16: Stress symbols for varying range of stress. (Smith, J. O., 1942)

After extensive investigation, it has been found that the level of minimum stress has a low influence on resulting in crucial impact on the fatigue life of metals. Experimentation results that were obtained show insignificant difference on the minimum stress whereas the total stress range has larger influence in determining fatigue life (Ohio Department of Transportation, 2009).

2.7   Earthquakes

According to a study conducted by Vavryčuk (2015), earthquakes are a set of phenomenon that often correlates with the abrupt rupture of rocks along fractures or faults exposed to stress field in the Earth's crust and lithosphere (Vavryčuk V., 2015). When the stresses managed to attain a pivotal value that surpasses the strength of faults and

cracks in the Earth's crust, the accumulated energy of elastic deformation is exerted on the anelastic deformations in the focal zone and is released in the form of seismic waves that radiate outwards (Heidbach *et al.*, 2008). These forces tend to result in a process known as "ridge push" where the lithospheric plates are pushed away from a spreading ridge or "slab pull" process where two plates are in collision and one of them is subducting into the asthenosphere (Fowler, C., 1990).

Global earthquake occurrences are known to be associated with tectonic setting, and tectonic activities both regional and local scales. Approximately around the Late Triassic, Permo-Triassic or even earlier periods, Thailand and the surrounding countries that adjoins her has occupied major parts of the two major blocks that have been joined together due to continent-continent collisions (Charusiri, P. & Palloplee, S., 2015). As shown in Figure 2.17, the two microcontinents mentioned above includes one part of Gonwanaland that is attached to the Australian continent (Shan-Thai (-Malay) craton (western half of Thailand); eastern Myanmar, northwest Malay Peninsula; and the other part composed of the Indochina craton (eastern half of Thailand, Laos, Kampuchea, southern Vietnam, and eastern Malay Peninsula (Charusiri, P. & Palloplee, S., 2015). Both blocks which consists principally of oceanic crustal materials have been dislocated by gigantic sinistral strike-slip faults and their N-trending have been modified by sinistral oroclinal bending associated with this faulting (Charusiri, P. & Palloplee, S., 2015).

1 = Mae Ping Fault, 2 = Three Pagoda, 3 = Red River Fault, 4 = Song Ma Fault, 5 = Mae Tha Fault, 6 = Nan-Uttaradit Fault or Suture, 7 = Ranong Fault, 8 = Klong Marui Fault, 9 = Bentong - Raub Fault or Suture, 10 = Malacca Fault, 11 = Mergui Fault, 12 = Indo-Burma Thrust, 13 = Tertiary Volcanic Belt, 14 = Pegu – Yoma (Sagaing) Belt, 15 = Sumatra Fault, 16 = Khorat Monoclin, 17 = Khorat Basin, 18 = Chao Phraya Basin, S = Sukho Thai Fold Belt, L = Loei Fold Belt

Figure 2.17: Tectonic map of Southeast Asia that shows major structures, basins, and tectonic blocks. Modified after (Charusiri, P. & Palloplee, S., 2015).

The present-day tectonic framework of Southeast Asia is dominated by the interaction of three adjoining major lithospheric plates: the continental-oceanic Indo-Australian plate in the west and the south; the continental Eurasian plate in the middle; and the oceanic West Pacific plate in the east (Charusiri, P. & Palloplee, S., 2015). Several concrete historical evidences have proved that Peninsular Malaysia does not necessarily have a low risk of experiencing seismic events. As a result, the regional tectonic setting has been thoroughly investigated to determine the potential of earthquake occurrences in the future (Yunus *et al.,* 2013). The tectonic framework for the whole of Malaysia covers between longitudes 90 E to 140 E and latitudes of 12 S to 20 N Malaysia was considered to have a low seismicity profile and it is located on the Sunda plate as part of the larger Eurasian plate (Yunus *et al.*, 2013). Moreover, the location of the Sunda plate that is outside the Pacific Ring of Fire more than enough justifies the tectonic stability (Shoushtari *et al.,* 2018). Despite the inherent stability, there have been reported cases of seismic effect in Peninsular Malaysia.

To date, significant evidences have shown that previous hypothesis on the earthquake-free condition of Malaysia is false. In contrast to the hypothesis, one of the more significant regional earthquakes was the 2004 Indian-Ocean Earthquake ($M_w = 9.1$) that resulted in an unprecedented and destructive tsunami resulted in significant casualties in the region. The aforementioned geological event resulted in the disturbance of tectonic plates surrounding the epicentre along with the deformation of the sunda-land core that subsequently caused the Peninsular to drift away from its original position along with post-seismic deformations for Southeast Asia. Observations by (Omar K. & Jhonny, 2009) have indicated that the significant deformation of Peninsular Malaysia due to the earthquake technically places the Peninsular at a closer distance to the epicentre which has a higher likelihood of increasing the severity of local effects due to the occurrences of earthquakes in the coming years. Moreover, it has been found that the reactivation of inactive faults due to the deformations on the sunda-land as shown in Figure 2.18 has the potential to trigger earthquakes that originate within Peninsular Malaysia (Yunus *et al.*, 2013).
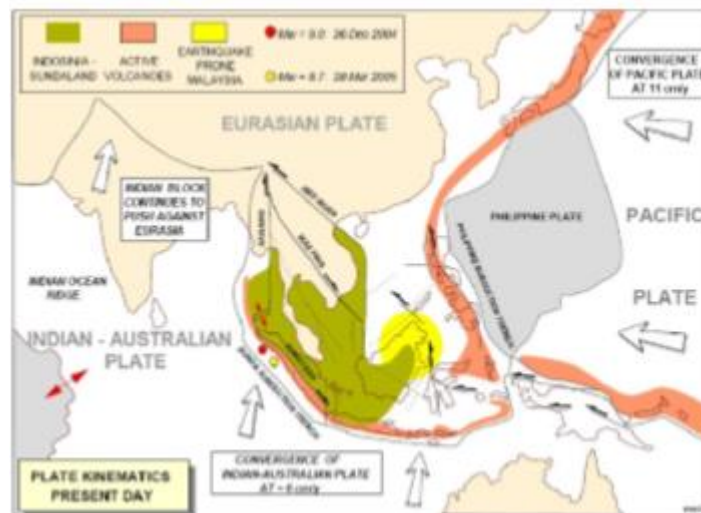
Figure 2.18 Earthquake-prone region of Malaysia. (Tjia, H., 2010)

On top of that, different scenarios has been detected in East Malaysia. Since the early 1870s, a least 21 earthquake cases have been detected in Sarawak whereas 94 cases have been reported in Sabah, notably the 1976 Lahad Datu Earthquake, 1991 Ranau Earthquake and 2004 Miri Earthquake (Yunus *et al.*, 2014).

The 2011 Tohoku earthquake in Japan of $M_w = 9.1$ is a prime example of overseas regional megathrust subduction earthquakes that resulted in critical impacts as far-field earthquakes. According to Shoushtari *et al.* (2017), Takewaki et al. (2011) reported that a large majority of high rise buildings in cities of Japan, such as Tokyo and Osaka with epicentral distances (R_{epi}) of approximately 385 and 761km respectively have been critically impacted by the ground motions induced by the quake (Shoushtari *et al.*, 2017). Moreover, the type of soil on a particular site of interest stands a a parameter that influences the damage amplification of low amplitude, long-period ground motions due to far-field earthquakes (Shoushtari *et al.*, 2017). A notable example of catastrophic damage caused by ground motion amplification can be seen in the 1985 Michoacán earthquake with $M_w = 8.1$. The earthquake produced large intensities in Mexico City and reached a level of IX on the Mercalli scale. As the peak ground accelerations (PGA) reached 0.17g, it surpassed the limits enforced by the building codes with the occurrences of higher than normal spectral amplifications and durations. This resulted in casualties of between 10000 to 35000 people and the destruction of approximately six thousand buildings (Ceballos *et al.*, 2017). The effect of soft soil on the seismic response of alluvial valleys (Type E soils) has the tendency to significantly amplify the ground motions induced by seismic activities. Its large amplitude ground motion and long duration records in the lacustrine plain sites in the Valley of Mexico was a result of the combination of significant sources, path and site effects (Ceballos *et al.*, 2017). The amplifications were significant as they reached at least 10 times the critical frequencies for Mexico City soil conditions (1-5s). As the uppermost soft layers trap the seismic wave energy, it resulted in significant ground motion amplifications by 10 to 50 folds (Ceballos *et al.*, 2017).

2.8 Tectonic Conditions of Peninsular Malaysia

Tectonic features affecting Peninsular Malaysia can be divided into two; far field earthquakes and near field earthquakes. In the case of far field earthquakes, the Sumatra Subduction Zone and the 1900km long Sumatra fault that is running through the entire Sumatra Island. The first being the source of gigantic earthquakes that poses a significant threat to Peninsular Malaysia. The summary of all cases of earthquakes that has affected Peninsular Malaysia are shown in Table 2.3.

Table 2.3: Earthquakes that affected Peninsular Malaysia

Date	Epicenter	Magnitude	Effect on Malaysia
1984/08/27	Northern Sumatera	5.2	Kuala Lumpur, Penang
1987/04/25	Northern Sumatera	6.3	Kuala Lumpur
1990/11/15	Northern Sumatera	6.9	Ipoh, Kuala Lumpur, Penang, Taiping
1994/10/11	Northern Sumatera	6.5	Southern Malaysia and Singapore
1997/08/20	Northern Sumatera	6.0	Alor Setar, Petaling Jaya, Penang
1998/04/01	Padang	6.9	Kuala Lumpur
2000/05/04	Sulawesi	7.4	Tawau
2000/06/04	Southern Sumatera	7.7	Johor, Kuala Lumpur, Petaling Jaya
2002/11/02	Simeulue	7.4	Kuala Lumpur, Port Klang
2004/07/25	Southern Sumatera	7.3	Southern Johor, Singapore
2004/12/26	Northern Sumatera	9.0	68 people killed in Penang, Langkawi, Kedah
2005/02/12	Sulawesi	7.0	Kota Kinabalu
2005/03/28	Northern Sumatera	8.6	West Coast Peninsular Malaysia
2005/04/10	Mentawai	6.7	Kuala Lumpur, Singapore
2005/04/10	Mentawai	6.5	Kuala Lumpur
2005/05/19	Nias	6.9	Penang, Kuala Lumpur, Sungai Ara, Tanjung Tokong
2005/07/05	Nias	6.7	Klang, Kuala Lumpur, Petaling Jaya, Sungai Ara

Source: (Yunus *et al.* 2013)

cont' Table 2.3: Earthquakes that affected Peninsular Malaysia

Date	Epicenter	Magnitude	Effect on Malaysia
2005/07/24	Nicobar Islands	7.2	George Town
2005/11/19	Simuelue	6.5	Ayer Itam
2006/12/17	Northern Sumatera	5.8	Kuala Lumpur, Singapore
2007/03/06	Southern Sumatera	6.4	Johor Bahru, Kuala Lumpur, Port Dickson, Skudai
2007/08/08	Jawa	7.5	Kuala Lumpur, Petaling Jaya, Sungai Ara
2007/09/12	Southern Sumatera	8.4	Setapak, Cheras, Pudu, Langkawi, Johor Bahru, Melacca
2007/09/20	Mentawai	6.7	Singapore
2009/08/16	Southern Sumatera	6.3	Kuala Lumpur, Penang, Johor
2009/09/30	Padang	7.9	Kuala Lumpur, Putrajaya George Town, Johor Bahru
2010/05/09	Northern Sumatera	7.2	Sungai Dua, Penang
2011/06/14	Northern Sumatera	5.6	Selangor, Melacca, Perak, Putrajaya, Negeri Sembilan
2012/04/11	Northern Sumatera	8.2	Penang, Kuala Lumpur
2012/06/24	Northern Sumatera	6.5	Kedah, Perak, Selangor, Negeri Sembilan
2012/07/25	Northern Sumatera	6.6	West coast Peninsular Malaysia

Source: (Yunus *et al.* 2013)

On the other hand, near field earthquakes that are originated within Peninsular Malaysia. These earthquakes started to occur since 2007 as presented in Table 2.4. Based on the study by Yunus *et al.* (2014), Shuib (2009) has commented on the reasons for the reactivations of ancient inactive faults being the result of intraplate stress after the 2004

Mega quake (Yunus *et al*, 2014). The main active seismic component that lay within Peninsular Malaysia is Bentong Fault Zone that includes the Bukit Tinggi Fault and Kuala Lumpur Fault (Yunus *et al.*, 2013).

Date	Case	Location
2007 – 2009	24	Bukit Tinggi, Kuala Lumpur
2009	4	Kuala Pilah, Perak
2009	1	Jerantut, Pahang
2009	1	Manjung, Perak
2010	1	Kenyir Dam, Terengganu
2012	1	Mersing, Johor

Table 2.4: Local earthquake occurrences in Peninsular Malaysia. Source: Modified after (Yunus *et al.* 2013)

2.9   Seismic Hazards in Peninsular Malaysia

Seismic hazard maps are used to divide a region into zones to allow for the communication of spatial distribution of frequency of future earthquake occurrences to the designer of future facilities. Said maps are about the predictions of future seismic activities and is not supposed to be a map which primarily focuses on the scientific record of historical activities (Looi *et al.*, 2017). Based on a study conducted by Shoushtari *et al*. (2017) have reassessed and updated the seismic hazard maps of Peninsular Malaysia with regards to the extended earthquake catalogue, upgraded seismic source parameters and compatible ground motion prediction equations (GMPE)'s (Shoushtari *et al*., 2017). The result was the generation of two probabilistic seismic hazard maps (PSHA) over a 12.5km grid in terms of its Peak Ground Acceleration (PGA) for 10% and 2% probabilities of exceedance (PE) in 50 years, with respect to RP475 and RP2475 years return periods. Both of which are presented in Figure 2.19 and Figure 2.20 respectively.
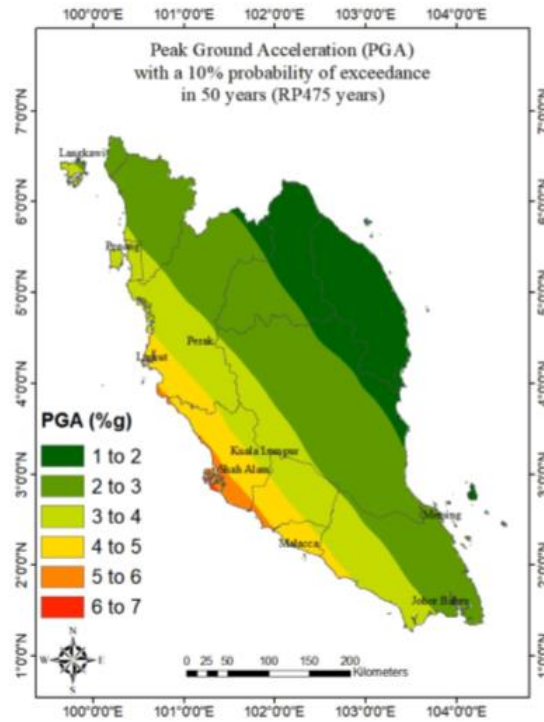
Figure 2.19 Probabilistic seismic hazard maps with 10% PE in 50-year (RP475-year) on rock site condition for Peninsular Malaysia due to only distant Sumatran earthquakes. (Shoushtari *et al.*, 2017)
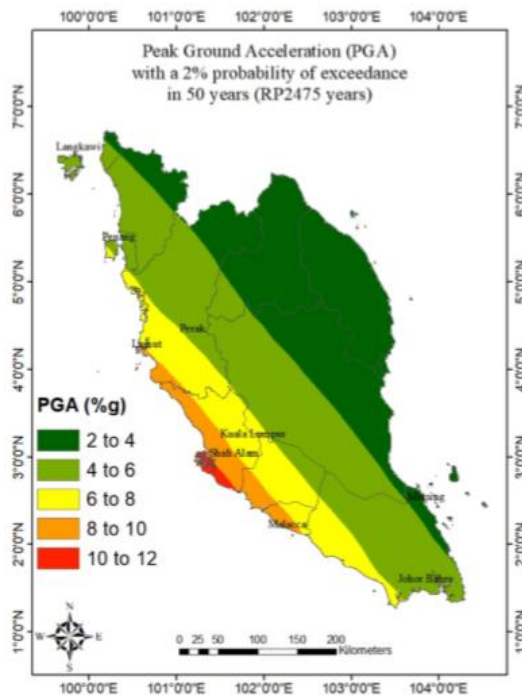
Figure 2.20: Probabilistic seismic hazard maps with 2% PE in 50-year (RP2475-year) on rock site condition for Peninsular Malaysia due to only distant Sumatran earthquakes. (Shoushtari *et al.*, 2017)

CHAPTER 3

METHODOLOGY

3.1 Introduction

This chapter discusses the work and methods that have been completed in this study on top of outlining the strategy, methods, approaches and process of the research. The methods on how the author models the bridge in SAP2000 software with the appropriate standards, conducts data collection and analysis will be presented in this chapter.

3.2 Bridge Description

In order to generate a model of the Sultan Abdul Halim Muadzam Shah Bridge (The Second Penang Bridge), detailed specifications of the bridge were sourced from the Client (Jambatan Kedua Pulau Pinang Sdn. Bhd.), the Consultant (AECOM) along with papers and proceedings regarding its design and construction. The Second Penang Bridge is the second dual-plane cable-stayed bridge in Malaysia that links Penang Island to mainland Batu Kawan following the completion of the first Penang Bridge. The bridge site is located in the Straits of Malacca and was constructed to relieve traffic congestion on its predecessor despite the recent widening works (Corbett *et al.,* 2010) The main bridge of the Second Penang Bridge consists of two-pylon that supports a three-span prestressed concrete deck with a span arrangement of (117.5m + 240m + 117.5m) and is supported by H-shaped pylons with parallel strand stay cables in a semi-fan arrangement anchored into the pylons by cable saddles (Man *et al.*, 2018).

The main span has a total of 4 stay cables planes that consists of 18 nos. of stay cables each. The stay cables are of high strength parallel strands with an ultimate tensile strength of 1860MPa at 150mm² for each strand. Stay cable no. 1 (M01 and S01) has a

larger mass and with 55 no. of strands, whereas the stay cables no. 2 to 18 (M02 to M18 and S02 to S18) were arranged with at angles of varying degrees in which the number of strands starts from 37 nos. on the second stay cable to 73.nos. in the outermost stay cable (Man *et al.*, 2018). The stay cables are anchored to the deck along the centreline of the diaphragms at a 6m centre to centre spacing for the first 16 stays and a 4m centre to centre spacing for the last 2 stays (Sham *et al.*, 2013). Along the vertical axis, the stays are arranged at a starting elevation of 5.5m above the deck and spaced at an equal distance of 2.525m centre-to-centre (Mohamed Taib, I. B., 2016).

Figure 3.1: Photograph of the Sultan Abdul Halim Muadzam Shah Bridge.
(Arup Malaysia, 2015)

3.3 Analytical Model of the Second Penang Bridge

The main structural components of the Second Penang Bridge are made up of stay cables, concrete bridge deck and concrete pylons, in which they are distinguished by different finite element variation in the model. This cable-stayed bridge consists of two cable planes with 64 stay cables on each side. The stay cables are defined by straight frame cable elements in SAP 2000 with applied tension force in the form of strain loads at the J-end, implying that the cables are stressed at the deck anchorage as the application of cable saddles at the pylons restrict any stressing activities to be conducted. The nonlinear behaviour of cables is achieved by the application of the equivalent tangential modulus,E_{eq} by Ernst over the existing modulus elasticity, E_p (Shrestha, B., 2014)

$$E_{eq} = \frac{E_P}{1 + \dfrac{w_p^2 d_p^2 E_P A_T}{12 F_{P,0}^3}} \qquad 3.1$$

Where, E_p=190GPa is the initial modulus of elasticity of cable strands, w_p is the weight of the stay cable per unit length (w_p=$\rho_s A_T g$, for ρ_s=7800kgm³ and g=9.81ms⁻²), dp is the horizontal projection of stay, A_T is the cross-section area of stay and $F_{p,0}$ is the initial prestress force of the element (Casado, A. C., 2011).
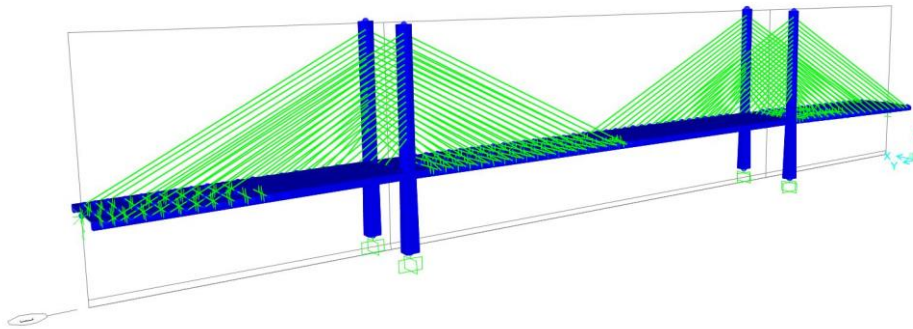
Figure 3.2: SAP 2000 model of the Sultan Abdul Halim Muadzam Shah Cable-Stayed Bridge Model

The concrete pylons and piers of the bridge with varying cross-section have been modelled in SAP 2000 with the use of non-prismatic frame elements. With regards to the geometry, the tower is divided into two segments and is assumed to have a fixed connection at the base. On the other hand, frame elements have been applied in the modelling of the concrete bridge deck. The bridge deck is assumed to be a continuous beam that spans between both abutments of the approach span, rigidly connected to the box girder cross beam of the H-pylons. The ends of the bridge are restrained in terms of vertical translation and rotation about the z-axis and y-axis respectively. The main deck girder is made of prestressed concrete with a grade of C55 concrete with strengths of f_{ck}=55N/mm² (Man *et al.*, 2018). On the other hand, the pylons are constructed of C50 concrete at an estimated concrete strength of f_{ck}=50N/mm² (Mohamed Taib, I.B., 2011).
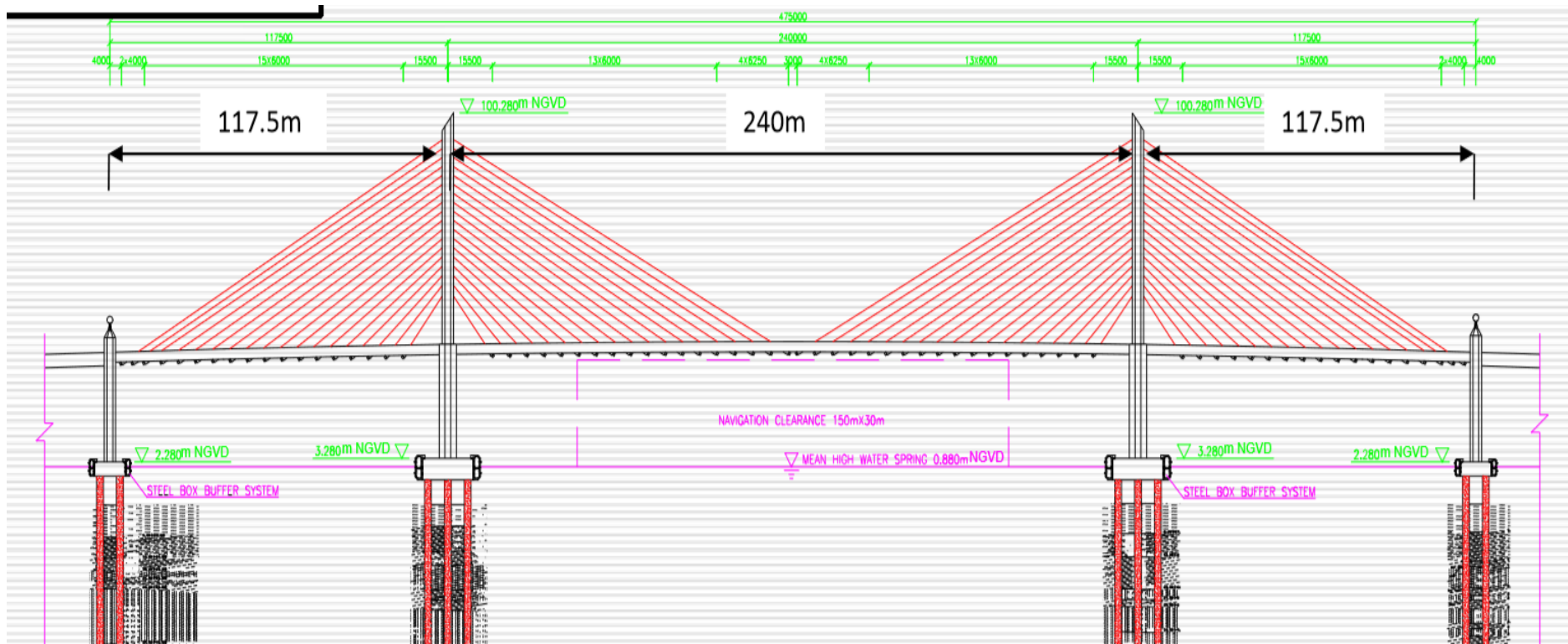
Figure 3.3: Longitudinal Layout of Cable-stayed portion of the Sultan Abdul Halim Muadzam Shah Bridge (Mohamed Taib, I. B., 2011).
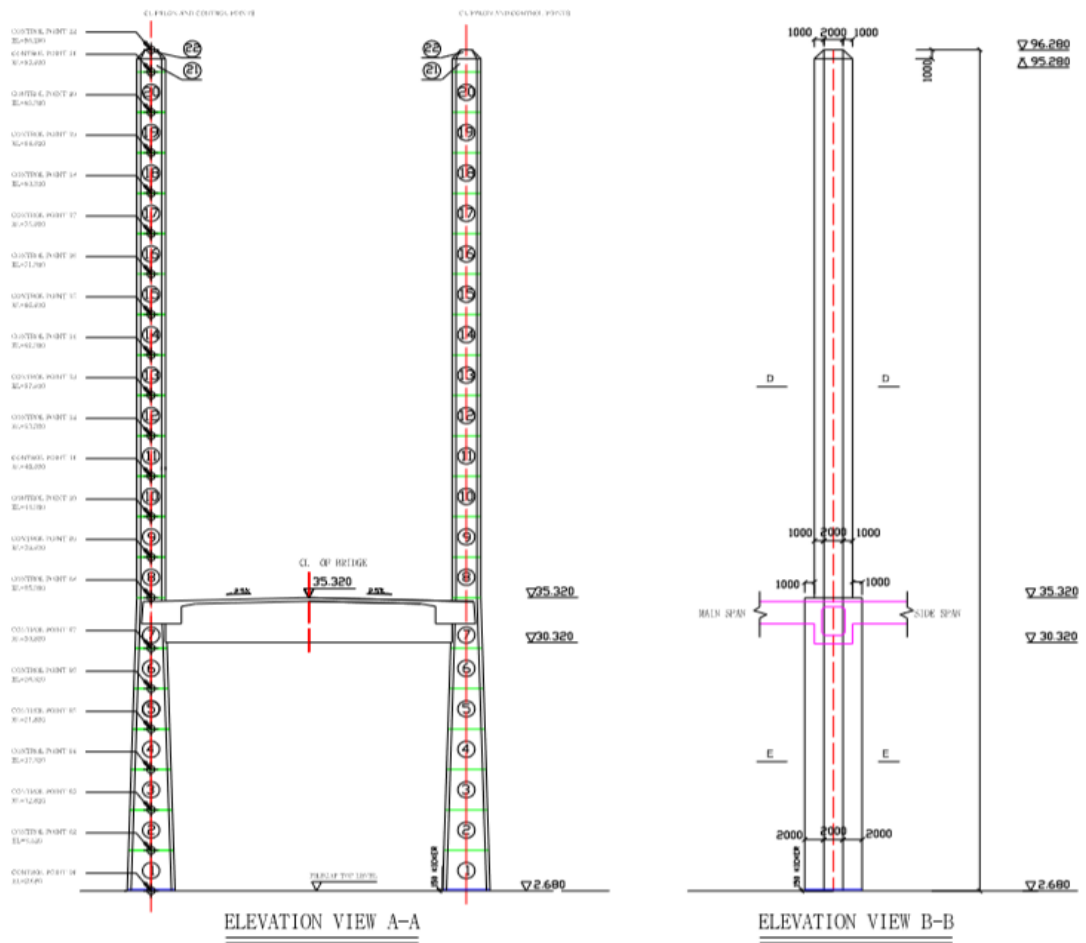
Figure 3.4: Elevation View of H-Pylons (Sham *et al.*, 2013).
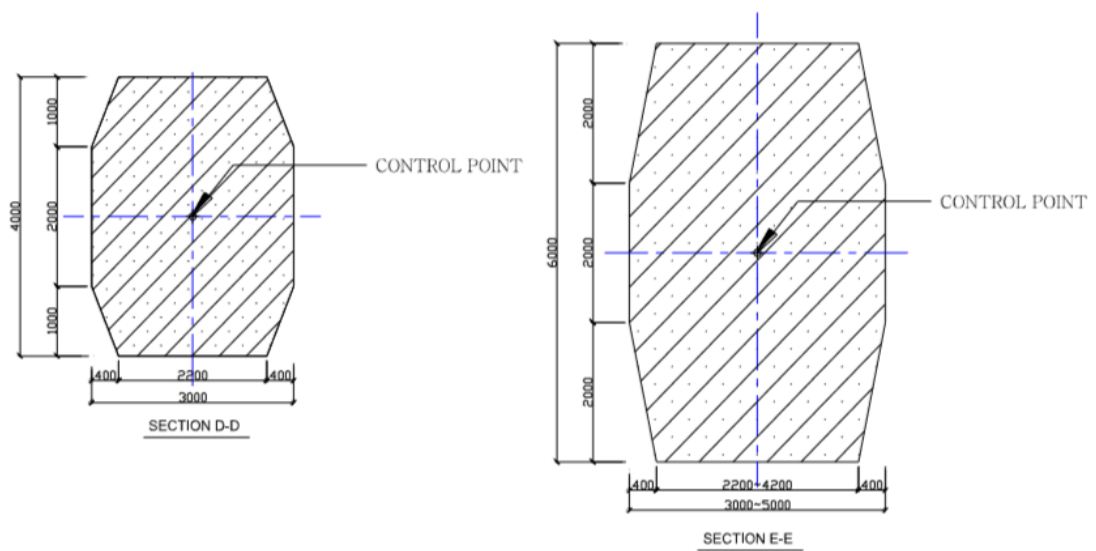
Figure 3.5: Cross-Section of Pylons (Sham *et al.*, 2013).
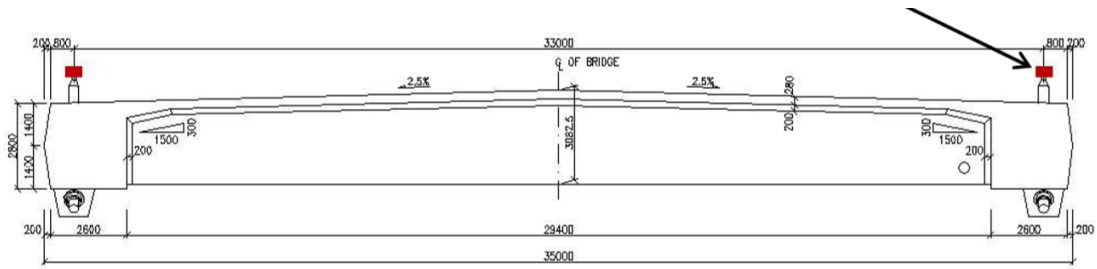
Figure 3.6: Cross-Section of Main Deck/Girder (Sham *et al.*, 2013).

According to Shreshta B. (2014), the equivalent modulus approach, is common among bridge designers such as the works of Abdel-Ghaffar and Nazmy (1990) in order to consider the effects of cable sag in the analysis of cable-stayed bridges for static loads. However, this approach is only accurate for static or quasi-static analysis and exhibits several drawbacks in the use of seismic analysis. Since the equivalent modulus of a cable depends on the cable tension that fluctuates constantly during seismic excitations. Cables will act as stiffening components when they experienced tensile forces whereas they become softening components when the cables grow slack as a result of force reduction in the cables. Hence, the usage of this method throughout the duration of seismic response is invalid when cable vibrations are considered (Tuladhar *et al.*, 1995). As the current study does not consider the influence of cable vibration on the dynamic response of the bridge, the equivalent modulus is considered. Therefore, each cable have been modelled with cable elements as a straight frame that eliminates the lateral vibration modes of the cables. As shown in Figure 3.7, the stay cable numbering and layout for the cable-stayed bridge is illustrated in a two-dimensional form for identification purposes.
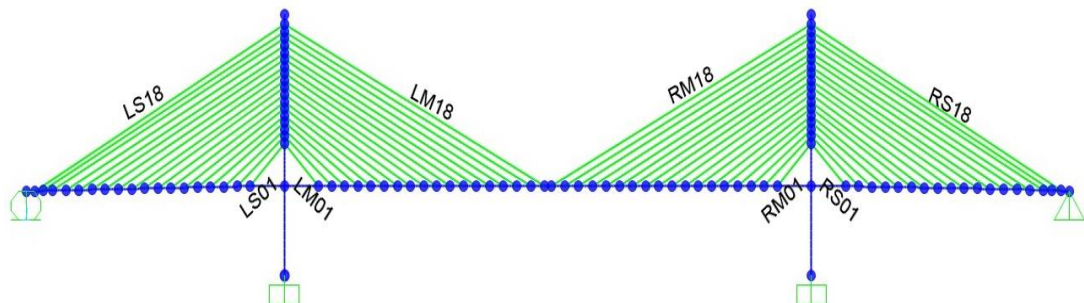
Figure 3.7: Stay cable numbering in SAP2000

3.4 Traffic Loadings

Traffic loadings are applied with regards to the Fatigue Load Models as stated in BS EN 1992-2:2004 in order to simulate actual traffic conditions on the bridge and thus resulting in the most critical theoretical fatigue damage towards the structural component in consideration. Equivalent vehicle models with specified loads for their individual axles will be applied in SAP 2000 in conjunction with the appropriate load patterns and critical lane placements as per the requirements of BS EN 1991-2:2003. Also, the speed of selected vehicles used in the analysis is based on the National Speed Limit of Malaysia.

3.4.1 Traffic Fatigue Load Model (FLM)

The development of fatigue damage is crucial to determine the ruggedness of highway bridges that primarily experiences traffic loads. The fatigue behaviour and ability of bridges to sustain loads are highly affected by factors such as the deterioration of materials, variation in traffic loadings as well as the surrounding environment. Therefore, the usage of fatigue load models that considers real traffic loads is crucial for fatigue analysis (Chen *et al.*, 2015).

The fatigue load models (FLM) as defined in BS EN 1992-2:2004 ranges from FLM 1 to FLM 5, each used under different conditions ranging from vehicle geometry, axle loads, vehicle spacing, traffic composition and the dynamic effects to simulate fatigue damage due to actual traffic loadings. They are intended to provide different levels of sophistication and economy (Flint & Niel Partnership Consulting Engineers, 2004). The number of heavy vehicles estimated annually for every slow lane is indicated in Table 3.1 whereas the axle definition for the Fatigue Load Models are depicted in Figure 3.8.

Table 3.1: Indicative number of heavy vehicles expected per year and per slow lane (BS EN 1991-2:2004).

	Traffic Categories	N_{obs} per year and per slow lane
1	Roads and motorways with 2 or more lanes per direction with high flow rates of lorries	2.0×10^6
2	Roads and motorways with medium flow rates of lorries	0.5×10^6
3	Main roads with low flow rates of lorries	0.125×10^6
4	Local roads with low flow rates of lorries	0.05×10^6

Note: N_{obs} is the number of estimated heavy vehicles (maximum gross vehicle weight of more than 100kN) per year per slow lane.

With regards to BS EN 1991-2:2004, Fatigue Load Models 1, 2 and 3 are commonly utilized to produce stress ranges instead of the provisions of counts of stress range. They are often used to check whether the fatigue life may be considered to be unlimited under a given a constant stress amplitude fatigue limit. Therefore, these Fatigue Load Models can only provide safe indications of unlimited life if they are conservative. On the other hand, Fatigue Models 4 and 5 are intended to be used on structures that assumes a limited fatigue life to assess the fatigue life with regards to the fatigue strength curves defined in BS EN 1992-2:2004.
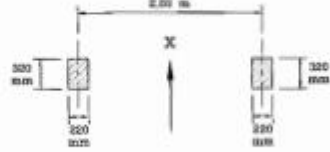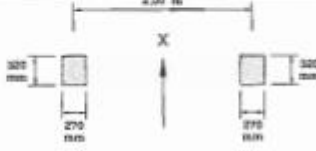
Figure 3.8: Definition of Axles for Fatigue Load Models (BS EN 1991-2:2004).

3.4.1.1 Fatigue Load Model 4

FLM 4 has better accuracy than FLM 3 for a wide range of bridges and traffic conditions which disregards the simultaneous presence of multiple lorries on the bridge. It comprises a description of a set of vehicles as shown in Figure 3.9 that are intended to replicate identical amount of fatigue damage as the typical traffic conditions on European roads that comprises a matching number of heavy goods vehicles (Flint & Niel Partnership Consulting Engineers, 2004); (BS EN 1992-2, 2004). A set of lorries relevant to the predicted traffic conditions for the route as defined in Figure 3.8 and 3.9 has to be taken into account in this load model. (BS EN 1992-2, 2004) For the purpose of simplifying the loading application and detailed analysis of this study, the equivalent lorry shall be classified under FLM4-A, FLM4-B, FLM4-C, FLM4-D and FLM4-E.

VEHICLE TYPE			TRAFFIC TYPE			
1	2	3	4	5	6	7
			Long distance	Medium distance	Local traffic	
LORRY	Axle spacing (m)	Equivalent axle loads (kN)	Lorry percentage	Lorry percentage	Lorry percentage	Wheel type
FLM4-A	4,5	70 130	20,0	40,0	80,0	A B
FLM4-B	4,20 1,30	70 120 120	5,0	10,0	5,0	A B B
FLM4-C	3,20 5,20 1,30 1,30	70 150 90 90 90	50,0	30,0	5,0	A B C C C
FLM4-D	3,40 6,00 1,80	70 140 90 90	15,0	15,0	5,0	A B B B
FLM4-E	4,80 3,60 4,40 1,30	70 130 90 80 80	10,0	5,0	5,0	A B C C C

Figure 3.9: Modified set of equivalent lorry for Fatigue Load Model 4. (BS EN 1991-2, 2004)

3.4.2   Load Model Selection

Based on the five different Fatigue Load Models (FLM), FLM 4 is the optimal selection for this study to be applied in the global analysis in SAP2000. This is because the analysis of fatigue does not consider an unlimited fatigue life for the bridge. As discussed in Section 3.4.1, both Fatigue Load Models 1 and 2 can only provide stress ranges that are effective to bridges with spans that are sensitive to individual axles instead of multiple moving loads. Therefore, these two models are unable to provide an proper model of stress cycle counts for a moderately spanned cable-stayed bridge. Although Fatigue Load Model 3 is intended to be used for fatigue life assessment, but the FLM 3 only has a single set of load cases that is capable of producing limited results. Unlike FLM 3, FLM 4 is capable of achieving greater accuracy for a wide range of subjects due to its wider range of standard sets of lorry with varying properties. Despite the utilization of FLM 5 that is capable of producing the most

optimal results via the application of actual traffic data, it is unsuitable for the current study due to several factors that includes time constraints and data acquisition.

3.4.3 Application of Fatigue Load Models

In this study, the global dynamic analysis of the model will be conducted in the form of 2-Dimensional and 3-Dimensional analysis. To simulate moving traffic across the bridge, traffic loads are applied along the entire length of the bridge that is situated on the centreline (y-axis) for the simplified 2-Dimensional model. A specific location of the placements of traffic loads is not required as the model only presents a side elevation of the bridge. Therefore, placement of the loads with respect to the x-axis does not result in a considerable amount of effect on the difference in nominal stress of stay cables. The 3-Dimensional model offers the option to simulate the placement of traffic on notional lanes of the carriageway. The deck is subjected to moving loads (Single Lorry and Convoy Lorry) with regards to BS EN 1991-2-2003. To determine the fatigue values, the location and numbering of the lanes should be selected depending on the traffic to be expected in normal conditions. The lane giving the most adverse effect is located furthest away from the centreline, namely Notional Lane 1L or Notional Lane 1R. The lane giving the second most adverse effect is the next closest lane to the centreline are Notional Lane 2L or 2R, where both of which are shown in Figure 3.8.

For the verification of individual load models on their respective notional lane, the load model should be applied on notional lanes that has the potential to produce the most adverse effect on the bridge with reference to their compatibility of the load application defined for each model. With regards to the National Annex for BS EN 1991-2:2003, fatigue damage should be evaluated in terms of the of stress cycles that are determined from two traffic lanes only. The lanes are the two notional lanes (1L and 1R) that will result in the most critical theoretical fatigue damage in the component (cables for this study) under consideration. In this study, the lane with a closer relative distance to the cable anchorage presents a higher degree of impact on the fatigue damage. Therefore, traffic load is only applied on the outermost lane, which is Notional Lane 1L. With regards to the carriageway layout of the actual bridge shown in Figure 3.10, it is made up of a pair of dual-lane carriageway with a 3.5 meter wide lane which starts at an offset distance of 1.5m from the centre. By taking the midpoint

of Notional Lane 1, traffic loads are placed at an offset distance of 6.75m from the centreline of the bridge deck.
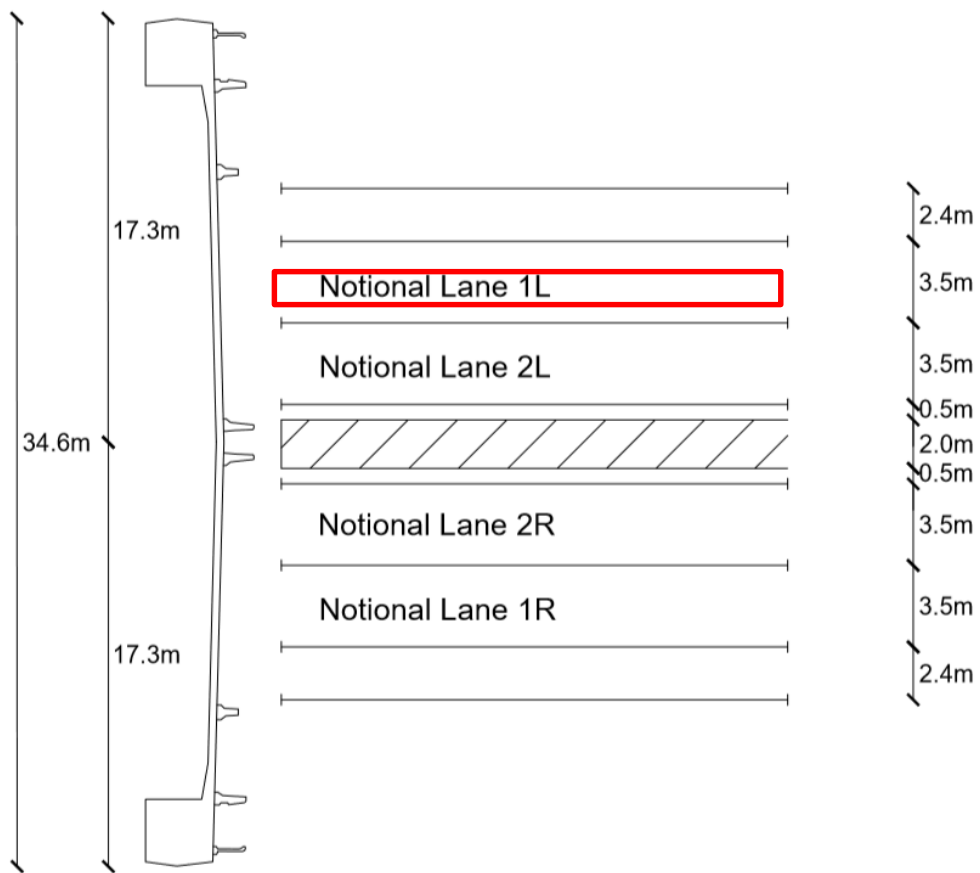
Figure 3.10: Detailed Carriageway Layout of Bridge Deck. (Man *et al,* 2018)

3.4.4 Vehicle Traverse Velocity

It is necessary to determine the speed limit of vehicles to simulate the dynamic effects on the bridge. In order to carry out global analysis for the study, it is required to specify the speed of vehicles in SAP 2000 for the application of traffic loads. In accordance with the Motor Vehicles (Speed Limit) Rules 1989 by the Government of Malaysia, lorry shall be categorized under goods vehicles that are rigid or articulated. In Malaysia, the speed limit for each type of vehicle is shown in Figure 3.11.

SCHEDULE
(Rule 3)

Class of Vehicle	Maximum Speed (kilometres per hour)	
	Roads described in Schedule to National Speed Limit Order 1989	Other roads
1. Motor vehicles fitted with pneumatic tyres on all wheels:		
(a) passenger vehicles		
(i) having a seating capacity not *exceeding twelve* persons, including the driver, and used for hire or reward	110	90
(ii) having a seating capacity exceeding twelve persons, including the driver	90	80
(iii) when drawing a trailer	80	70
(iv) motor van	90	80
(b) goods vehicles (rigid or articulated)—		
(i) when not drawing a trailer or semi-trailer and the maximum permissible laden weight of which does not exceed 7,500 kilogrammes	90	80
(ii) when not drawing a trailer or semi-trailer and the maximum permissible laden weight of which exceeds 7,500 kilogrammes	80	70
(iii) when drawing a trailer or semi-trailer, excluding a trailer drawn by land tractor	80	70
(iv) 3 wheelers including motor cycles with side cars	70	60

Figure 3.11: Malaysia National speed limits based on the type of vehicle (Motor Vehicle (Speed Limit) Rules 1989, 2010).

With regards to the figure, rigid goods vehicle that has a minimum laden weight of more than 7,500 kilograms (approximately 73.6 kN) and goods vehicle that is drawing a trailer or semi-trailer has a speed limit of only 80 km/h. In accordance to the set of equivalent lorries defined in Fatigue Load Model 4 (FLM4), the minimum weight equates to 200kN (refer to Figure 3.9), satisfying condition (ii) of the National Speed Limit. In addition to 2 sets of rigid lorries, an additional 3 sets consists of lorries that draw trailers or semi-trailers, satisfying condition (iii) of the National Speed Limit. Therefore, the speed limit used in this analysis is 80km/hr.

3.4.5   Traffic Alone

Fatigue Load Model 4 comprises of 5 sets of equivalent lorries. As mentioned previously, Notional Lane 1 and Notional Lane 2 shall be used as a basis of stress cycle counting to result in the greatest theoretical fatigue damage. A single lorry is assumed to be travelling along the entire span of the bridge for each set. Each consecutive set of lorry will proceed in similar fashion after the rear axle of previous sets of lorries completely clears the modelled bridge span. In order to measure the exact duration for each lorry to clear the bridge, the speed of the vehicles have been fixed at a constant vale based on the speed limits shown in Figure 3.11. The loading configuration for Single Lorry is shown in Table 3.2.

Table 3.2: Traffic Loading Pattern for Single Lorry

Vehicle	Starting Point, m	Start Time, s	Velocity, ms^{-1}	Load Duration, s
FLM4 – A	0	0	22.2222	
FLM4 – B	0	22.0111	22.2222	
FLM4 – C	0	44.0222	22.2222	150
FLM4 – D	0	66.0333	22.2222	
FLM4 – E	0	88.0444	22.2222	

3.4.6   Traffic in Convoy

Similarly, traffic in a convoy configuration will employ the exact procedure of utilizing two traffic lanes for traffic placement to simulate critical fatigue damage for the structural component in consideration. The only differentiating factor would be the positions of the lorries whilst travelling across the bridge. With regards to BS EN 1991-2:2003, traffic in convoy requires a spacing of 40 meters, centre of rearmost axle of the front vehicle to centre of the foremost axle of the vehicle directly behind the

lorry as shown in Figure 3.12. In contrast to "traffic alone", the lorries will travel continuously across the entire length of the bridge at constant spacing and velocity.
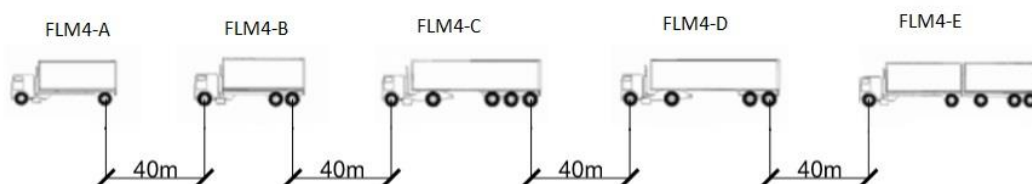
Figure 3.12: Modified traffic arrangement in convoy at a 40m equidistant spacing. Modified after NA to BS EN 1991-2:2003

Table 3.3: Traffic Loading Pattern for Lorry in Convoy

Vehicle	Starting Point, m	Start Time, s	Velocity, ms^{-1}	Load Duration, s
FLM4 – A	0	0	22.2222	
FLM4 – B	0	2.0925	22.2222	
FLM4 – C	0	4.2525	22.2222	45
FLM4 – D	0	6.9975	22.2222	
FLM4 – E	0	10.2465	22.2222	

3.5   Ground Motion Records

Ground motion data will be applied in the form of Time-History Records. In order to make up for the lack of sufficient data of local earthquake events, earthquake time functions records were obtained via the Pacific Earthquake Engineering Research Center (PEER) of the University of California. The main source of seismic data was obtained with regards to Shallow Crustal Earthquakes in Active Tectonic Regimes. Within NGA-West2's ground motion database, large sets of ground motion records

across the globe in terms of shallow crustal quakes that features meta-data with different distance measured, site characteristics, earthquake source data and magnitude to name a few.

3.5.1 Ground Motion Data Selection

The selection of appropriate seismic data for the study places an emphasis on filtering through a set range of characteristics that possess similarities with the location of the Penang Second Bridge in terms of the approximate distance from the epicentre, fault types, moment magnitude of quake event and maximum peak ground acceleration of the monitoring stations. With regards to the tectonic conditions surrounding the site of interest, most of the quakes often occur along the Sumatran Fault that is located on the Eurasian Tectonic Plate as mentioned in Section 2.7. Based on the earthquake event mapping from the USGS Earthquake Catalogue as shown in Figure 3.13, a large majority of seismic events with a moment magnitude of at least $M_w=5.0$ that occur around the site has a distance of not less than 250km from the site of interest. Therefore, the earthquake occurrences surrounding the site of interest are categorized under far-field earthquakes (epicentre distance greater than 20km). In order to determine the type of geological properties under the monitoring stations, monitoring stations of pre-selected sets of data were cross-checked with data sets from the Center for Engineering Strong Motion Data (CESMD) which includes additional information on the geological make-up that a particular station situates on.
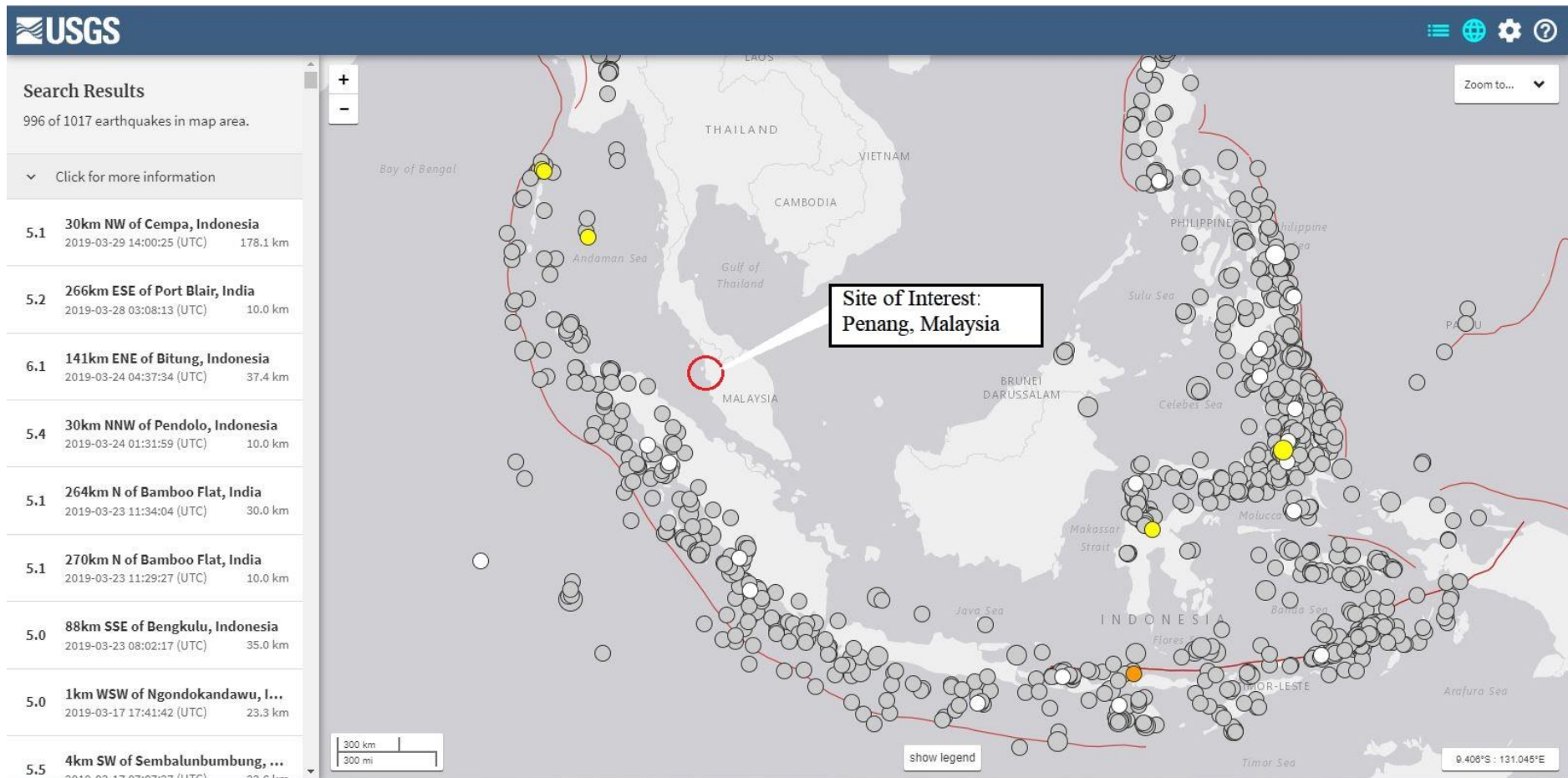
Figure 3.13: Earthquake Event Map for Earthquakes of $M_w > 5.0$. (United States Geological Survey, 2019)

A study conducted by Man *et al.* (2018) has stated that the seismic design of the bridge is divided into to design evaluation levels. Level 1 (Design earthquake) features a return period of 475 years with an expected peak ground acceleration (PGA) of 0.072g; whereas the Level 2 (Maximum credible earthquake) has a return period of 2500 years with a PGA of 0.109g (Man *et al.* 2018). An analysis on the tsunami generation from the 2004 Sumatra-Andaman Earthquake by Eric Geist from the United States Geological Survey (USGS) provided an insight on the tectonic setting and seismological characteristics of the earthquake. It has been determined that the Sumatra subduction zone is characterized by decoupled faulting that results in nearly pure reverse thrust faulting along the intraplate thrust and strike-slip faults in the overriding plate, notably along the Great Sumatran Fault. By overlaying Figure 3.13 and Figure 3.14, a large majority of earthquake events are a result of strike-slip faults in comparison to the lower events along the thrust faults. Therefore, a combination of thrust/reverse faults and strike-slip faults need to be considered for the seismograph stations upon selecting the suitable seismic data (Geist, E–USGS, 2008).
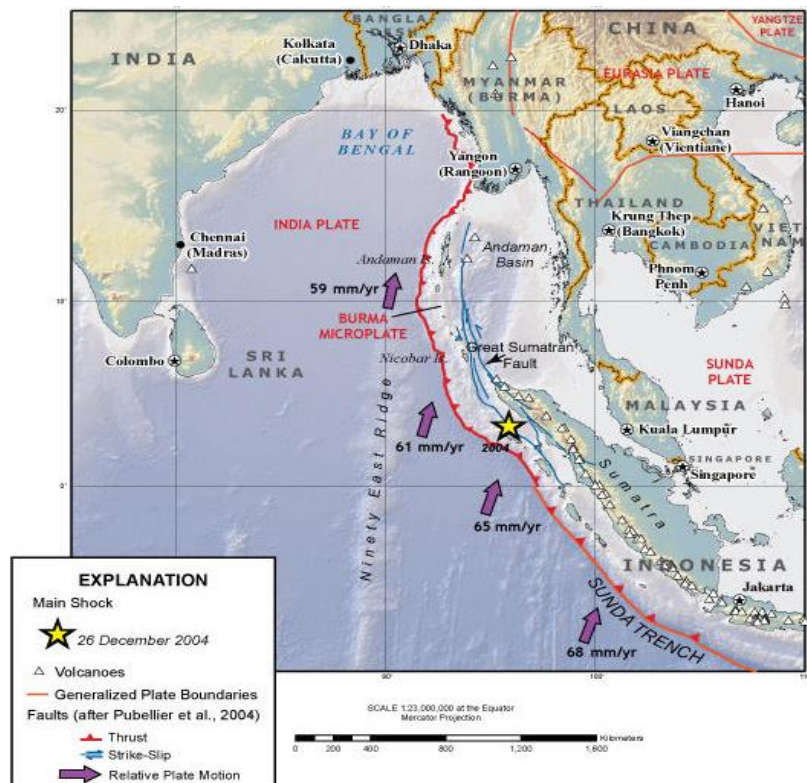
Figure 3.14: Tectonic base map of the Sumatra Subduction Zone showing major faults. (Geist, E–USGS, 2008)

In order to conduct a comprehensive simulation of seismic events and also mimic the worst case scenario, the obtained records will be scaled to match two forms of PGA: Level 2 (Maximum credible earthquake) PGA of 0.109g corresponding to the 2500 years return period that was used to design the bridge, and a PGA of 0.04g that corresponds to the probabilistic seismic hazard maps with 10% PE in a 50-year (RP475-year) condition for Peninsular Malaysia which allows the condition to closely depict the estimated ground acceleration in terms of the seismic hazard map of Malaysia for a return period of 475 years.

3.5.2   Ground Motion Data Sets

For the purpose of this study, three sets of time-history records that have been obtained from PEER as shown in Table 3.4 features the 2002 Denali Earthquake Event in Alaska, the 2002 Kocaeli Earthquake Event in Turkey, and the 2003 San Simeon Earthquake Event in California, United States with moment magnitudes of M_w=7.9, M_w=7.51, and M_w=6.52 respectively. Both of which will represent far-field earthquakes that occur along the Sumatra Fault in addition to depicting seismic mechanisms of Reverse + Strike-Slip faults and Reverse Oblique faults.

Table 3.4: Ground motion parameters of far-field ground motions.

No.	Earthquake	Station	Year	Magnitude, M_w	Mechanics	R_{epi} (km)	5-95% Duration (s)	PGA, g	Scale (0.109g)	Scale (0.04g)
1	Denali, Alaska	Anchorage – DOI Off. Of Aircraft	2002	7.9	Strike-slip	272.5	118.5	0.03	3.633	1.333
2	Kocaeli, Turkey	Bornova	2002	7.51	Reverse+ Strike-Slip	315.89	71.9	0.04	2.725	1.000
3	San Simeon, California, USA	Beverly Hills Pac Bell Bsmt	2003	6.52	Reverse Oblique	272.92	154.2	0.02	5.45	2.000

Source: (Ancheta *et al.* – Pacific Earthquake Engineering Research Centre PEER NGA-WEST2 Database, 2019)

3.5.3   Application and Analysis of Ground Motion Records

Similarly to traffic loadings, seismic events will be simulated in a 2-Dimensional and 3-Dimensional space. Ground motion acceleration data from time-history records of seismic activities are often represented by 3 sets of data that represent the horizontal (U1 and U2 for x-axis and y-axis) and vertical ground motions (U3 for z-axis). In order to identify the nominal stress of stay cables due to seismic ground motions, the study will consider the horizontal and vertical components of ground motions listed in Table 3.4. For the 2-Dimensional analysis, horizontal components (H) about the y-axis are applied in accordance with the orientation of the bridge's longitudinal section with the direction of ground motion data. Proceeding to the 3-Dimensional analysis, both horizontal and vertical ground motions (H+V) are applied to the model synchronously with similar consideration for the bridge's orientation as per the 2D analysis. As shown in Figure 3.15, the applied ground motions will result in the propagation of seismic waves from the LHS side span towards the RHS side span.
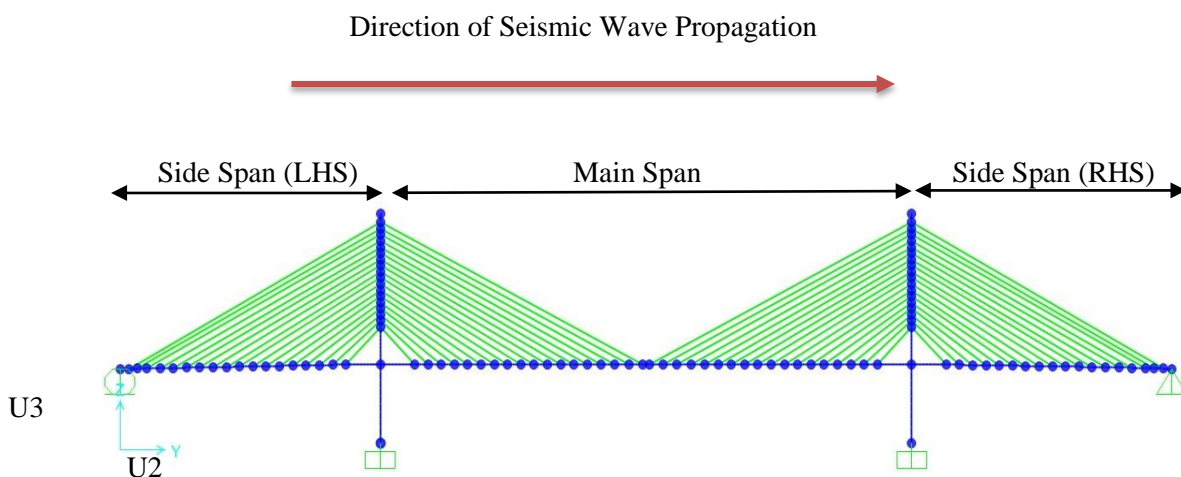
Figure 3.15: Direction of seismic wave propagation along the length of the cable-stayed bridge

For this study, linear direct integration methods have been adopted for the analysis as a substitute for non-linear analysis to determine the stress range of the stay cables. Based on a study conducted by Shreshta & Tuladhar (2012), it has been proved that the use of linear time-history analysis is viable for the determination of the seismic response of cable-stayed bridge (Shreshta B. & Tuladhar R., 2012). Comparisons that were been made between a linear time-history analysis and non-linear direct integration time-history analysis concluded that linear

modal time-history analysis has the capability of producing accurate results for cable tensile forces with marginal differences of 1 to 8%. With the above justifications, the time-history function will be analysed with regards to linear direct integration methods according to the selected data sets. For the study of the influence of seismic activities on the stress range of stay cables, loadings due to dead load combined with the post-tensioning force of cables and seismic loading (DL+PS+EQ) was focused to evaluate the performance.

3.6   Global Analysis

In order to determine the effect of traffic loading and seismic loads on the stress ranges of stay cables, the global analysis of the cable-stayed bridge model has been conducted in terms of its initial equilibrium condition, traffic loading analysis and ground motion loading analysis.

3.6.1   Initial Equilibrium Condition

The initial equilibrium condition of the cable-stayed bridge is the equilibrium condition caused by the presence of the bridge's self-weight and tensile forces in the stay cables. The initial design strain loads are applied on each individual dead load and static analysis with dead loads are conducted. The nominal stresses in the cables will then be compared with the actual data obtained from the bridge specifications to determine if the model has been modelled correctly.

3.6.2   Traffic Loading Analysis

Direct-integration time-history analysis have been applied to determine the effect of Fatigue Load Models on the global response of the bridge model. It is a linear method of dynamic analysis that fully integrates the equilibrium equation of motion as dynamic traffic loading is applied. Time-history analysis allows kinetic equation of dynamic loads of a structure to be solve by analysing the reaction through the structural characteristics in relation to the moving loads at any time (Wang X.Q. & Jin W. C., 2011). With regards to the fatigue load model selected, the vehicles are assumed to move in only one direction with an integration time step of 0.1s with a total loading duration of 150s and 45s for both single lorry and lorry in convoy respectively. In SAP2000, this process involves the direct integration of structural properties at series of time steps in relation to the overall loading duration, allowing results to be presented with regards to a time-series function plot.

Once the analysis have been completed, the nominal stress in each cable were obtained along with the plot function of the moving loads for each stay cable. The initial stress will be obtained with load case with characteristic dead loads only. Then, subsequent stress will be based on single lorry and lorry in convoy for the maximum nominal stress due to traffic loads. The overall maximum stress will be calculated by summing up the maximum stress for single lorry + seismic and convoy lorry + seismic respectively. On the other hand, only the stay cables closest to the critical notional lane selected for application of fatigue load model will be selected as it represents the most critical loading and strain on the stay cables. Moreover, the plot function have been analysed by comparing the peak and troughs of the applied force in cables to determine the maximum stress range generated by the each traffic load configuration.

3.6.3 Ground Motion Loading Analysis

Direct-integration time-history analysis have been applied to determine the effect on ground motions on the global response of the bridge model. It is a linear method of dynamic analysis that fully integrates the equilibrium equation of motion with the applied ground motions on the horizontal and vertical axis. With regards to the ground motions selected, the horizontal acceleration are have been applied in both x and y directions whereas the vertical acceleration have been applied on along the z-axis. The loading duration of each ground motion will be applied separately based on the duration of the seismograph readings. Furthermore, the time step for each ground motion have been set to 0.05s to increase the accuracy of the applied force in the plot function. In SAP2000, this process involves the direct integration of structural properties at series of time steps in relation to the overall loading duration, allowing results to be presented with regards to a time-series function plot. Similarly with Section 3.6.2, the subsequent stress will be based on each individual ground motion for the maximum nominal stress due to far-field seismic excitations. Moreover, the plot function have been analysed by comparing the peak and troughs of the applied force in cables to determine the maximum stress range generated by the each traffic load configuration.

CHAPTER 4

RESULTS AND DISCUSSION

4.1   Introduction

The combination of several load parameters has an impact on the dynamic behaviour of cable-stayed bridges in terms of the induced cable forces and fatigue. Thus, global analysis on the cable-stayed bridge is required to determine its structural performances due to moving traffic and seismic excitation as both loads possess similar cyclic loading characteristics that are crucial to the evaluation of the fatigue life of steel elements. This chapter presents the static analysis with regards to different loading conditions to determine the structural behaviour of The Second Penang Bridge due to moving loads and earthquake ground motions. Therefore, Fatigue Load Model 4 (FLM4) has been applied on all two-spans of the cable stayed bridge to simulate and analyse the effect of cyclic loading on stay cables. In addition, seismic excitations will also be applied in the form of Time-History Records to simulate the effect of seismic loadings on the same elements.

4.2   Static Behaviour of Cable-Stayed Bridge

In order to ensure the structural stability of the cable-stayed bridge model in SAP2000, the initial behaviour of the bridge has to be determined in terms of varied loading conditions. The preliminary behaviour is produced by considering the self-weight of the cable-stayed bridge. Without any stressing force in the cables, the central span and both side spans tend to sag downwards due to the lack of vertical supports by the stay cables. As shown in Figure 4.2 a), it causes the pylons to bend inwards as a result of the significant central load and the lack of stay cable forces that balances the entire span. With the structural self-weight and post tensioning forces applied, the central span of the bridge has the tendency to curve upwards as depicted in Figure 4.1 b) due to the

strain loads that were applied on the cables. The vertical restraints at both ends of the side span prevents the occurrence of vertical translation, in which they significantly reducing the vertical displacement of the furthest cable anchorage. Coupled with the post tensioning force in the outer stay cables, the pylons will deflect outwards as the central span is free to deflect vertically.

Uniform loads that are applied on the central span as shown in Figure 4.1 a) will be supported by the internal stays and transferred to the pylon. This will cause the main span to deflect downwards. Thus, resulting in backstays to withstand tensile force as a means of balancing out both ends of the pylons. As stated previously, the restrained vertical translation of the back stays will emit a pulling action to prevent the main span from sagging downwards. Hence, it resulted in the higher tensile forces in the cables. The verification of the bridge model through this method will allow further stress analysis to proceed for this study.

a) Uniform Load on Central Span

b) Uniform Load on Side Span
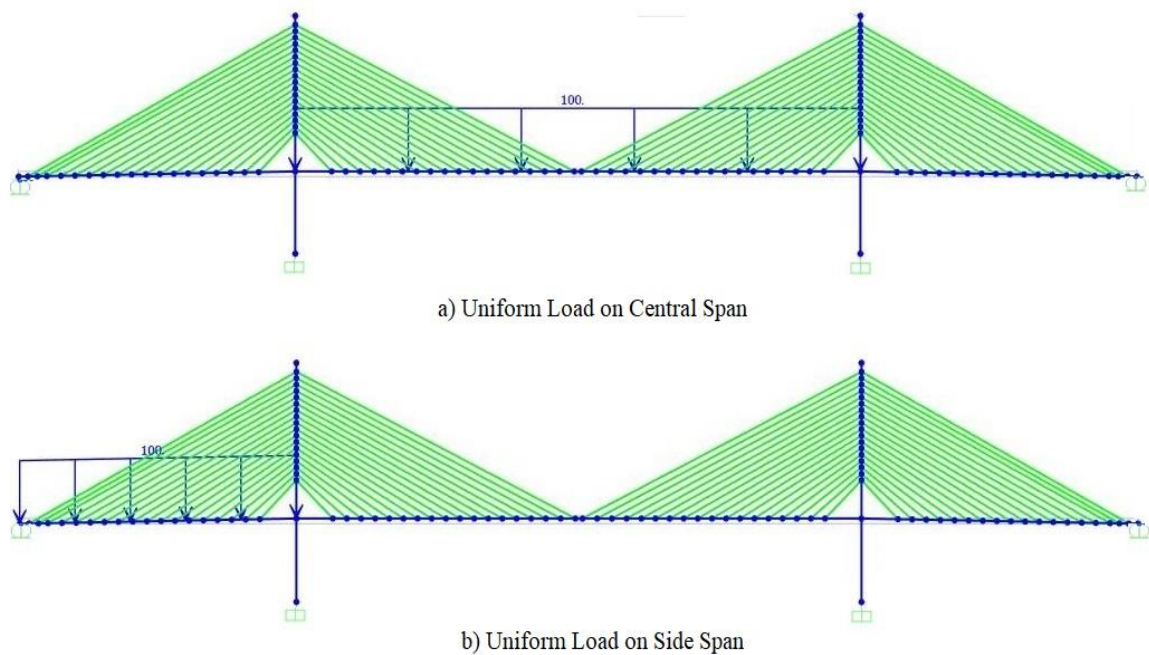
Figure 4.1: Live load configuration with 100kN/m was added to the permanent self-weight of the cable-stayed bridge

a) Dead Load Only

b) Dead Load + Post-Tension

c) Dead Load + Post-Tension + Uniform Load on Central Span

d) Dead Load + Post-Tension + Uniform Load on Side Span
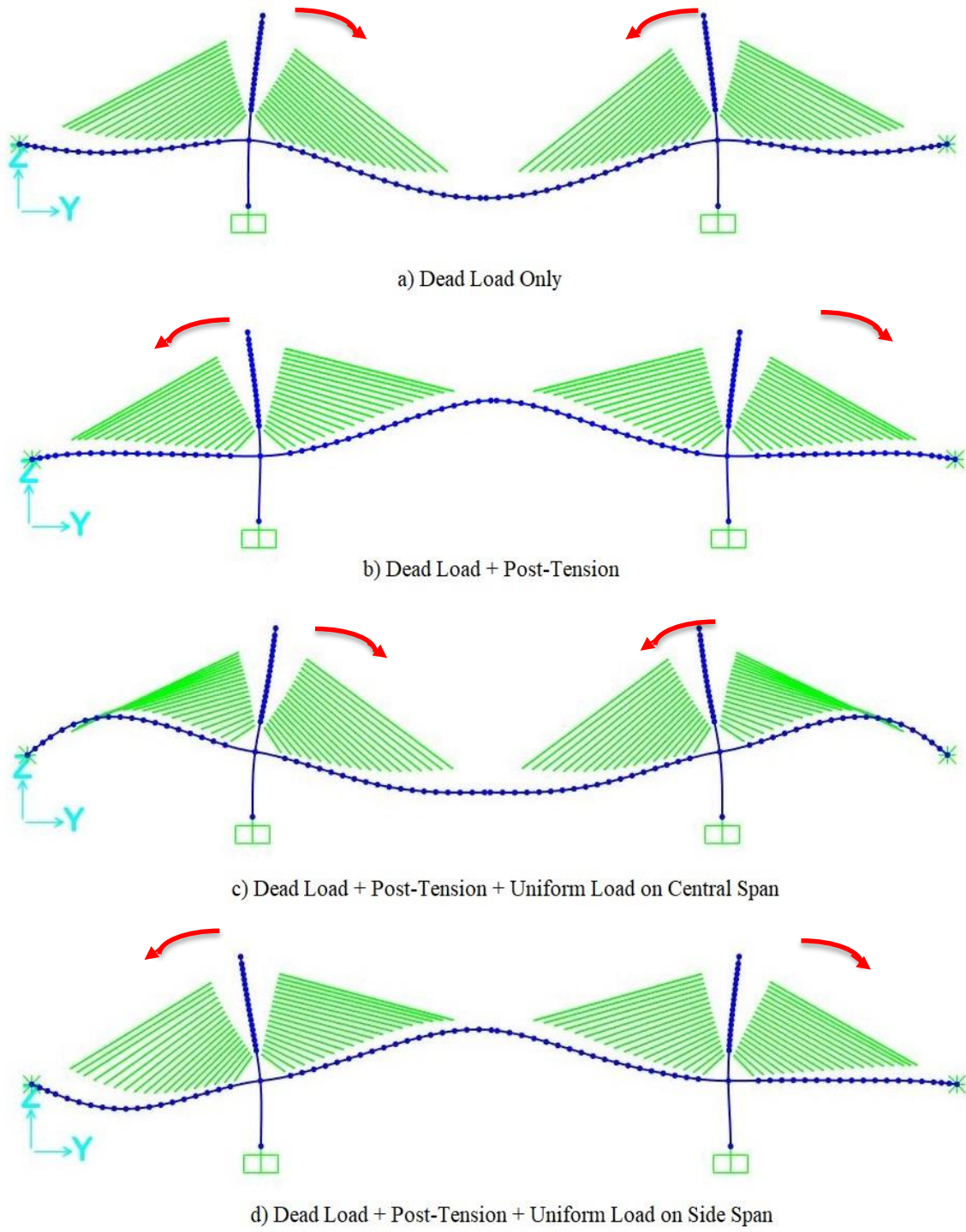
Figure 4.2: Deformed shape of cable-stayed bridge due to different loading configurations

4.2.1 Baseline Stay Cable Forces and Stress Range

Based on the initial analysis from SAP 2000, the different baseline stresses of each stay cable has been obtained as shown in Figure 4.3. The fourth stay cable on both side spans (LS04 and RS04, refer to) presents the largest initial stress of 638.69N/mm² whereas the fifteenth stay cable (LM15 and RM15) on the main span is subjected to the smallest initial stress of 492.553N/mm². In this study, the baseline stress of the cable-stayed bridge is indicated with the load case that only includes the self-weight of structural elements and the strain forces in stay cables (DL+PS) is considered. Based on Figure 4.3, a fluctuating pattern can be seen on the initial stress throughout the side spans and main span. For the side span, the cable closest to the pylons (LS01 and RS01) has similar initial stresses of 632.82N/mm². As the horizontal distance between the cable anchorage and pylons increases, the stresses in the cables that follows tend to fluctuate between high and low points. On the main span, a decreasing trend of the cable stresses with greater consistency can be seen. Starting from initial stresses of 561.94 N/mm² for the cables closest to the pylons (LM01 and RM01), the cable stresses shows a steep increment to 622.89 N/mm² on cables (LM04 and RM04). Moving further away from the pylons towards the mid-span, a gradual decreases in nominal stress accompanied by minor fluctuations to 493.021 N/mm² at LM18 and RM18 can be observed.
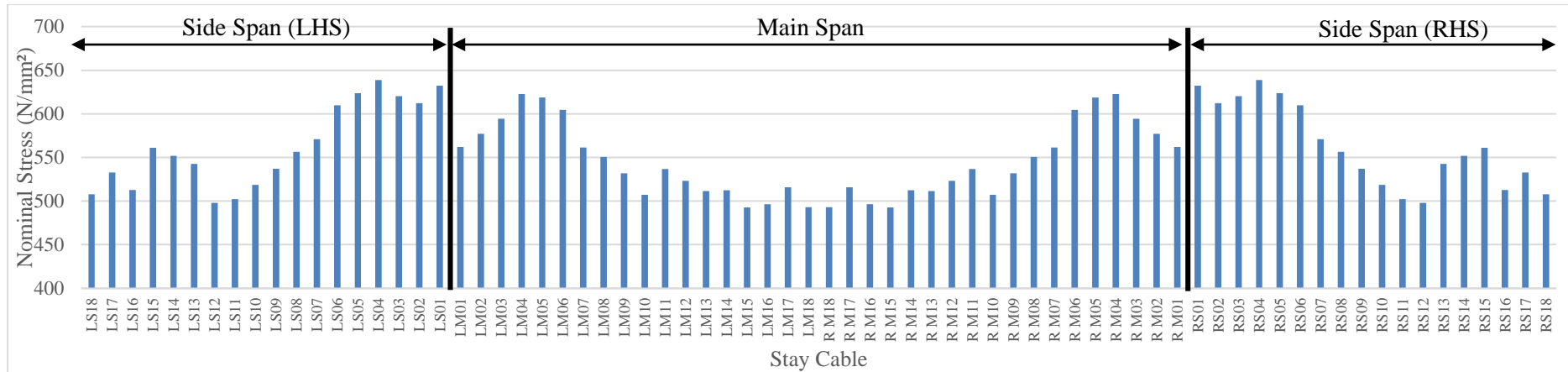
Figure 4.3: Initial nominal stress in stay cables due to structural self-weight of cable-stayed bridge and post-tensioning force
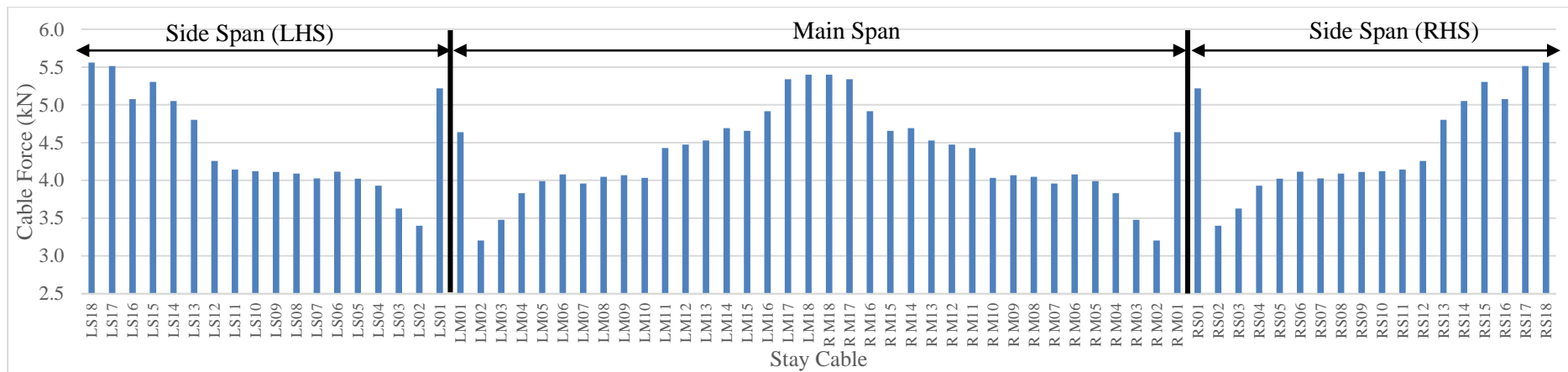
Figure 4.4: Initial tensile force in stay cables due to structural self-weight of cable-stayed bridge and post-tensioning force

69
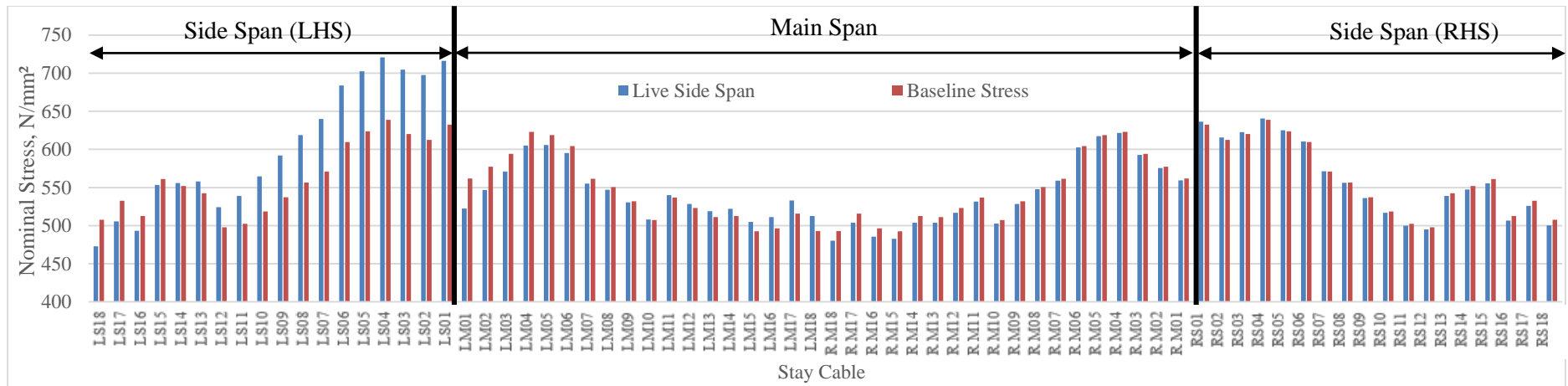
Figure 4.5: Comparison of nominal stress in stay cables due to uniform load on side span with baseline stress
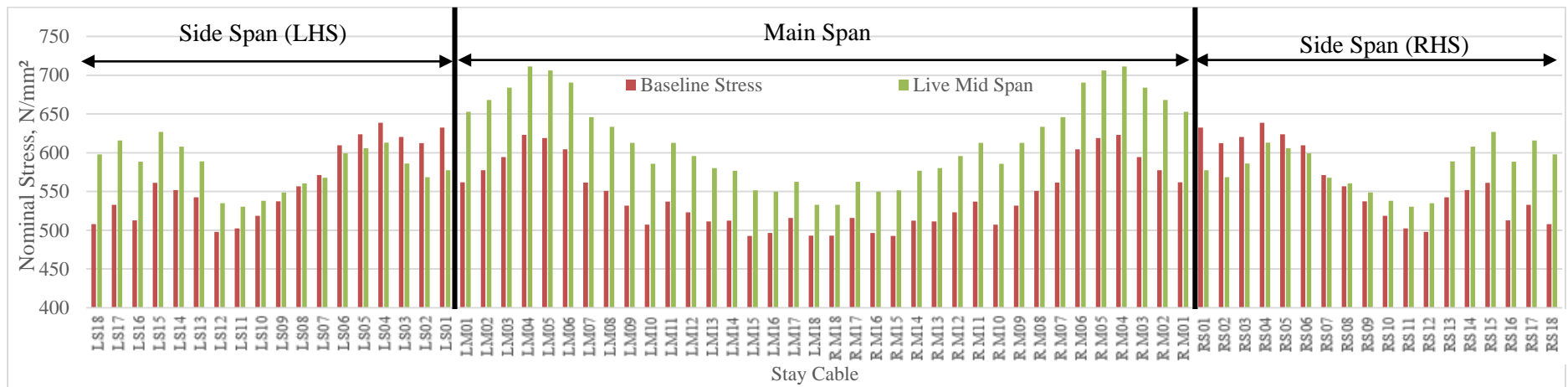
Figure 4.6: Comparison of nominal stress in stay cables due to uniform load on main span with baseline stress

70

This form of stress pattern is caused by the variation of cable strands along the length of the bridge. Stay cable no. 1 (LS01, LM01, RM01 and RS01) consists of 55 number of strands; whereas stay cables no. 2 through no. 18 (LS02 to LS18, LM02 to LM18, RM02 to RM18 and RS02 to RS18) is arranged with varying numbers of strand that increases gradually from 37 nos. to 73 nos. (Man *et al.*, 2018). Therefore, the different allocation of cable strands across a single cable plane resulted in stay cables with smaller cross-sectional areas closer to the pylons and larger areas for stay cables placed further away from the pylon. This ties in with the stress pattern mentioned above as the amount of stress is inversely proportional to the cross-sectional area for a given force. Even though cables no.18 (LS18, LM18, RM18, & RL18) for the side span and main span does not have the largest nominal stress, Figure 4.4 shows that stay cable no. 18 on the mid span (LM18 & RM18) and side span (LS18 & RS18) are subjected to the maximum amount of tensile force of 5398.58kN and 5559.238kN respectively. This is a result of the cables being required to sustain larger dead loads due to the increase in span length from the pylons.

As depicted in Figure 4.1, different load configurations have been placed on the bridge model to depict the action of moving traffic loads and determine the resulting stress range for the affected cables. Variations of nominal stress due to the respective applied loads are shown in Figure 4.5 and Figure 4.6 along with a comparison with the initial nominal stress in stay cables. With the uniform load applied on the side spans, stays closer to the pylons experienced a positive increase in tensile stress, specifically stay no. 3 (LS03) that produced the largest stress range of 85.152N/mm² as shown in Figure 4.5. On the other hand, stays no.15 through 18 (LS15 – LS18) is subjected to a reduction in nominal stress. This was caused by the concentration of force in the middle of the side span that resulted in the side span deflecting downwards (refer Figure 4.2 d)). The large mid-span deformation increases the strain on the cables close to the point of load concentration and induces larger stresses on the specific cables. Simultaneously, the exaggerated concentrated action pulls the pylons outwards and increases the amount of slack on the outer cables due to the small deformation at the anchorages nearer to the end span, and consequently reduces their nominal stress. Further observations on the behaviour and stress variation due to this load configuration suggests that the highly impacted areas are local as large changes are only found on stay cables that being subjected to the uniform load in contrast to the remaining stays on the main span and right side span (RHS).

On the other hand, load configuration with uniform load along the main span generated stress ranges on a wider spectrum of stay cables. From the comparison shown in Figure 4.6, a larger number of cables are affected due to the load placement. Due to the larger concentration of stress on the main span, stay cables anchored on both of the side spans experienced large tensile stress in order to support the additional loads and prevent large mid-span sagging. By referring to both Figure 4.6 and Figure 4.2 c), it shows that the back stays (LM18 & RM18) experienced significant effect on their nominal stress with similar stress range of 90.065 N/mm². As previously mentioned for the stress behaviour due to uniform loads on the side span, the amount of stress is relative to the higher vertical restraint on the back stay's anchorage that allows the bridge to balance out the forces on both sides of the main span. As the pylons have the tendency to bend inwards, the back stays plays a role in counteracting the movement and were required to sustain large amounts of internal forces. The stay cables along the main span were subjected to large increments in their nominal stress which results in the maximum stress range of 91.025N/mm² on stay no. 1 (RM01) and an average variation of 74.412 N/mm² throughout the central stays. Due to the behaviour of the pylons, reduction of nominal stress can be seen on cables no.1 through 7 on the side spans (LM01 – LM07 and RM01 – RM07) because of the effects of cable sag. From the application of both load cases, it is apparent that the presence of loads on the main span is capable of affecting a wider range of stay cables and better depicts the effect of moving traffic load.

4.3   Stay Cable Behaviour Due To Moving Traffic

In order to produce the effects of traffic loads on the variation of stress range on stay cables, Fatigue Load Model 4 (FLM4) has been applied on the cable-stayed bridge model to represent the loads caused by moving traffic. To simulate this type of loading, two load combinations have been applied in this study: self-weight of structural elements, post-tensioning force and single lorry traffic loads (DL+PS+SL) that represent ultimate loads caused by single traffic; self-weight of structural elements, post-tensioning force and convoy lorry traffic loads (DL+PS+CL) that represent ultimate loads caused by convoy traffic. As mentioned in Chapter 3, FLM 4 is the preferred load model due to its capability to simulate the same amount of fatigue damage that is equivalent to the typical traffic condition on European roads. For this study, both single and convoy lorry configuration traverses along a similar path that is located on the slow lane of the bridge with the same velocity to reduce the complexity of the data collection.

4.3.1 Cable Stresses Due To Single Lorry Configuration

Upon completion of the time-history analysis in SAP 2000, results have shown that the application of traffic loads in single lorry configuration has produced minor increments in the maximum nominal stress across all stay cables of the cable-stayed bridge as shown in Figure 4.8. The data shown is obtained by selecting the maximum stress generated for each stay cable when each lorry completely crosses the entire length of the cable-stayed bridge (total of 475m). Based on Figure 4.7, a uniform increase in cable stress along the entire span of the bridge can be seen without any form of irregularities. The maximum nominal stress generated by load combination (DL+PS+SL) is 646.331N/mm² on stay cable RS04. By comparing the difference in maximum stress generated, the stay cables experienced an average stress increment of 5.712N/mm². On the other hand, the stay cable that experienced the largest stress increment was found to be stay cable LS02 with 8.313N/mm², compared to that of RS04 which produced slightly lower increments of 7.641N/mm² and 8.084% reduction in the maximum stress produced. The critical stay cables were then selected based on the 85th percentile of the difference between the maximum stay cable stress and the baseline stress. It has been determined that critical stay cables LM01, LM02, LM03, RS01, RS02, RS03, RM04, RM05, RM06, RM07, and RS18 fall within the 85th percentile with respective stress increments of 9.424 N/mm², 9.238 N/mm², 8.937 N/mm², 9.213 N/mm², 9.153 N/mm², 8.936 N/mm², 8.7 N/mm², 8.779 N/mm², 8.799 N/mm², 8.756 N/mm², and 8.72N/mm².

Although the critical stays have been determined via the maximum nominal stress, fatigue assessment requires the use of stress range under the cumulative damage method as per BS EN 1993-1-9:2005 where the maximum stress range generated in each stay cable due to the entire load duration of moving traffic as depicted in Figure 4.8. It has been determined that cables that were subjected to very large stress ranges are primarily concentrated around both pylons whereas the smallest stress range is generated in stay cables that are located around the middle of the main span (LM15 – LM13) and both side spans (LS13 & RS13). Furthermore, observation shows that a similar trend on the variation of maximum generated stress range in stay cables can be seen on the main and side spans. In terms of the variation on the main span, the maximum stress range tends to reduce gradually with increments on the horizontal distance between stay cables until the central region of the span. Based on data obtained, it has been observed that stay cable RM16 generated the smallest peak stress range within the main span with only 4.2289 N/mm².
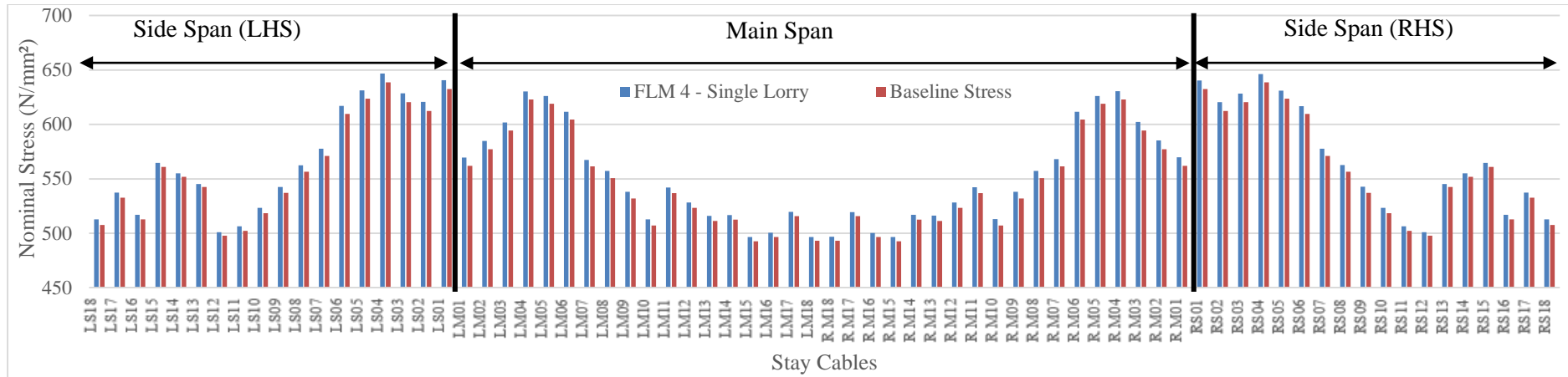
Figure 4.7: Comparison of maximum nominal stress in stay cables due to Single Lorry traffic loads with baseline stress of cable-stayed bridge
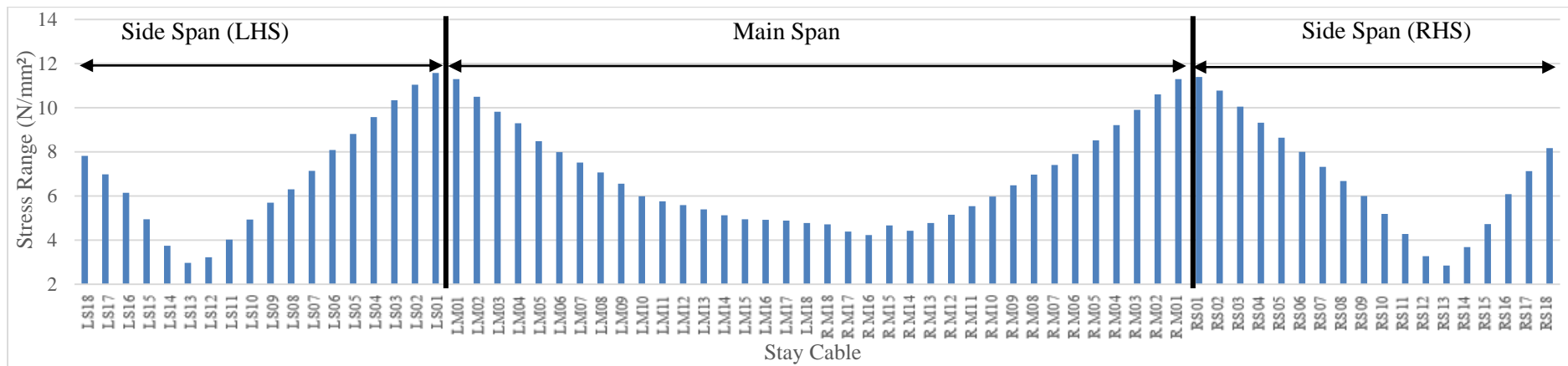
Figure 4.8: Maximum generated stress range of all stay cables due to Single Lorry traffic load configuration

SAP2000   Filename: Penang Second Bridge   Case: Single Lorry   Time 48.9

FLM4-C

Side Span (LHS)   Main Span   Side Span (LHS)
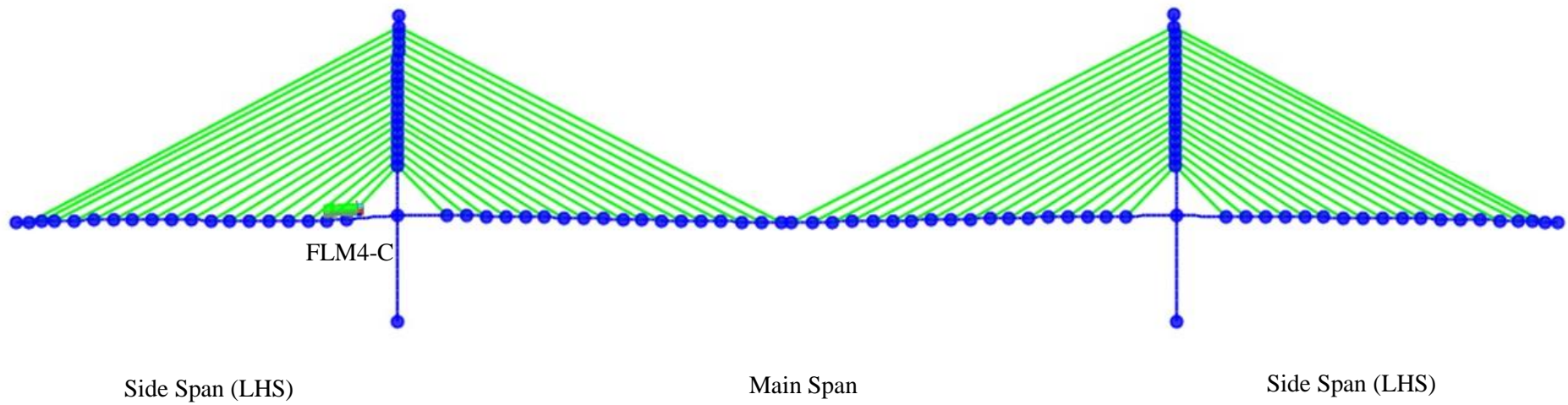
Figure 4.9: Location of equivalent lorry (FLM4-C) that resulted in maximum stress range in stay cable LS01 at T=48.2s

Diving further in to the load-history plot function of single lorry traffic load application, 5 distinct loading timeframes can be easily identified based on the peaks generated by the moving load. The peak applied force of 65.862 kN was generated in stay cable no. 1 (LS01) at a time of 48.2 seconds. By comparing the peaks in Figure 4.10 and the travel time of each equivalent lorry to cross the entire span, it has been found that each peak is caused by the coincidence of the lorry's centroid with the centreline of the cable anchorage as shown in Figure 4.9. When the lorry moves closer to the stay anchorage, a steep increase of the applied force is present, whereas the applied force reduces at a similar rate once the lorry passes through the anchorage. This pattern is a result of traffic load that is supported by the subsequent stays as the lorry moves along the entire span of the bridge, leaving the current stay cable of interest unloaded. Based on Figure 4.11, it can be seen that the placement of traffic loads will affect the applied force on all stay cables on the bridge. When cable LS01 is experiencing the most amount of applied force at T=48.2 seconds, stay cables LS02 through LS12 is in taut condition as they experience positive tension force as a result of load distribution and positive deflection in the direction of gravity. From LS13 through LS18, the cables are under the sagging condition due to the presence of negative applied forces as mentioned previously. On the other hand, stay cables on the main span and side span (RHS) does not experience a drastic variation in applied force.

When the full brunt of the load is being subjected towards the stay cable, the resulting tensile force keeps the stay cable in taut condition. Once the lorry is far enough that the loads are no longer distributed to the stay cable of interest, it experiences negative applied force as the cable becomes slack. This behaviour ties in with the previous observation seen in Figure 4.1, Figure 4.3 and Figure 4.4 where the dynamic effects of deck and pylon deformation due to different location of applied loads results in cables experiencing different amounts of sag and tension. Once the cable-stayed bridge is absent of any traffic load around the 108.9 second mark, the stay cable continues to experience variations of applied force which fluctuates under 5kN for both positive and negative forces as a result of residual vibrations left by the movement of traffic loads. Without the use of dampers on the actual bridge, the damping of vibrations relies mainly on the natural damping properties of the bridge's structural components.
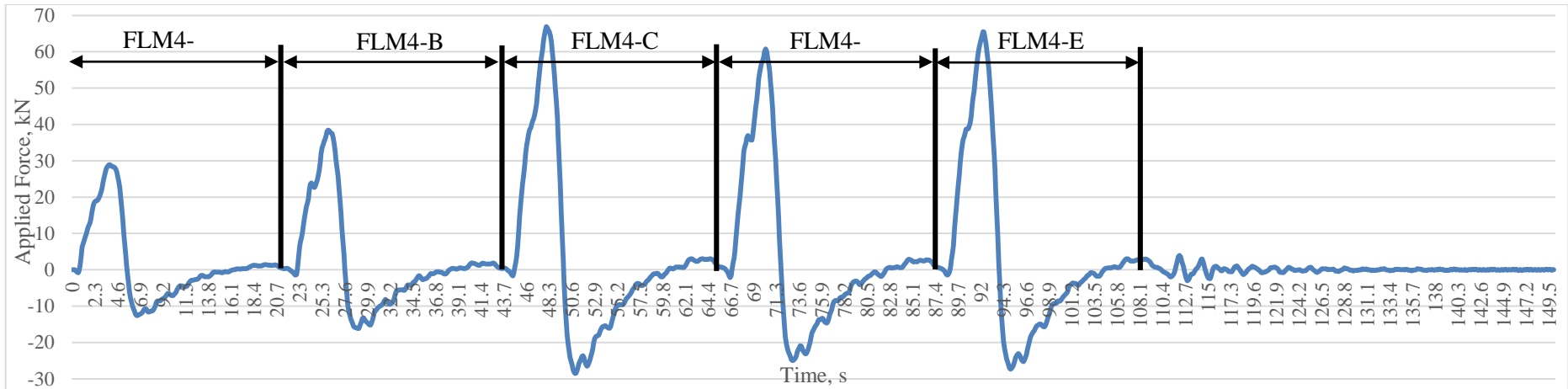
Figure 4.10: Time-history plot function of applied force on stay cable LS01 due to Single Lorry load configuration
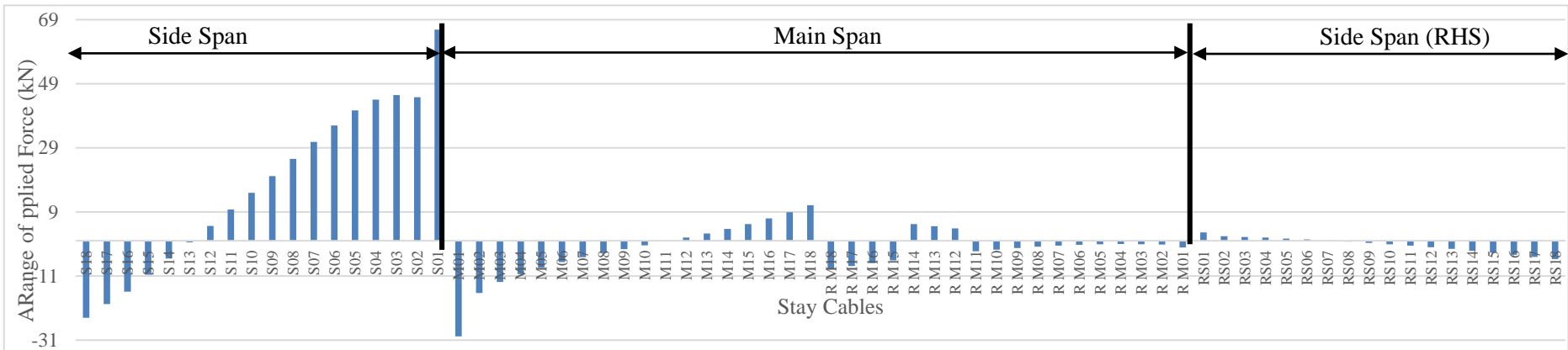
Figure 4.11: Variation of applied forces for all stay cables when cable LS01 is subjected to the maximum applied force.

77

4.3.2   Cable Stresses Due To Convoy Lorry Configuration

Similarly with the Single Lorry load combination (DL+PS+SL), the maximum nominal stress of all stay cables due to Convoy Lorry load combination (DL+PS+CL) have been determined as shown in Figure 4.12. Based on the obtained results, all stay cables were subjected to maximum nominal stresses that are higher than that produced by a Singly Lorry load combination.   The maximum nominal stress generated by the load combination (DL+PS+CL) is 647.075N/mm² on stay cable LS04 which is 8.385N/mm² higher than the baseline stress of the stay cable, whereas on average, the stress increments throughout all stay cables is 7.304N/mm².   From on initial observations, the higher load produced by lorry arranged in convoy configuration directly resulted in higher stress increments in the cables in comparison to that produced by single lorry configuration of 5.172N/mm².   Therefore, it is equivalent to a difference of 2.132N.mm² or 41.22% increment.

Likewise with the situation observed for (DL+PS+SL), the stay cable with the maximum nominal stress does not necessarily relate to the largest stress increment. In this case, stay cable LM01 experienced the highest stress increment of 9.424N/mm² but with maximum nominal stress of only 571.364N/mm². By assessing the maximum stress increments of stay cables that fall within the top 85th percentile, a large majority of stay cables that experienced higher stress increments portray similar positions as in the Single Lorry configuration that is, being concentrated around the pylons with an additional stay cable located near the side span supports. It has been determined that critical stay cables LM01, LM02, LM03, RS01, RS02, RS03, RM04, RM05, RM06, RM07, and RS18 fall within the 85th percentile with respective stress increments of 9.424 N/mm², 9.238 N/mm², 8.937 N/mm², 9.213 N/mm², 9.153 N/mm², 8.936 N/mm², 8.7 N/mm², 8.779 N/mm², 8.799 N/mm², 8.756 N/mm², and 8.72N/mm².
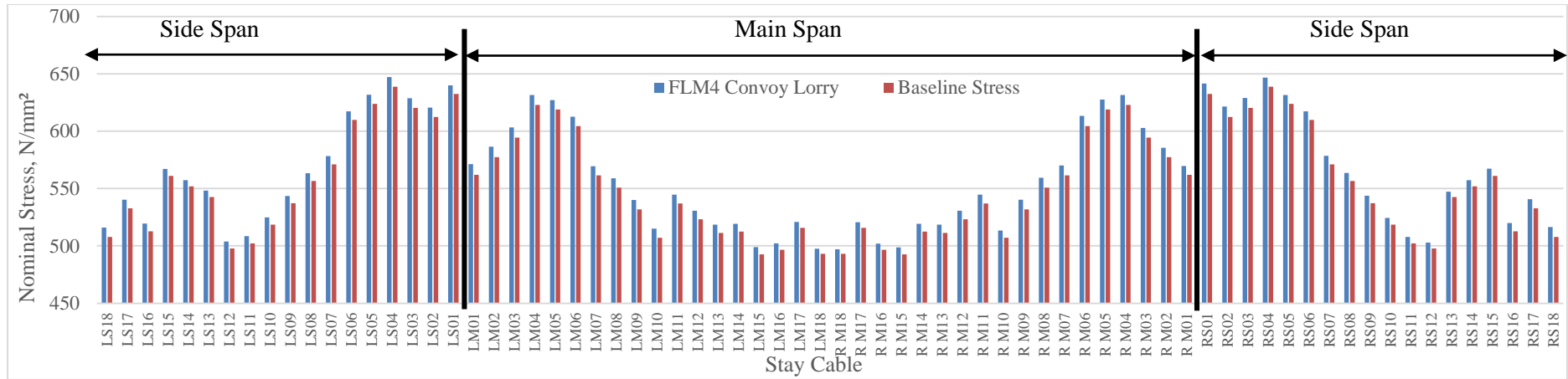
Figure 4.12: Comparison of maximum nominal stress in stay cables due to Convoy Lorry traffic loads with baseline stress of cable-stayed bridge
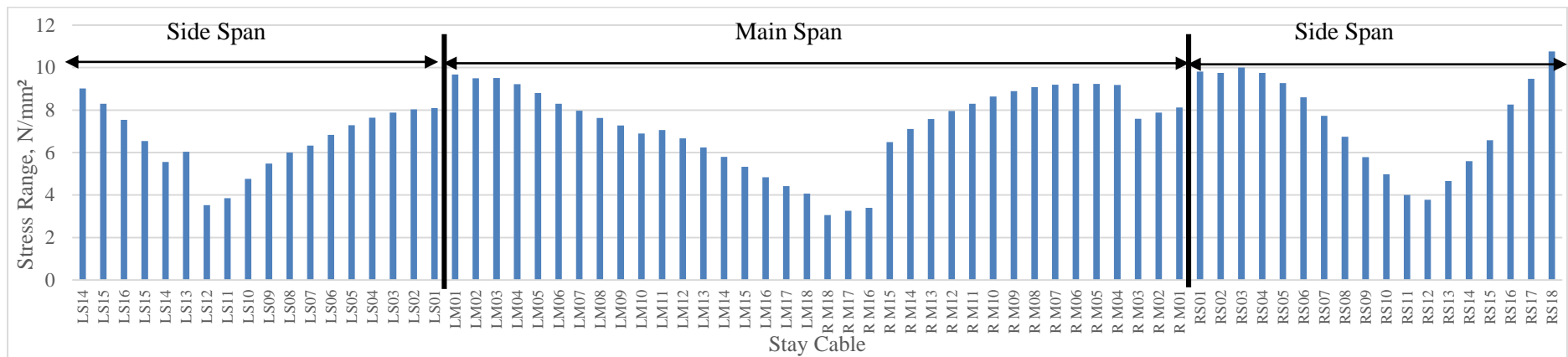
Figure 4.13: Maximum generated stress range of all stay cables due to Convoy Lorry traffic load configuration

In terms of the maximum stress range generated in each stay cable during the entire loading duration, Figure 4.13 shows that a significantly higher overall stress range has been generated throughout all the stay cables in comparison to the stress range due to Single Lorry configuration. Similarly, the cables located in the middle of both side spans and main span has a reduced maximum stress range with cables closer to the pylons generating a higher value. Stay cables on the (RHS) side span were subjected to higher overall peak stress range when compared to the (LHS) side span. For each side span, stay cables LS18 and RS18 experienced the highest maximum stress range of 9.014N/mm² and 10.760N/mm² respectively, with the minimum being LS12 and RS12, both with 3.524N/mm² and 3.772N/mm² respectively. On average, the stress range experienced by stay cables on the right side span is 0.934N/mm² higher than those on the left side span. In terms of the main span, the maximum stress range experienced by stay cables LM01 through LM03 and RM07 through RM04 falls in the higher spectrum compared to the remaining stay cables on the main span.

Stay cable LM01 had the highest maximum stress range of 9.668N/mm² whereas stay cable RM18 was subjected to the lowest maximum stress range of 3.063N/mm². Furthermore, Figure 4.13 reflects a gradual decrease in the maximum stress range of each stay cable connected to the left pylon on the main span. In contrast, the variation of the maximum stress range of stay cables connected to the right pylon has a completely different trend. Based on Figure 4.13, the maximum stress ranges on stay cable RM15 experienced a drastic jump from 3.394N/mm² of stay cable RM16 to 6.485N/mm². From stay cable RM15, the maximum stress range proceeds to increase at a gradual rate until it reaches a plateau at stay cable RM04, followed by a sharp drop to stay cable RM03. Overall, there isn't a distinctively large maximum stress range in the stay cables with the exception for stay cable LS01 and RS18 on the side spans. As previously speculated with the maximum nominal stress for this load combination, stay cables close to the pylons have a higher maximum stress range compared to the rest, specifically from stay cables LM01 to LM04 and RS01 to RS04.

As depicted in Figure 4.15, the load-history plot function of convoy lorry traffic load application on stay cable RS18 shows a fluctuation in applied force of ±20kN from T=0s to T=9s. Then, it increases with time at a steep gradient to a peak applied force of 95.448kN at T=16.2s and proceeds to drop at a similar rate until T=25.6s where the applied force is approximately -22.37kN. Further increments in loading time reveals large fluctuations of applied force between -40kN and 10kN until the convoy completely crosses the end of the right side span supports at T=30.7s. Comparison of the peak applied force with the travel time of the convoy lorry shows that none of the lorries is in-line with the anchorage point of stay cable RS18 as depicted in Figure 4.14.

The resulting behaviour of the cable-stayed bridge closely depicts the behaviour produced by placing uniform loads on the main span of the cable-stayed bridge. As shown in Figure 4.12 the back stays of both side spans are highly affected by load placements at the main span that results in the cables to become taut due to the vertical deformation at the main span. Due the position of the anchorage of stay cable RS18 that is close to the side span supports, placement of loads close to the stay anchorage will result in the reduction of cable stresses as shown in Figure 4.3. As the convoy moves closer to the stay cable, the effect of loading on the positive applied force of the back stays significantly reduces. By referring to Figure 4.15 and Figure 4.16, when stay cable RS18 is experiencing the most amount of applied force at T= 16.2s, all of the stay cables on the main span were subjected to a high tensile force that causes them to become taut. On both of the side spans, stay cables S01 through S07 were subjected to negative applied force as they grow slack due to the portion of the side span bending upwards. From stay cable S08 onwards until S18, a gradual increase in tensile force is observed with the outer-most stay cables being critically affected by the loads on the main span, peaking at 95.448kN on RS18 and 89.088kN on LS18. Once the cable-stayed bridge is absent of any traffic load around the 30.7 second mark, the stay cable continues to experience fluctuations of applied force within ±5kN at a less vigorous rate compared to that of Single Lorry configuration as a result of residual vibrations left by the movement of traffic loads.
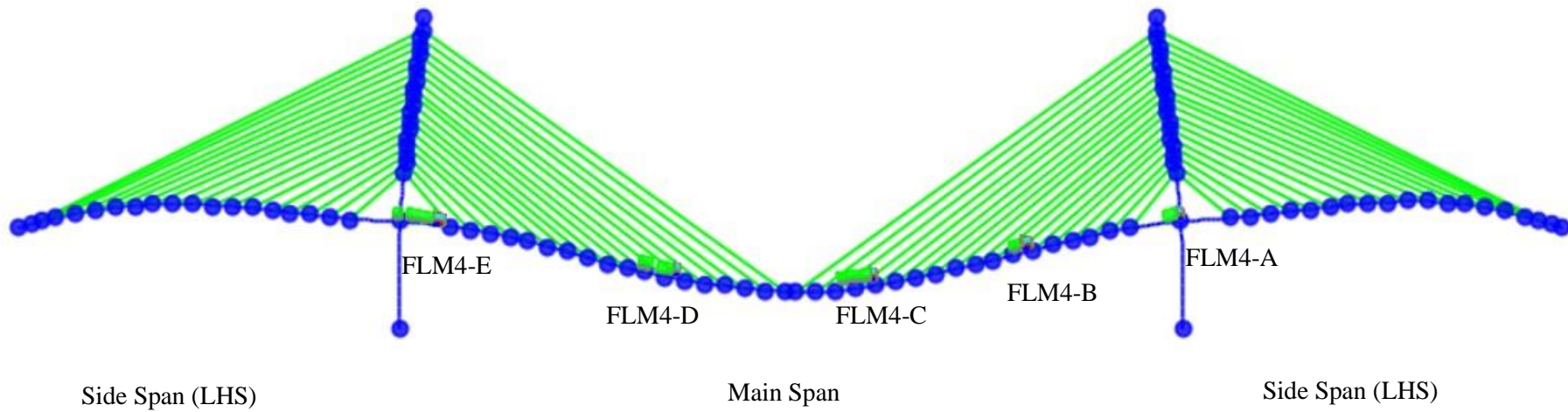
Figure 4.14: Deformation shape of cable-stayed bridge due to Convoy Lorry configuration at T=16.2s
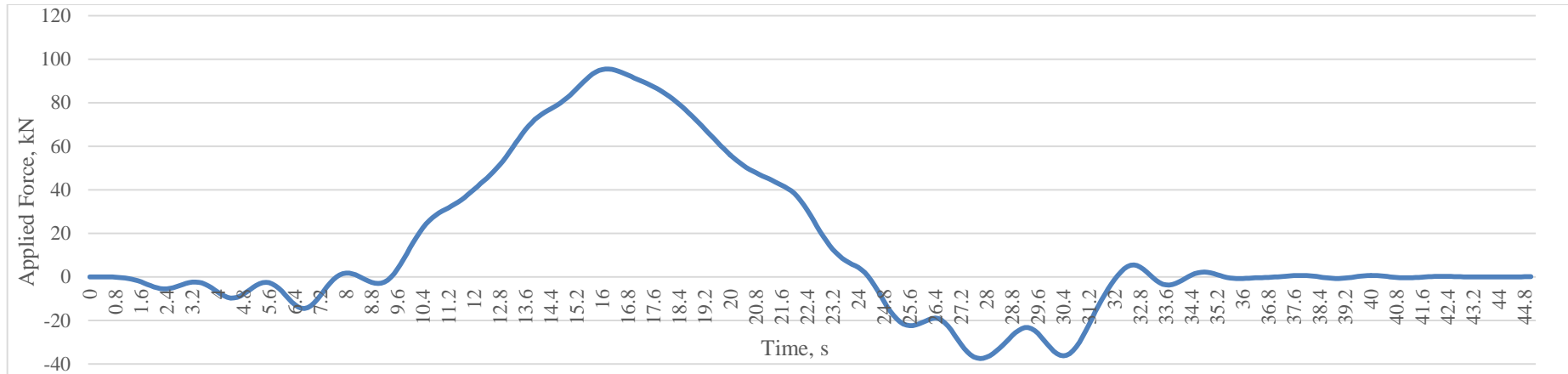
Figure 4.15: Time-history plot function of applied force on stay cable RS18 due to Convoy Lorry load configuration.
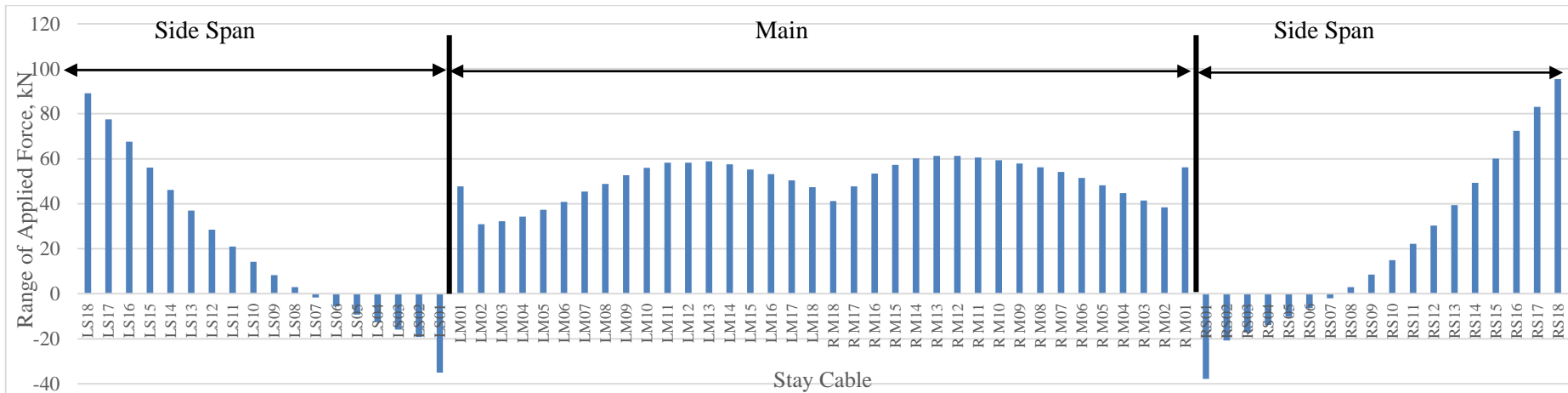
Figure 4.16: Variation of applied forces for all stay cables when cable RS18 is subjected to the maximum applied force.

4.4   Influence of Far-Field Ground Motion

In order to determine the effects of ground motions on the stress range of the stay cables, four ground motion records have been selected for the analysis. Each ground motion has been used in three separate load combinations: self-weight of structural elements, post-tensioning force and Kocaeli Bornova ground motions (DL+PS+KCL); self-weight of structural elements, post-tensioning force and Denali ground motions (DL+PS+DNL); and self-weight of structural elements, post-tensioning force and San Simeon ground motions (DL+PS+SSN),   As mentioned in Chapter 3, the ground motions will be scaled to meet the design criteria of the bridge to a PGA of 0.109g and probabilistic seismic hazard maps with 10% PE in 50-year (RP475-year) to a PGA of 0.04g to depict the worst case scenario that will be experienced by the cable stayed bridge for two levels of earthquake severity. For the purpose of this study, the ground motions were applied to determine its effect on the stay cables in terms of varying magnitudes and different epicentral distance. Furthermore, the ground motions were scaled based on the design PGA and probabilistic seismic hazard map to simulate the expected response when met with the worst case scenario.

4.4.1   Correlation of Peak Ground Acceleration and Magnitude of Ground Motions on Cable Stresses

To determine the effect of ground motion magnitude on the stress range of the stay cables, the ground motion records have been scaled to PGA of 0.109g and 0.04g in two separate sets of analysis. On the other hand, the effect of unscaled ground motions has been analysed in this study. By comparing Figure 4.10 and Figure 4.17, it confirms the initial assumption that ground motions have similar cyclic loading effect. The figure shows both variations that depict a cyclic action of applied load as a function of time. Thus, the calculation of stress ranges in stay cables can utilize the same methods. Based on the results obtained as shown in Figure 4.18, all of the applied ground motion resulted in increments in the maximum nominal stress in all stay cables. The maximum nominal stress of 642.898N/mm² and stress increment of 4.208N/mm² found on stay cable LS04 was a result of the (DL+PS+DNL) load combination where the earthquake event experienced a moment magnitude of M_w=7.9; whereas the minimum nominal stress of 493.392N/mm² was experienced by stay cable RM15 under the load combination (DL+PS+KCL) that features an earthquake with a moment magnitude of M_w=7.2. Based on the initial results, it can be said that a higher nominal stress in stay cables can be resulted by ground motions of a large magnitude. Further observations on the results

show that pylons that experienced high stresses are also concentrated around the pylons whereas those with low nominal stress are located at the centre of the main span.
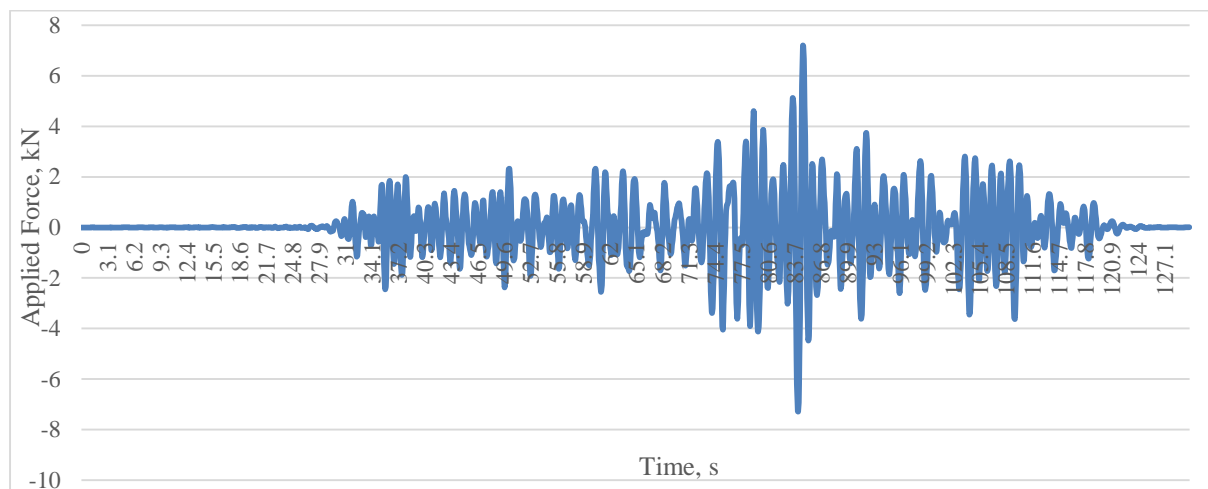
Figure 4.17: Variation of applied force on stay sable LS01 against time of applied ground motion.

The average stress increments throughout all stay cables with regards to load combinations (DL+PS+KCL), (DL+PS+DNL) and (DL+PS+SSN), are 1.730N/mm², 2.788N/mm² and 1.616N/mm²respectively. Despite the ground motions of the San Simeon earthquake originating from a lower magnitude, the average stress increment is significantly larger than the Kocaeli earthquake that had a moment magnitude of $M_w=7.51$. Therefore, an initial analysis reveals that a general consensus on the increase of maximum cable stress with increments to the magnitude of earthquakes can be used, although not all of which will necessarily produce the expected results. As the maximum nominal stress that occurs in stay cables is not the main factor to be considered in determining the fatigue performance of metallic elements, further investigations have been conducted to determine the stress range caused by the ground motions above.
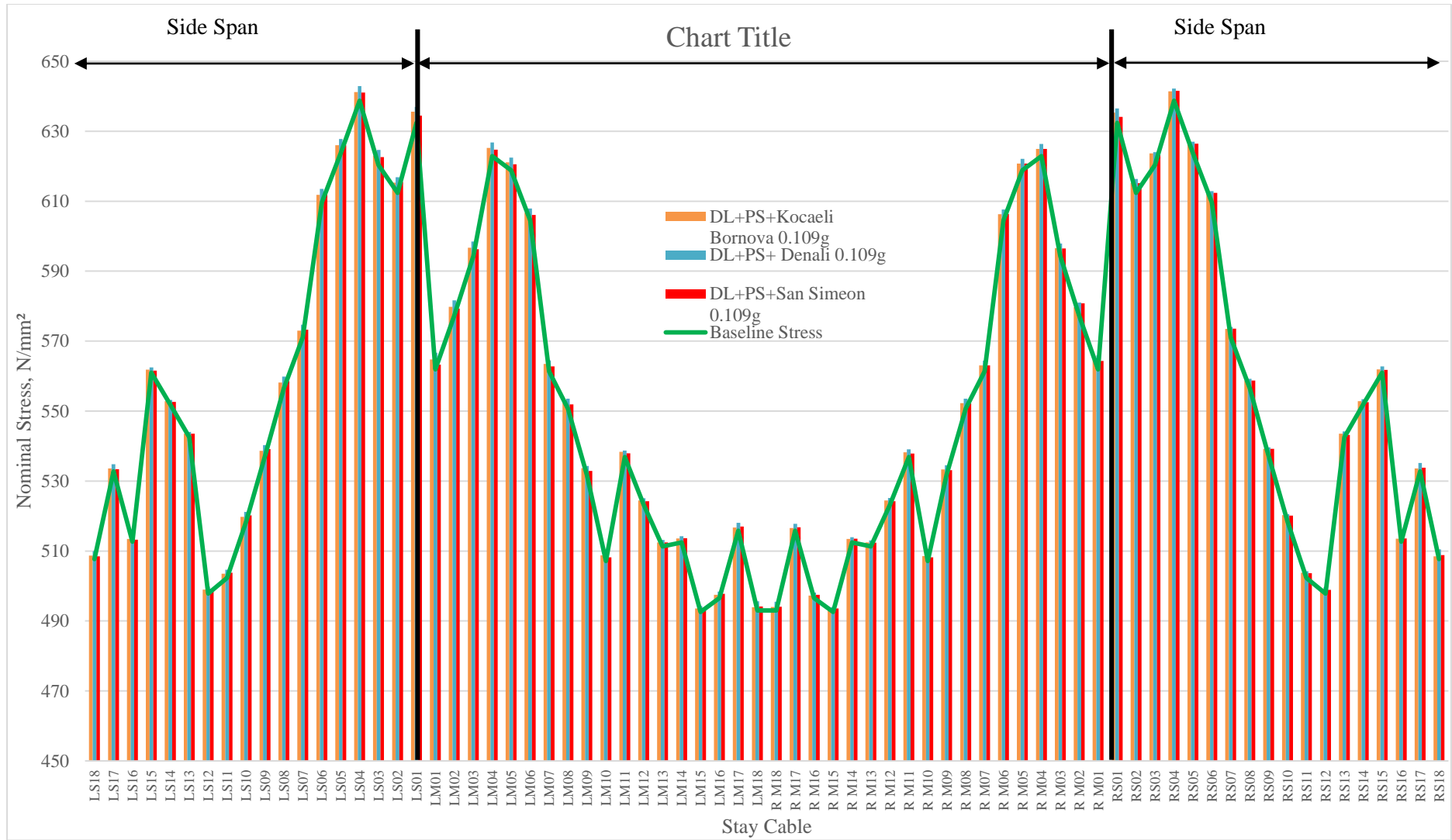
Figure 4.18: Comparison of maximum nominal stress in stay cables due ground motion records with baseline stress of cable-stayed bridge.

As shown in Figure 4.19, the maximum generated stress range by the Kocaeli Bornova earthquake is 6.473N/mm² on stay cable LM01 when scaled to a PGA of 0.109g whereas the same could be said when scaled to a PGA of 0.04g but with a reduced amount of 2.375N/mm². By comparing the stay cables connected to each side of the pylons, the maximum generated stress range on the left pylons is slightly higher than of the pylons on the right-hand side. Taking the highest stress range of each side that is located on stay cables LS01 and RS01, the maximum stress range of LS01 is 0.418N/mm² larger than the latter. On the other hand, the mean difference between the stay cables connected to both pylons is approximately 0.183N/mm². Based on obtained results, stay cables that experienced high stress ranges are located close to the pylons whereas the cables on the central region of the main span and those anchored on the ends of both side spans were subjected with minimum stress ranges. Taking the stress ranges resulted by scaling the ground motion to a PGA of 0.109g, critical stay cables that were subjected to stress ranges in the top 85th percentile along with their stress ranges are as follows: LS03, LS02, LS01, LM01, LM02, LM03, RM02, RM01, RS01, RS02 and RS03 with their respective maximum stress range of 5.709 N/mm², 6.045 N/mm², 6.385 N/mm², 6.473 N/mm², 6.073 N/mm², 5.741 N/mm², 5.570 N/mm², 5.911 N/mm², 6.054 N/mm², 5.667N/mm² and 5.656N/mm². By comparing the eleven critical stay cables above, six of the cables are located on the left pylon whereas the remaining five are on the opposite pylon. From the data obtained, a uniform distribution of seismic forces can be seen throughout the stay cables on both sides of the cable-stayed bridge.

Based on Figure 4.20, the overall reaction of the maximum stress range experienced by stay cables due to the 2002 Denali earthquake have close similarities to that produced by the Kocaeli earthquake. By comparing both results, both cases reflects the stay cables close to the pylons tend to fall into the higher spectrum of the maximum stress range, with cables connected to the central region of the main span and ends of both side spans subjected to lower stress ranges throughout the entire loading period of the ground motions. Moreover, the stay cables closer to the left pylon depicts a significantly higher maximum stress range than the stay cables surrounding the right pylons. The stay cable with the highest maximum stress range is stay cable LS01 with 9.141N/mm² whereas the stay cable (RS01) only experienced a stress range of 7.412N/mm². On average, stay cables connected to the left pylons experienced stress ranges of 5.31N/mm² and the cables connected to the right pylon were subjected to stress ranges of 4.960N/mm², resulting in an average difference of 0.349N/mm². Similarly to the stress ranges resulted by the Kocaeli earthquake, ground motions scaled to a PGA of 0.109g shows a higher

generated maximum stress range in stay cables over the data that were scaled to a PGA of 0.04g.

Comparing the maximum stress ranges of stay cable LS01 from different scaled ground motion, the stay cable only experienced a mere 3.355N/mm² and is therefore approximately 54.74% lesser than the values that were based on ground motion scaled to 0.109g. Therefore, the use of stress range data that has been based on ground motion scaled to 0.109g is a better suited to determine the worst case scenario that the cable-stayed bridge will experience. By referring the stress ranges resulted by scaling the ground motion to a PGA of 0.109g, critical stay cables that were subjected to stress ranges in the top 85th percentile are fairly to the previous results from Figure 4.17 aside from a few stay cables. The critical stay cables are LS05, LS04, LS03, LS02, LS01, LM01, LM02, LM03, RM02, RM01 and RS01, with their respective maximum stress range of 7.546 N/mm², 7.960 N/mm², 8.361 N/mm², 8.770 N/mm², 9.141 N/mm², 8.983 N/mm² N/mm², 8.358 N/mm², 7.746 N/mm², 7.470 N/mm², 7.777 N/mm² and 7.412 N/mm². Comparisons between the eleven critical stay cables above shows that eight of the cables are located on the left pylon whereas the other three cables are on the opposite pylon. This provides a good indication on the distribution of seismic forces where the left portion of the bridge was subjected to a significantly larger amount of exposure compared to the right portion of the cable-stayed bridge. In addition, the results above also show a higher deck-tower interaction the closer the deck to the pylons which directly increases the applied force in the stay cables when seismic forces are applied to the cable-stayed bridge.
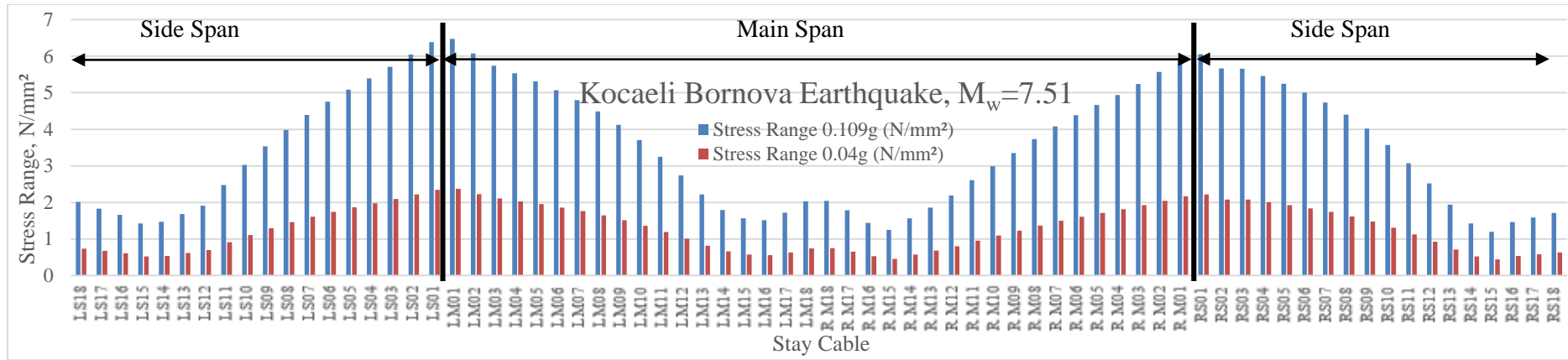
Figure 4.19: Maximum generated stress range of all stay cables due to Kocaeli Bornova ground motion
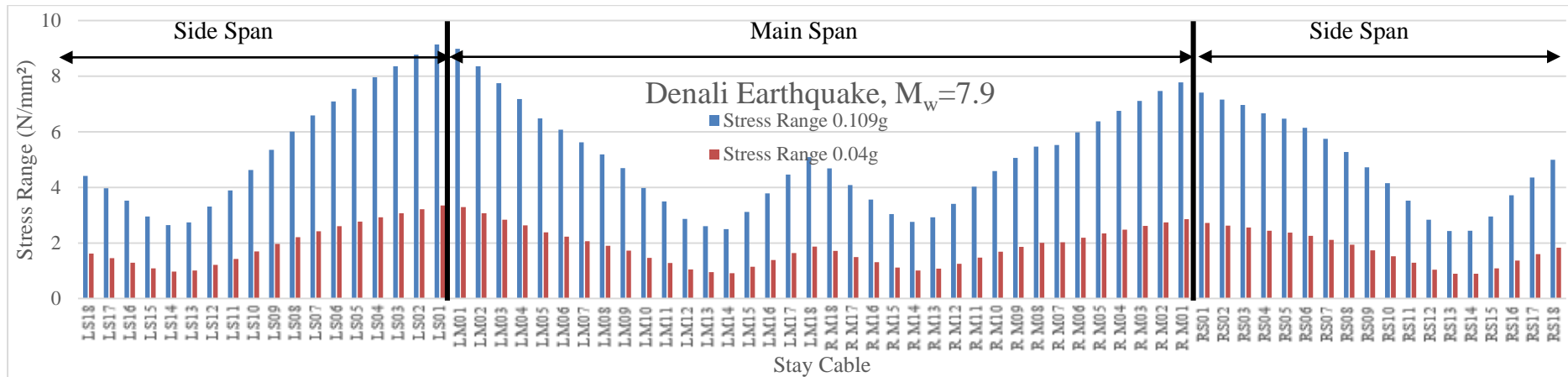
Figure 4.20: Maximum generated stress range of all stay cables due to Denali ground motion

89

In spite of this, the stress ranges resulted from the San Simeon earthquake has several variations that are notable when compared to the maximum stress range from Kocaeli and Denali. Figure 4.21 presents the maximum stress range experienced by all stay cables when the ground motion records of the 2005 San Simeon earthquake was analysed in SAP 2000. In terms of the overall trend, stay cables with a higher spectrum of stress range are located around the pylons with several exceptions such as stay cable RS01 that only experienced a small maximum stress range of 4.292 N/mm² compared to stay cables RM01 and RS02 with 6.038 N/mm² and 6.942 N/mm². In this case, the ground motion resulted in irregularities of the maximum stress range experienced by several cables. Moreover, the presence of extreme difference was also found on stay cable LS02 that saw a sudden surge from 5.694 N/mm² of stay cable LS03 to 7.938 N/mm². The subsequent stay cable, LS01 also presented a significantly lower value of 4.802 N/mm² compared to LS02.

If the irregularities were disregarded, stay cables RS03 through RS18 has a larger overall maximum stress range and a mean of 4.249 N/mm² compared to stay cables LS03 through LS18 that only produced a mean of 3.791 N/mm² for the maximum stress range produced in each cable. The maximum stress range for stay cables on the side spans tends to decrease as the cables projects further away from the side supports (LS18 – LS15 and RS18– RS14) and then increase gradually the closer the stay cables are to the pylons (LS14 – LS03 and RS13 – RS02). Moreover, stay cables in the central region of the main span (LM08 – RM08) depicts a rather flat variation for the maximum stress range in each cable, averaging in at 2.864 N/mm².

By taking account of the data for all stay cables, stay cable LS02 presented the largest maximum stress range on the left portion of the cable-stayed bridge with 7.939N/mm², whereas stay cable RM02 experienced the peak maximum stress range of 7.308 N/mm² on the right portion of the bridge. Similarly with the two previous ground motions, the maximum stress range experienced by the stay cables that have been scaled to a PGA of 0.109g also presented a higher value compared to the ground motion scaled to 0.04g. In terms of the stress ranges resulted by scaling the ground motion to a PGA of 0.109g, critical stay cables that were subjected to stress ranges in the top 85th percentile are different from previous two results due to the irregular maximum stress ranges experienced by the cables mentioned above. For this ground motion, the critical stay cables includes LS05, LS04, LS03, LS02, RM02, RM01, RS02, RS03, RS04, RS05, RS06 and RS07, with maximum stress range of 5.691 N/mm², 5.732

N/mm², 5.694 N/mm², 7.938 N/mm², 7.308 N/mm², 6.038 N/mm², 6.942 N/mm², 7.028 N/mm², 6.990 N/mm², 6.825 N/mm², 6.534 N/mm² and 6.109 N/mm². Out of the nine critical stay cables, seven stay cables are located on the right pylon whereas the remaining two belongs to the left pylon. This shows a significant amount of force that is experienced by the right pylons. Thereby, more attention should be paid if earthquakes with similar characteristics as the San Simeon earthquake were to be encountered.

Initial observations on the first two sets of ground motions (Kocaeli and Denali) show that ground motion records that originate from events of large magnitude will result in larger maximum stress range in stay cables, provided that the readings were taken at roughly the same epicentral distances. Furthermore, the strength of earthquakes increases exponentially on the Richter scale and a slight increment in magnitudes will result in larger effects on a cable—stayed bridge. By comparing the maximum stress range resulted from all three ground motions as shown in Figure 4.21, a relationship between the magnitude of an earthquake and its corresponding effect on the stay cables. Although a general conclusion could be drawn from the overall increment of maximum stress range with the increase of an earthquake's magnitude, it does not necessarily reflect a uniform variation throughout the stay cables. Comparison between the maximum stress ranges resulted from the Kocaeli ground motion with the San Simeon ground motion revealed that the stay cables on the sides spans (LS14 – LS04, RS02 – RS18) and the central region of the main span (LM13 – RM12) experienced higher overall maximum stress range for the San Simeon quake with a magnitude of M_w=6.52 over the results obtained from the Kocaeli quake that has a larger magnitude of M_w=7.2.

On the other hand, the application of ground motion records from the 2002 Denali earthquake with a magnitude of M_w=7.9 resulted in overall maximum stress ranges that were significantly higher than the Kocaeli quake for a large majority of the stay cables with exception for stay cables LS13 through LS11, LM10 through LM12, and RS10 through RS12. Overall, averages of the maximum stress range and maximum nominal stress increment experienced by the stay cables due to the ground motions of (DL+PS+KCL), (DL+PS+DNL) and (DL+PS+SSN) are shown in Table 4.1. Based on the data obtained, it shows that earthquakes of higher magnitude will generally to induce larger amounts of force on the cable-stayed bridge and consequently, result in larger stress ranges that are experienced throughout all of the stay cables. On the other hand, ground motions that are unscaled show that the higher the magnitude of an earthquake, the greater the effect on a cable-stayed bridge and the higher

the stress range in stay cables are produced. Similarly with Figure 4.22, the unscaled motions of Figure 4.23 also show that a smaller earthquake will still result in larger stress ranges in the back stays of the cable-stayed bridge. Therefore, regardless of the magnitude of an earthquake, the back stays and stay cables in the central region are equally affected compared to the stay cables closer to the pylons.

Table 4.1: Average values of the maximum stress range and nominal stress experienced by stay cables of a cable-stayed bridge due to different magnitudes of ground motion records.

Ground Motion	PGA Scaling: 0.04g		PGA Scaling: 0.109g	
	Mean Stress Range (N/mm²)	Mean Nominal Stress (N/mm²)	Mean Stress Range (N/mm²)	Mean Nominal Stress (N/mm²)
Kocaeli	1.3005	554.554	3.5445	556.500
Denali	1.8844	554.945	5.135	559.625
San Simeon	1.0591	554.510	3.8447	556.391
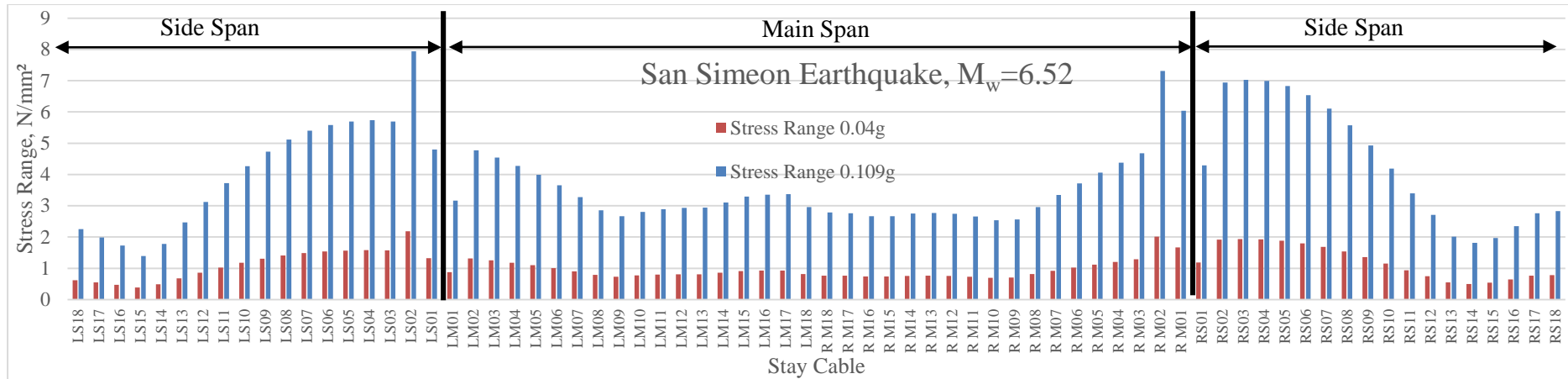
Figure 4.21: Maximum generated stress range of all stay cables due to San Simeon ground motion
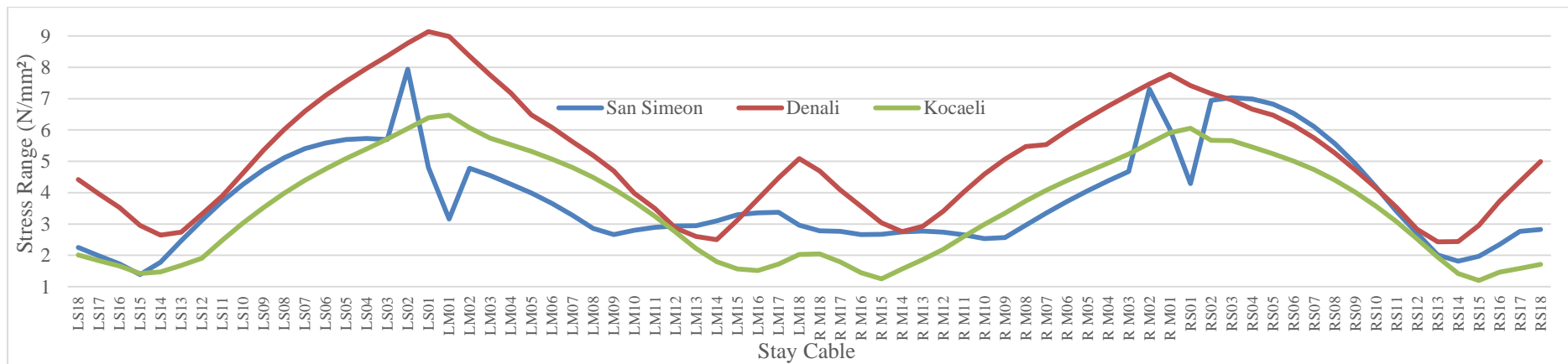
Figure 4.22: Comparison of maximum generated stress range of all stay cables due to ground motions of varying magnitudes scaled to 0.109g

93
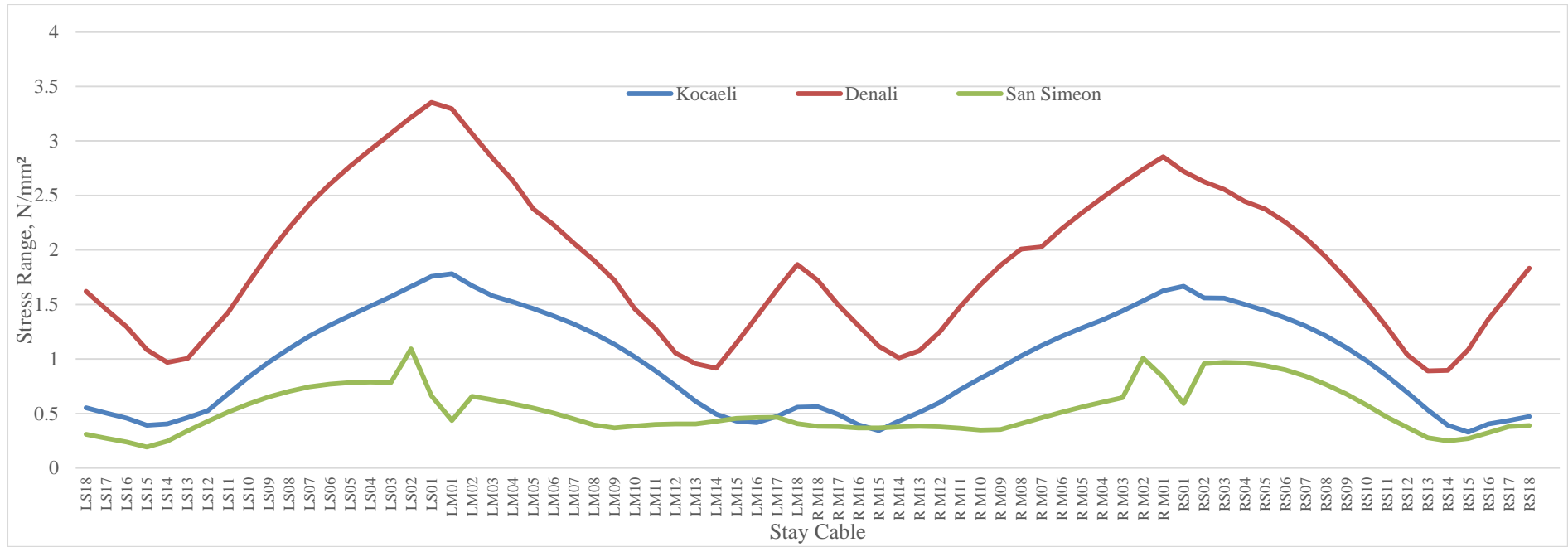
Figure 4.23: Comparison of maximum generated stress range of all stay cables due to ground motions of different magnitudes (unscaled)

4.5   Influence of Ground Motions and Traffic Loadings

The nominal stress obtained by combing the results due to ground motions and traffic loadings are shown in Figure 4.24. To enable the maximum achievable nominal stress due to the combination of both loadings, both of the previous traffic load combinations (DL+PS+SL) and (DL+PS+CL) were used to combine with the most critical ground motion (DL+PS+DNL). Based on the results obtained, the influence of ground motions on a cable-stayed bridge with moving traffic resulted in the increase in the nominal stress range experienced by all of the stay cables. By combining the peak stress range produced by moving traffic and scaled ground motions, the resulted stress range can be seen in Figure 4.25 for single lorry and convoy lorry configuration. Based on the Figure 4.25, a larger maximum achievable stress range was produced for all of the stay cables when the resulting peak stress range of each cable due to traffic loads and seismic loads were added up. The combination of single traffic loading and seismic loads resulted in higher maximum stress range in stay cables LS11 through LM02 and RM03 through RS02. Nonetheless, the combination of convoy traffic loading and seismic loads revealed a higher maximum stress range throughout most of the stay cables. Compared to single traffic loadings, the combination of convoy traffic and seismic loads induced a higher range of applied force in 83% of the all the stay cables on the cable-stayed bridge. Although all stay cables are able to achieve higher stress range with the merging of both load combinations, the likelihood of all stay cables achieving such stress ranges solely depends on the peak applied force of both loadings coinciding.

However, the effect of far-field ground motions is less likely to result in large increments towards the maximum stress range as the PGA generated will be significantly reduced on the receiving end. By comparing similar sets of ground motions were scaled to a PGA of 0.04g and 0.109g, the motions scaled to 0.04g only resulted in miniscule influence on the peak stress range. Referring to Figure 4.25, the inclusion of convoy traffic loads with ground motions scaled to 0.04g and 0.109g show that increments to the maximum stress range experienced by the cable-stayed bridge due to the load combination (DL+PS+CL) with ground motion scaled to 0.04g is relatively minor compared to load combination (DL+PS+CL) with ground motion scaled to 0.109g. Moreover, events with similar PGA of 0.109g is less likely to occur due to its larger return period of 2500 years compared to those close to 0.04g of a smaller return period of 475 years. Therefore, traffic loads remains as the optimal parameter

followed by ground motions scaled to a PGA of 0.04g in determining the maximum stress range for selecting critical stays for replacement and maintenance
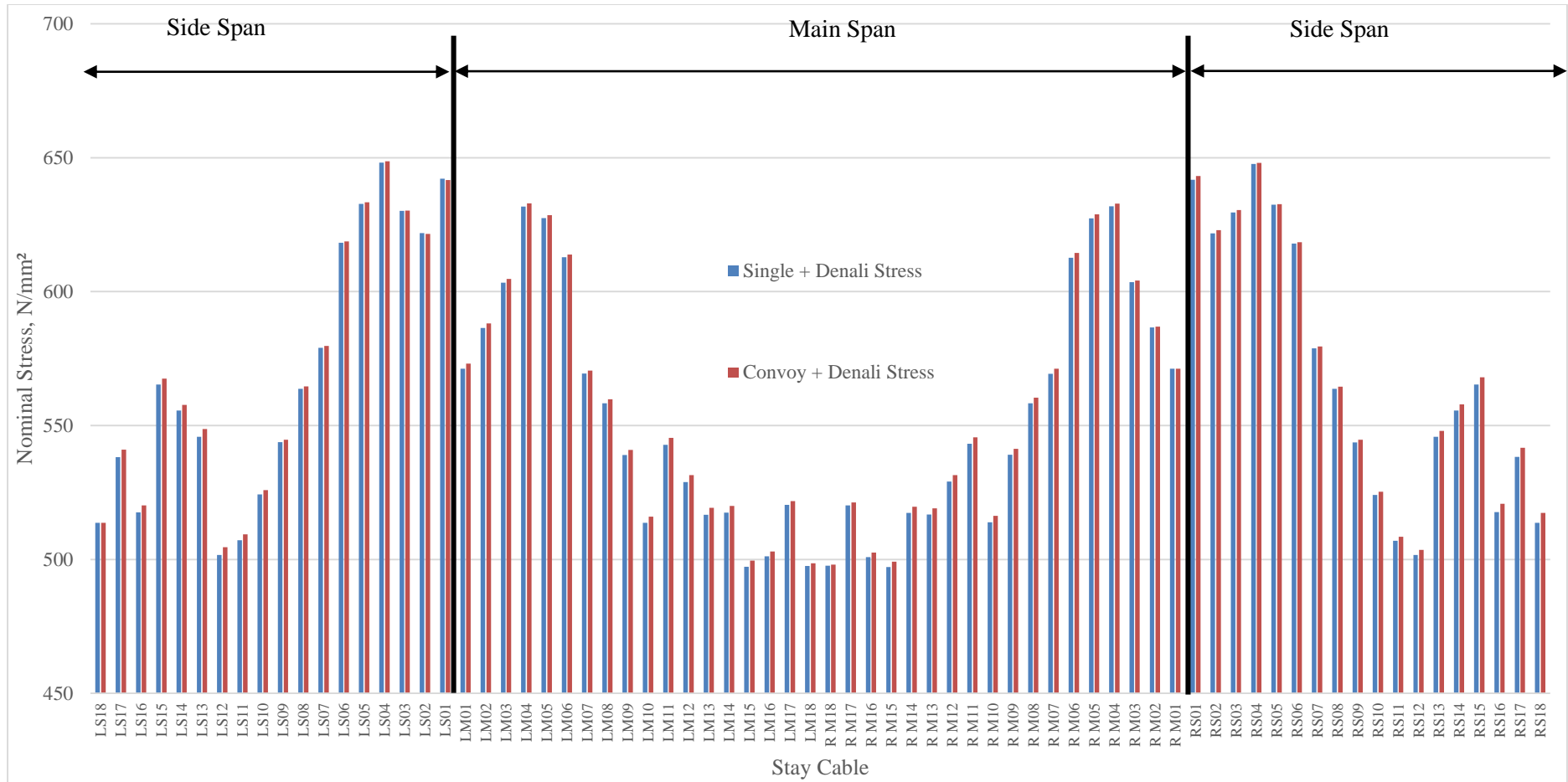
Figure 4.24: Nominal stress in stay cables due to Single Lorry and Convoy Lorry configuration with Denali ground motion
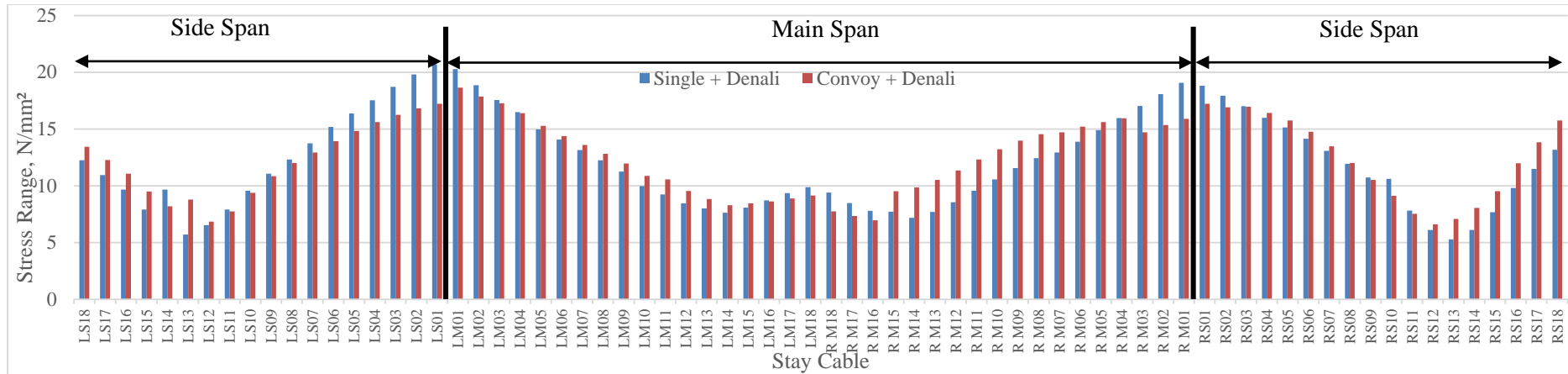
Figure 4.25: Maximum stress range in stay cables due to Single Lorry and Convoy Lorry configuration with Denali ground motions
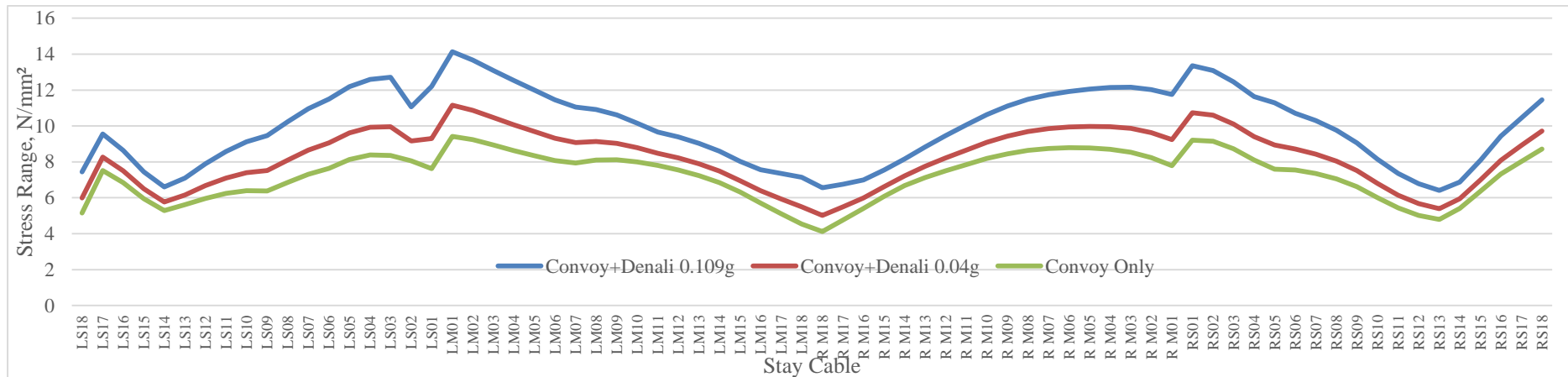
Figure 4.26: Maximum stress range comparison between Convoy lorry configurations with no applied ground motion, ground motion scaled to 0.04g and ground motion scaled to 0.109g

4.6   Concluding Remarks

The finite element modelling in this Chapter has presented the static behaviour of a cable-stayed bridge subjected to structural self-weight, strain force and the application of uniform live loads on the side span and main span. The behaviour has shown that the different combination of force application will affect the deformation of the pylons and bridge deck that varies from the different placement of loads such as uniform live loads on the side span and main span. In relation to the different deformation behaviour, it directly affects the stresses in stay cables along the entire span of the bridge as the primary principle of a cable-stayed bridge consists of the balancing of both ends of the span. Regardless of the location of the applied loads, all of the stay cables will be directly affected. In relation to the applied loads on the cable-stayed bridge, their respective influence on the stress ranges on the stay cables have also been determined. It has been found that the placement of uniform live load on the side span will have a significant local effect on the stay cable's stress range, whereas uniform loads that are placed on the main span resulted in large stress range for all of the stay cables connected to the main span as well as most of the back-stays.

The results in this Chapter has also shown the influence of moving traffic loads and far-field ground motions on the nominal stresses and maximum stress range in the stay cables. The application of moving traffic loads in singly lorry configuration managed to produce stress ranges above the 85th percentile on the critical stay cables that are closed to the pylons whereas minimal amounts of stress ranges have been detected in the stay cables connected to the central region of the main span and both side spans. Moreover, the overall trend of the produced stress range is fairly similar to the placement of uniform loads on the side span. In contrast, the application of moving traffic loads in convoy lorry configuration produced stress ranges above the 85th percentile on the critical stay cables close to the RHS pylon and connected to the main span. Unlike the single lorry configuration, results of the convoy lorry configuration reflected large effects on the stress ranges throughout a large majority of stay cables on the cable-stayed bridge.

Furthermore, the application of three sets of far-field ground motions that have been scaled to two PGA (0.109g and 0.04g) resulted in the increments of overall nominal stress in the stay cables over the baseline stresses. It has been revealed that ground motions behave in the same way as traffic loadings in terms of their cyclic loading

behaviour, therefore rendering them applicable for the calculation of stress ranges. The results have also indicated that critical stay cables that were subjected to large stress ranges are mainly concentrated around both sides of the pylons whereas the stay cables connected to the central region of the main span and the back stays have experienced moderate amounts of stress ranges. Also, ground motions that have been scaled to 0.109g resulted in significantly larger stress ranges but have a lower probability of such events occurring due to its 2500 years return period. On top of this, the ground motions scaled to 0.04g is more suitable for the prediction of stress ranges experienced by the stay cables in the event of earthquakes occurring in the region. However, it has been found that ground motions of different regions have the probability to cause the cable-stayed bridge to behave differently. Therefore, the use of local seismic data is a more reliable source to determine the actual behaviour of the stay cables in terms of their stress range. Based on the mean stress range that was experienced by the stay cables, it can be said that ground motions that originated from earthquakes of higher magnitudes will generally result in a larger amount of forces in stay cables, therefore increasing the stress range experienced.

It has been found that the combination of moving traffic loads and ground motions resulted in an overall larger stress range throughout all of the stay cables should the peak applied force of each respective loads coincide with each other. With the lower probability of seismic forces being applied towards the cable-stayed bridge in comparison to the constant bombardment of fluctuating loads due to actual traffic conditions, traffic loadings remains as the primary consideration in terms of identifying critical stay cables for further fatigue analysis. However, the ever-increasing frequency of earthquake occurrences in the region requires seismic forces to be considered to identify the critical stay cables for the purpose of maintenance and replacements.

CHAPTER 5

CONCLUSION

5.1 General Overview

This chapter summarizes the findings obtained from this research on the diversity of stress ranges in stay cables of the cable-stayed bridge due to traffic loads and far-field seismic excitation on top of the limitations of this research and the recommendations for future studies. This study presents an investigation on the stress ranges in stay cables of an actual two-span cable-stayed bridge (Penang Second Bridge) with the finite element software (SAP2000 Version 20 & 21) for the global analysis. The primary objective of this research was to determine the varying nominal stresses and stress range in the stay cables of a cable-stayed bridge under the influence of traffic loads and ground motions for far-field earthquakes as summarised in the next sub-section.

5.2 Main Conclusion

The findings of this study are concluded with regards to the objective outlined in sub-section 1.3. The first objective was to analyse the cable-stayed bridge with a suitable fatigue load model (FLM) based on Eurocode. In accordance to Eurocode 1: Action on Structures – Part 2: Bridges, 5 Fatigue Load Models have been considered in the selection of the optimal FLM for this study. By comparing the use case and characteristics of each FLM, Fatigue Load Model 4 has been selected for this study as the author assumes the fatigue life of a stay cable to be limited. Moreover, results that are more accurate and similar to traffic on conventional European roads can be produced with the load model. In the direct integration time-history analysis, each set of equivalent lorry has been applied in SAP2000 as moving traffic loads in single lorry and convoy lorry configuration on the outermost path of the carriageway at a fixed speed of 80km/h.

The next objective was to analyse the cable-stayed bridge with the effect of selected ground motion due to seismic excitation. Three sets of ground motion records have been obtained based on the monitoring stations of three different far-field earthquake events (Kocaeli, Denali and San Simeon) with varying magnitudes to depict the effect of ground acceleration on the cable-stayed bridge. Each set of ground motions have been scaled to 0.109g and 0.04g corresponding to a return period of 2500 years and 475 years to depict the different levels of earthquake severity and determine their effect on a cable-stayed bridge.

By conducting linear time-history analysis on the applied traffic and seismic loads, the obtained nominal stresses and maximum stress ranges that were experienced by the stay cables of the cable-stayed bridge has been determined. Under the influence of moving traffic in single lorry configuration, all the stay cables experienced minor increments in terms of their nominal stresses on top of their baseline values and it has been observed that the stay cables with higher nominal stresses are located close to the pylons. Relatively, the stay cables that experienced maximum stress ranges in the 85th percentile are also located close to the pylons. On the other hand, the convoy lorry configuration resulted in slightly higher increments in the nominal stresses in stay cables compared to the single lorry configuration. In contrast to the previous configuration, stay cables which experienced significant stress ranges are located close to the pylons and the side-span supports as a result of a higher overall applied load by the placement of all five lorries on the main span. Comparison between the trend of stress range experienced by single lorry and convoy lorry configuration shows that the convoy lorry configuration resulted in an overall larger maximum stress range throughout all of the stay cables located on the main span and those that are nearer to the side span supports.

The presence of seismic loads that were applied as ground motions for their linear time-history analysis resulted in the increase of nominal stresses in the stay cable for all three earthquake events. Generally, the stress ranges that occurred in stay cables behaved similarly to the results of a single lorry traffic load. It has been found that the maximum stress ranges increases with the reduction in the horizontal projection of stay cables from the pylons. Moreover, the increase in an earthquake's magnitude has resulted in increments towards the maximum stress ranges experienced by the cables although ground motions tend to vary from one another and will produce different forms of

reactions on the bridge. The simultaneous presence of moving traffic loads and seismic excitation will also increase the stress range and nominal stresses experienced by the stay cables. Critical stay cables with peak stress range values have been identified near to the columns and side span supports. Therefore, more attention should be focused on these particular cables for stay cable replacement in order to reduce the probability of fatigue failure. Ground motions with the highest magnitude result in the largest maximum stress range, but they do not necessarily produce significant stress range between ground motions of varying magnitudes.

5.3   Limitations of Research

The focus of this research was to determine the fatigue performance of a cable-stayed bridge by obtaining the stress ranges that have occurred in the stay cables. Despite being successful in obtaining the required data, there have been several factors that have impeded the process of obtaining the desired results. The limitations of this research are as follows:

- Lack of detailed specifications of the bridge model. Due to the limited information that was available online, a true-to-life model of the bridge could not be modelled in SAP2000. As the specifications were only limited to the details as mentioned in Chapter 3 of this study, elements such as the superimposed loads on the bridge deck, actual number of parallel-wire strands and the specifications of high damping rubber bearings on the side spans could not be assigned correctly. Furthermore, a detailed drawing and design report of the stay cable anchorages are also required for the modelling in other Finite Element software to determine its fatigue performance. Therefore, a set margin for the possible errors has to be considered in this study.

- The limited time of research. In order to determine the fatigue performance of the stay cable anchorages on the cable-stayed bridge, the use of multiple software and varying methods of calculating the equivalent fatigue damage are required. The lack of sufficient time to consider the additional processes limits how far the research can achieve. In this case, SAP2000 places a larger emphasis in terms of global analysis that allows the author to determine the stress ranges in the stay

cables. A detailed investigation will require the aid of other Finite Element software such as ANSYS, ABAQUS and MIDAS 2000.

- Insufficient local seismic data for ground motion application. Due to the limited budget that has been allocated for this research, actual ground motion data of stations located throughout Peninsular Malaysia could not be acquired from the Malaysia Meteorological Department (MET). Moreover, the lack of local site spectral data prevents the author from scaling the external ground motions accurately. Therefore, the assumptions in sub-section 3.5.1 were required in order to produce results that are close as possible to the actual seismic condition that will be experienced by the cable-stayed bridge.

- Lack of actual traffic data of the cable-stayed bridge. In order to simulate the actual stress ranges that are being subjected towards the stay cables of the cable-stay bridge, actual traffic data should be applied under Fatigue Load Model 5 instead of just current Fatigue Load Model 4 that could only provide a rough representation of the conditions experienced by European roads. The current research time frame does not permit the author to gain sufficient resources in terms of contacting the local authorities and the governing agencies that overlooks the maintenance of the Penang Second Bridge. Even if the author were to gain sufficient backing to obtain the required data, the limited time will still inhibit the production of a sufficient sample size for the provisions of accurate and reliable data.

5.4   Suggestions and Future Recommendations

This research has been conducted to determine the theoretical stress ranges that will be experienced by the stay cables on a cable-stayed bridge due to traffic loads and seismic loads that contribute to cyclic loadings. The aim is to predict the stay cables that are critically affected by these conditions in order to allow for the preparation of stay cable replacement and schedules maintenance to prevent the occurrence of sudden fatigue failure.   However, further investigations are required in order to conduct more comprehensive and detailed research based on the parameters and conditions set out in this study. The following endeavours could be undertaken in future works:

- For the application of traffic loads on the cable-stayed bridge, Fatigue Load Model 5 (FLM 5) should be used over Fatigue Load Model 4 (FLM 4) since it involves actual traffic data that can better simulate moving traffic loads for fatigue performance assessment. Moreover, the use of this load model can permit the consideration of growth in traffic volume.

- In order to produce the largest theoretical fatigue damage, traffic loads from Fatigue Load Models should include both lanes of the carriageway with their respective traffic percentage for fatigue assessment as recommended in the standard procedure of EC.

- Further consideration on the Dynamic Amplification Factor (DAF) which correlates with the vehicle's travel velocity should be taken account for because the acceleration and deceleration will affect the dynamic behaviour of stay cables and anchorages.

- Further studies can be conducted based on the data obtained in this research for local fatigue analysis at the cable anchorage with other Finite Element software such as ANSYS and ABAQUS.

- In order to accurately predict the effects of ground motions on the cable-stayed bridge of interest, more accurate seismic data in Malaysia should be obtained from MET as it will provide an actual representation of the seismic forces that will be experienced by the bridge.

- A more accurate bridge model could be produced by obtaining an in-depth blueprint of the Penang Second Bridge drawing.

REFERENCES

Abdelghaffar, A. M. & Nazmy, A. S. (1991) 3-D Nonlinear Seismic Behavior of Cable-Stayed Bridges. Journal of Structural Engineering-Asce 117(11): p. 3456-3476.

Albrecht, P. & Wright, W. (2000) Fatigue and fracture of steel bridges. European Structural Integrity Society 26: p. 211 - 234.

Arciniega-Ceballos, A., Baena-Rivera, M. & Sánchez-Sesma, F. J. (2018) The 1985 (M8.1) Michoacán Earthquake and Its Effects in Mexico City. Proceedings of Living Under the Threat of Earthquakes. Springer, Cham, pp. 65 - 75.

Arup Malaysia. (2015), Second Penang Bridge. [Photograph]. [Accessed on November 2018]. https://www.arup.com/-/media/arup/images/projects/s/second-panang-bridge/image-1_second-penang-bridge--arup-malaysia_2000x1125.jpg?h=1125&la=en&w=2000&hash=1764FEF328BFF39B81BB0D44E7145D025AF51991

Ayres, C. (2015) 14 Primary Pros And Cons Of Arch Bridges [Online]. [Accessed 13th November 2018]. Available from World Wide Web: https://greengarageblog.org/14-primary-pros-and-cons-of-arch-bridges

Billington, D. P. & Nazmy, A. (1991) History and Aesthetics of Cable-Stayed Bridges. Journal of Structural Engineering 117(10):3103-3134.

Boardman, B. & Deer and Company (1990) Fatigue Resistance of Steels. ASM Handbook 1.

BSI (2005) BS EN 1993 Part 1-9: Design of Steel Structures: Fatigue. London: British Standards Institution.

BSI (2003) BS EN 1991-2 Part 2: Traffic Load on Bridges. London: British Standards Institution.

BSI (2008) NA to BS EN 1991 Part 2: Traffic Loads on Bridges. London: British Standards Institution.

Cajka, M. & Drysdale, J. (1989) Intensity Report of the November 25, 1988 Saguenay, Québec, Earthquake [Online]. [Accessed 12 January 2019]/ Available from World Wide Web: http://www.earthquakescanada.nrcan.gc.ca/historic-historique/events/19881125_int-en.php2018

Camara, A. (2018) Seismic Behaviour of Cable-Stayed Bridges: A Review. Medcrave Online Journal of Civil Engineering 4(3): p. 161 - 169.

Casado, A. C. (2011) Seismic Behaviour of Cable-Stayed Bridges: Design, Analysis and Seismic Devices. In Department of Continuum Mechanics and Theory of Structures. Universidad Politécnica de Madrid, Madrid.

Chang, K. C., Mo, Y. L., Chen, C. C., Lai, L. C. & Chou, C. C. (2004) Lessons Learned from the Damaged Chi-Lu Cable-Stayed Bridge. Journal of Bridge Engineering 9(4): p. 343-352.

Charusiri, P. & Palloplee, S. (2015) Regional Tectonic Setting and Seismicity of Thailand with Reference to Reservoir Construction. Proceedings of GEOTHAI'07 International Conference on Geology of Thailand: Towards Sustainable Development and Sufficiency Economy, p. 248 - 287.

China Communications Construction Company Ltd. (2010) Chaotianmen Yangtze River Bridge Project in Chongqing City. [Online]. [Accessed on November 2018]. http://en.ccccltd.cn/business/btbot/BT/201011/t20101112_1609.html

Corbett, P. W., Buckby, R. J. & Wee, E. L. (2010) Penang Bridge Widening: Design and Construction Challenges. Proceedings of the Institution of Civil Engineers - Bridge Engineering 163(3): p. 125-135.

European Steel Design Education Programme (1998) Lecture 12.2: Advanced Introduction to Fatigue. [Online]. [Accessed on 22 October 2018]. Available from World Wide Web:http://fgg-web.fgg.uni-lj.si/~/pmoze/ESDEP/master/wg12/l0200.htm2018).

Filliatrault, A., Tinawi, R. & Massicotte, B. (1993) Damage to Cable-Stayed Bridge During 1998 Saguenay Earthquake II: Dynamic Analysis. Journal of Structural Engineering 119. p.1450 - 1463.

Flint & Niel Partnership Consulting Engineers (2004) Derivation of the UK National Annex to Clause 4.6: Fatigue Load Models: Eurocode 1: Actions on structures - Part 2: Traffic loads on bridges. London.

Föhl, K. (2005) Pont de Dryburgh Abbey, Imag2381, [Photograph]. [Accessed on 1st December 2018]: https://files1.structurae.de/files/photos/1720/imag2381.jpg

Fowler, C. (1990) The Solid Earth. An Introduction to Global Geophysics. Cambridge University Press, Cambridge.

Geist, E. (2008) Tsunami Generation from the 2004 M=9.1 Sumatra-Andaman Earthquake. Pacific Coastal and Marine Science Center, United States Geological Survey (USGS) [Online]. [Accessed March 2019]. Available from World Wide Web: https://www.usgs.gov/centers/pcmsc/science/tsunami-generation-2004-m91-sumatra-andaman-earthquake?qt-science_center_objects=0#qt-science_center_objects2019

Gimsing, N. J. & Georgakis, C. T. (2012) Cable Supported Bridges: Concept and Design Third Edition. Sussex: John Wiley & Sons.

Griffin, A. (2018) Why did the Genoa bridge collapse? Engineering experts weigh in on disaster that left 35 dead. [Online]. [Accessed 16th December 2018]. Available from World Wide Web: https://www.independent.co.uk/news/science/genoa-bridge-collapse-italy-why-did-disaster-engineering-experts-a8491811.html2018

Heidbach, O., Tingay, M., Barth, A., Reinecker, J., Kurfeß, D. & Müller, B. (2008) The world stress map database release 2008.

Hobbs, R. E. & Ghavami, K. (1982) The Fatigue of Structural Wire Strands. International Journal of Fatigue 4(2):69-72.

Hou Man, L. B., Peng Yun Dong, Chang Chung Man (2018) Design of Main Bridge of Second Penang Bridge in Malaysia. International Journal of Transportation Engineering and Technology 4(2): p. 65 - 42

Imam, B. M. & Chryssanthopoulos, M. K. (2012) Causes and Consequences of Metallic Bridge Failures. Structural Engineering International 22(1): p. 93-98.

Kumar, S. R. S. & Kumar, A. R. S. (2012) Fatigue of steel structures. Indian Institute of Technology Madras.

Kundu, B., Legrand, D., Gahalaut, K., Gahalaut, V. K., Mahesh, P., Kamesh Raju, K. A., Catherine, J. K., Ambikapthy, A. & Chadha, R. K. (2012) The 2005 volcano-tectonic earthquake swarm in the Andaman Sea: Triggered by the 2004 great Sumatra-Andaman earthquake. Tectonics 31(5):n/a-n/a.

Looi, D. T. W., Tsang, H. H. & Hee, M. C. (2017) Seismic Hazard Modelling for Malaysia and Singapore. Proceedings of The 2017 World Congress in Advances in Structural Engineering and Mechanics (ASEM17), 28 August – 1 September 2017, Ilsan(Seoul), Korea.

Manson, S. S., Smith, R. W. & Hirschberg, M. H. (1964) Fatigue Behavior of Materials Under Strain Cycling In Low and Intermediate Life Range. National Aeronautics and Space Administration (NASA), Lewis Research Center, Cleveland, Ohio.

Marto, A., Soon, T. C., Kasim, F. & Yunus, N. Z. M. (2013) Seismic Impact in Peninsular Malaysia. Proceedings of The 5th International Geotechnical Symposium, pp. 22 - 24.

Mendes, T. a. A. (2010) Composite Steel-Concrete Bridges with Double Composite Action. Technical University of Lisbon, Portugal.

Mohamed Taib, I. B. (2011) The Second Penang Bridge: In: Universiti Teknologi Malaysia Seminar Kejuruteraan Awam (SEMKA) Program Perdana Semester II Sesi 2010/2011.).

Mohamed Taib, I. B. (2016) Jambatan Sultan Abdul Halim Mu'adzam Shah Sustainable Design, Construction & Maintenance: In: Seminar Kejuruteraan Awam (SEMKA) Program Perdana Semester II Sesi 2015/2016.

Morales, M. & Bauer, D. (2006) Fatigue and remaining life assessment of steel bridges more than 50 years old. Proceedings of 7th International Conference on Short & Medium Span Bridges 2006.

Muhamad Khairussaleh, N. a. B. (2016) Fatigue Of Cable Anchorages On A Cable-Stayed Bridge. Department of Civil and Environmental Engineering. University of Surrey, Guildford, Surrey.

Nabilah, A. B. & Balendra, T. (2012) Seismic Hazard Analysis for Kuala Lumpur, Malaysia. Journal of Earthquake Engineering 16(7): p. 1076-1094.

Nakamura, S. & Hosokawa, H. (1989) A study on the fatigue design of parallel wire strands on cable-stayed bridges. Doboku Gakkai Ronbunshu 6(410): p. 157-166.

Ohio Department of Transportation. (2009) Bridge Inspector's Reference Manual. In Section 12- Special Bridges. [Online]. [Accessed December 2018]. Available from World Wide Web: http://www.dot.state.oh.us/Divisions/Engineering/Structures/bridge%20operations%20and%20maintenance/Bridge%20Inspectors%20Reference%20Manual/Forms/AllItems.aspx

Omar, K. & Jhonny (2009) Crustal Deformation Study in Peninsular Malaysia Using Global Positioning System. Proceedings of Postgraduate Seminar Faculty of Geoinformation Science & Engineering 2009.

Park, S. H. & Lee, C. S. (2017) Relationship between mechanical properties and high-cycle fatigue strength of medium-carbon steels. Materials Science and Engineering a-Structural Materials Properties Microstructure and Processing 690: p. 185-194.

Parke, G. A. R. (2014) Engineering Materials Unit 2: Fatigue University of Surrey, Surrey.

Pollock, E. (2018) Italy's Morandi Bridge Collapse—What Do We Know? [Online]. [Accessed on 21st October 2018]. Available from World Wide Web: https://www.engineering.com/BIM/ArticleID/17517/Italys-Morandi-Bridge-CollapseWhat-Do-We-Know

Rötzel, K. (2005) Akashi Kaikyō Bridge, Bridge.Jpg, [Photograph]. [Accessed on 8th October 2018]: https://commons.wikimedia.org/wiki/File:Akashi_Bridge.JPG

Roylance, D. (2001) Fatigue. Department of Materials Science and Engineering, Massachusets Institute of Technology. [Online]. [Accessed on 12th November 2018]. Available from World Wide Web: https://ocw.mit.edu/courses/materials-science-and-engineering/3-11-mechanics-of-materials-fall-1999/modules/MIT3_11F99_fatigue.pdf

Schijve, J. (2009) Fatigue of Structures and Materials. India, Springer Netherlands.

Sham, R., Fan, F. & Feng, L. Y. (2013) Construction Of The Cable-Stayed Bridge. Proceedings of Second International Seminar on the Design & Construction of the Second Penang Bridge.

Shoushtari, A. V., Bin Adnan, A. & Zare, M. (2018) Incorporating the local faults effects in development of seismic ground-motion hazard mapping for the Peninsular Malaysia region. Journal of Asian Earth Sciences 163(168): p. 194-211.

Shrestha, B. (2014) Seismic response of long span cable-stayed bridge to near-fault vertical ground motions. KSCE Journal of Civil Engineering 19(1): p. 180-187.

Shrestha, B. & Tuladhar, R. (2012) The response of Karnali Bridge, Nepal to near-fault earthquakes. Proceedings of the Institution of Civil Engineers - Bridge Engineering 165(4): p. 223-232.

Smith, J. O. (1942) The Effect of Range of Stress on the Fatigue Strength of Metals. Engineering Experiment Station Bulletin Series No. 334 XXXIX (No. 25).

Timothy D. Ancheta, R. B. D., Jonathan P. Stewart, Emel Seyhan, Walter J. Silva, Brian S.J. Chiou, Katie E. Wooddell, Robert W. Graves, Albert R. Kottke, David M. Boore, Tadahiro Kishida, and Jennifer L. Donahue. (2013) PEER NGA-West2 Database. Pacific Earthquake Engineering Research Center, University of California, Berkely. [Online]. [Accessed on March 2019]. Available from World Wide Web: https://ngawest2.berkeley.edu/

Tjia, H. (2010) Geohazard in Malaysia Context: In: Seminar Teknikal Kebangsaan Gempa Bumi & Tsunami di Malaysia (NatSET 2010).

Tuladhar, R., Dilger, W. H. & Elbadry, M. M. (1995) Influence of Cable Vibration on Seismic Response of Cable-Stayed Bridges. Canadian Journal of Civil Engineering 22(5):1 p. 001-1020.

Vavryčuk, V. (2015) Earthquake Mechanisms and Stress Field. In: Encyclopedia of Earthquake Engineering. (Beer, M., Patelli, E., Kougioumtzoglou, I., andAu, I. S.-K. (eds)) Springer-Verlag, Pp. 1-21.

Virlogeux, M. (1999) Recent evolution of cable-stayed bridges. Engineering Structures 21(8): p. 737-755.

Virlogeux, M. (2005) State-of-the-art in cable vibrations of cable-stayed bridges. Bridge Structures 1(3), p.133-168.

Walther, R., Houriet, B., Isler, W., Moia, P. & Klein, J. F. (1999) Cable Stayed Bridges Second Edition. Thomas Telford.

Table A.1: Nominal tresses in stay cables LS18-LM18 experienced during the initial condition, the placement of live load on left side span, and the placement of live load on main span.

Stay No	Baseline Stress (DL+PS) (N/mm²)	Live Side Span Stress (N/mm²)	Live Mid Span Stress (N/mm²)
LS18	507.693	472.751	597.758
LS17	532.747	505.404	615.769
LS16	512.675	493.072	588.414
LS15	561.023	553.226	626.946
LS14	551.902	555.907	607.937
LS13	542.558	558.064	588.920
LS12	497.861	524.331	534.872
LS11	502.271	539.032	530.390
LS10	518.431	564.668	538.110
LS09	537.182	591.972	548.850
LS08	556.492	618.839	560.521
LS07	571.069	639.972	567.723
LS06	609.699	684.036	599.086
LS05	623.704	702.441	605.710
LS04	638.690	720.764	612.907
LS03	620.304	704.581	585.969
LS02	612.380	697.532	568.328
LS01	632.382	716.184	577.414
LM01	561.940	522.477	652.965
LM02	577.243	546.621	667.983
LM03	594.300	570.916	683.882
LM04	622.890	605.238	711.244
LM05	618.831	605.751	705.971
LM06	604.500	535.137	690.374
LM07	561.378	555.120	645.831
LM08	550.710	547.129	633.519
LM09	531.835	530.652	612.683
LM10	507.133	508.180	585.629
LM11	536.877	540.075	612.636
LM12	523.224	528.559	595.713
LM13	511.347	518.850	580.033
LM14	512.482	522.214	576.816
LM15	492.553	504.697	551.618
LM16	496.522	511.143	549.737
LM17	515.791	532.928	562.586
LM18	493.021	512.624	532.779

Table A.2: Nominal tresses in stay cables RM18-RS18 experienced during the initial condition, the placement of live load on left side span, and the placement of live load on main span.

Stay No	Baseline Stress (DL+PS) (N/mm²)	Live Side Span Stress (N/mm²)	Live Mid Span Stress (N/mm²)
R M18	493.021	480.385	532.779
R M17	515.791	503.936	562.586
R M16	496.522	485.638	549.737
R M15	492.553	482.750	551.618
R M14	512.482	503.821	576.816
R M13	511.347	503.803	580.033
R M12	523.224	516.774	595.713
R M11	536.877	531.472	612.636
R M10	507.133	502.699	585.629
R M09	531.835	528.271	612.683
R M08	550.710	547.898	633.519
R M07	561.378	559.183	645.831
R M06	604.500	602.768	690.374
R M05	618.831	617.389	705.971
R M04	622.890	621.543	711.244
R M03	594.300	592.827	683.882
R M02	577.243	575.388	667.983
R M01	561.940	559.431	652.965
RS01	632.382	636.244	577.414
RS02	612.380	615.544	568.328
RS03	620.304	622.822	585.969
RS04	638.690	640.618	612.907
RS05	623.704	625.074	605.710
RS06	609.699	610.519	599.086
RS07	571.069	571.331	567.723
RS08	556.492	556.173	560.521
RS09	537.182	536.252	548.850
RS10	518.431	516.851	538.110
RS11	502.271	500.001	530.390
RS12	497.861	494.863	534.872
RS13	542.558	538.792	588.920
RS14	551.902	547.343	607.937
RS15	561.023	555.653	626.946
RS16	512.675	506.501	588.414
RS17	532.747	525.888	615.769
RS18	507.693	500.182	597.758
Maximum Stress		720.764	711.244
Minimum Stress		480.385	530.390
Median Stress		547.621	588.920
Mode Stress		720.764	588.920
Mean Stress		567.539	600.081

Table A.3: Nominal tresses in stay cables LS18-LM18 experienced during the initial condition, the application of traffic load in Single Lorry configuration and the application of traffic load in Convoy Lorry configuration.

Stay No	Baseline Stress (DL+PS) (N/mm²)	DL + PS + Single Lorry(SL) Stress (N/mm²)	DL+PS+Convoy Lorry (CL) Stress (N/mm²)
LS18	507.693	512.775	515.857
LS17	532.747	537.427	540.264
LS16	512.675	516.939	519.523
LS15	561.023	564.732	566.976
LS14	551.902	555.068	557.193
LS13	542.558	545.200	548.181
LS12	497.861	500.918	503.835
LS11	502.271	506.313	508.518
LS10	518.431	523.276	524.831
LS09	537.182	542.631	543.573
LS08	556.492	562.428	563.357
LS07	571.069	577.672	578.382
LS06	609.699	616.867	617.337
LS05	623.704	631.271	631.839
LS04	638.690	646.627	647.075
LS03	620.304	628.523	628.663
LS02	612.380	620.693	620.438
LS01	632.382	640.499	640.000
LM01	561.940	569.465	571.364
LM02	577.243	584.750	586.481
LM03	594.300	601.761	603.237
LM04	622.890	630.339	631.523
LM05	618.831	626.132	627.179
LM06	604.500	611.580	612.574
LM07	561.378	567.249	569.331
LM08	550.710	557.290	558.817
LM09	531.835	538.035	539.952
LM10	507.133	512.869	515.132
LM11	536.877	542.136	544.674
LM12	523.224	528.215	530.772
LM13	511.347	516.032	518.585
LM14	512.482	516.803	519.330
LM15	492.553	496.587	498.879
LM16	496.522	500.427	502.232
LM17	515.791	519.569	520.906
LM18	493.021	496.621	497.557
R M18	493.021	496.714	497.143

Table A.4: Nominal tresses in stay cables RM18-RS18 experienced during the initial condition, the application of traffic load in Single Lorry configuration and the application of traffic load in Convoy Lorry configuration.

Stay No	Baseline Stress (DL+PS) (N/mm²)	DL + PS +Single Lorry(SL) Stress (N/mm²)	DL+PS+Convoy Lorry (CL) Stress (N/mm²)
R M18	493.021	496.714	497.143
R M17	515.791	519.470	520.551
R M16	496.522	500.319	501.931
R M15	492.553	496.619	498.642
R M14	512.482	516.865	519.169
R M13	511.347	516.106	518.485
R M12	523.224	528.362	530.727
R M11	536.877	542.372	544.728
R M10	507.133	512.989	513.318
R M09	531.835	538.060	540.289
R M08	550.710	557.252	559.355
R M07	561.378	568.155	570.134
R M06	604.500	611.528	613.299
R M05	618.831	626.177	627.610
R M04	622.890	630.547	631.590
R M03	594.300	602.164	602.837
R M02	577.243	585.177	585.474
R M01	561.940	569.784	569.727
RS01	632.382	640.201	641.595
RS02	612.380	620.336	621.533
RS03	620.304	628.166	629.040
RS04	638.690	646.331	646.797
RS05	623.704	631.086	631.495
RS06	609.699	616.773	617.256
RS07	571.069	577.758	578.421
RS08	556.492	562.685	563.551
RS09	537.182	542.755	543.807
RS10	518.431	523.273	524.452
RS11	502.271	506.288	507.711
RS12	497.861	500.971	502.883
RS13	542.558	545.200	547.356
RS14	551.902	555.056	557.313
RS15	561.023	564.705	567.388
RS16	512.675	516.883	519.994
RS17	532.747	537.342	540.778
RS18	507.693	512.664	516.413
Maximum Stress		646.627	647.075
Minimum Stress		496.587	497.143
Median Stress		555.062	557.253
Mode Stress		545.200	647.075
Mean Stress		561.173	564.071

Table A.5: Nominal tresses in stay cables LS18-LM18 experienced during the initial condition, application of Kocaeli Bornova (KCL) ground motions at 0.109g, application of Denali(DNL) ground motions at 0.109g, and application of San Simeon(SSN) ground motions at 0.109g.

Stay No	Baseline Stress (DL+PS) (N/mm²)	DL+PS+ Kocaeli(KCL) Stress 0.109g (N/mm²)	DL+PS+Denali(DNL) Stress 0.109g (N/mm²)	DL+PS+San Simeon(SSN) Stress 0.109g (N/mm²)
LS18	507.693	508.684	509.984	508.448
LS17	532.747	533.637	534.781	533.415
LS16	512.675	513.463	514.470	513.257
LS15	561.023	561.831	562.510	561.557
LS14	551.902	552.811	553.213	552.606
LS13	542.558	543.569	544.038	543.546
LS12	497.861	498.971	499.785	499.118
LS11	502.271	503.478	504.614	503.777
LS10	518.431	519.729	521.160	520.158
LS09	537.182	538.644	540.257	539.103
LS08	556.492	558.189	559.871	558.574
LS07	571.069	572.984	574.712	573.275
LS06	609.699	611.815	613.549	611.985
LS05	623.704	626.013	627.754	626.031
LS04	638.690	641.192	642.899	641.020
LS03	620.304	623.011	624.652	622.598
LS02	612.380	615.314	616.854	615.498
LS01	632.382	635.554	636.969	634.430
LM01	561.940	564.738	566.651	563.299
LM02	577.243	579.807	581.673	579.309
LM03	594.300	596.698	598.456	596.277
LM04	622.890	625.233	626.791	624.758
LM05	618.831	621.106	622.481	620.566
LM06	604.500	606.689	607.888	606.083
LM07	561.378	563.469	564.479	562.793
LM08	550.710	552.682	553.521	551.933
LM09	531.835	533.660	534.343	532.866
LM10	507.133	508.783	509.295	508.179
LM11	536.877	538.325	538.745	537.920
LM12	523.224	524.447	525.063	524.248
LM13	511.347	512.466	513.144	512.429
LM14	512.482	513.567	514.227	513.636
LM15	492.553	493.591	494.261	493.764
LM16	496.522	497.508	498.374	497.738
LM17	515.791	516.733	518.036	516.994
LM18	493.021	493.928	495.631	494.121

Table A.6: Nominal tresses in stay cables RM18-RS18 experienced during the initial condition, application of Kocaeli Bornova (KCL) ground motions at 0.109g, application of Denali(DNL) ground motions at 0.109g, and application of San Simeon(SSN) ground motions at 0.109g.

Stay No	Baseline Stress (DL+PS) (N/mm²)	DL+PS+ Kocaeli(KCL) Stress 0.109g (N/mm²)	DL+PS+Denali(DNL) Stress 0.109g (N/mm²)	DL+PS+San Simeon(SSN) Stress 0.109g (N/mm²)
R M18	493.021	493.991	495.462	494.050
R M17	515.791	516.575	517.786	516.809
R M16	496.522	497.241	498.114	497.505
R M15	492.553	493.392	494.018	493.559
R M14	512.482	513.455	513.959	513.509
R M13	511.347	512.448	513.049	512.377
R M12	523.224	524.446	525.180	524.241
R M11	536.877	538.210	539.084	537.863
R M10	507.133	508.564	509.582	508.209
R M09	531.835	533.351	534.495	533.117
R M08	550.710	552.297	553.550	552.180
R M07	561.378	563.023	564.373	563.031
R M06	604.500	606.279	607.630	606.313
R M05	618.831	620.759	622.109	620.786
R M04	622.890	624.969	626.337	624.970
R M03	594.300	596.555	597.914	596.493
R M02	577.243	579.704	581.036	580.824
R M01	561.940	564.624	565.908	564.324
RS01	632.382	635.313	636.528	634.098
RS02	612.380	615.252	616.320	615.173
RS03	620.304	623.664	624.032	623.139
RS04	638.690	641.420	642.213	641.515
RS05	623.704	626.353	627.019	626.468
RS06	609.699	612.245	612.852	612.348
RS07	571.069	573.484	574.024	573.549
RS08	556.492	558.739	559.208	558.756
RS09	537.182	539.225	539.630	539.190
RS10	518.431	520.233	520.571	520.141
RS11	502.271	503.797	504.185	503.649
RS12	497.861	499.083	499.629	498.882
RS13	542.558	543.558	544.178	543.217
RS14	551.902	552.848	553.374	552.563
RS15	561.023	561.917	562.747	561.762
RS16	512.675	513.521	514.791	513.577
RS17	532.747	533.569	535.172	533.829
RS18	507.693	508.500	510.434	508.819
Maximum Stress		641.420	642.899	641.515
Minimum Stress		493.392	494.018	493.559
Median Stress		552.490	553.294	552.057
Mode Stress		493.392	642.899	493.559
Mean Stress		556.500	559.625	556.391

Table A.7: Nominal tresses in stay cables LS18-LM18 experienced during the initial condition, the combination of Single Lorry traffic & Denali ground motions scaled to 0.109g, and the combination of Convoy Lorry traffic & Denali ground motions scaled to 0.109g.

Stay No	Baseline Stress (DL+PS) (N/mm²)	DL+PS+DNL(0.109g)+SL Stress (N/mm²)	DL+PS+ DNL(0.109g) +CL Stress (N/mm²)
LS18	507.693	515.066	518.148
LS17	532.747	539.461	542.298
LS16	512.675	518.734	521.318
LS15	561.023	566.219	568.463
LS14	551.902	556.379	558.504
LS13	542.558	546.680	549.661
LS12	497.861	502.842	505.759
LS11	502.271	508.656	510.861
LS10	518.431	526.005	527.560
LS09	537.182	545.706	546.648
LS08	556.492	565.807	566.736
LS07	571.069	581.315	582.025
LS06	609.699	620.717	621.187
LS05	623.704	635.321	635.889
LS04	638.690	650.836	651.284
LS03	620.304	632.871	633.011
LS02	612.380	625.167	624.912
LS01	632.382	645.086	644.587
LM01	561.940	574.176	576.075
LM02	577.243	589.180	590.911
LM03	594.300	605.917	607.393
LM04	622.890	634.240	635.424
LM05	618.831	629.782	630.829
LM06	604.500	614.968	615.962
LM07	561.378	570.350	572.432
LM08	550.710	560.101	561.628
LM09	531.835	540.543	542.460
LM10	507.133	515.031	517.294
LM11	536.877	544.004	546.542
LM12	523.224	530.054	532.611
LM13	511.347	517.829	520.382
LM14	512.482	518.548	521.075
LM15	492.553	498.295	500.587
LM16	496.522	502.279	504.084
LM17	515.791	521.814	523.151
LM18	493.021	499.231	500.167

Table A.8: Nominal tresses in stay cables RM18-RS18 experienced during the initial condition, the combination of Single Lorry traffic & Denali ground motions scaled to 0.109g, and the combination of Convoy Lorry traffic & Denali ground motions scaled to 0.109g.

Stay No	Baseline Stress (DL+PS) (N/mm²)	DL+PS+DNL(0.109g)+SL Stress (N/mm²)	DL+PS+ DNL(0.109g) +CL Stress (N/mm²)
R M18	493.021	499.155	499.584
R M17	515.791	521.465	522.546
R M16	496.522	501.911	503.523
R M15	492.553	498.084	500.107
R M14	512.482	518.342	520.646
R M13	511.347	517.808	520.187
R M12	523.224	530.318	532.683
R M11	536.877	544.579	546.935
R M10	507.133	515.438	515.767
R M09	531.835	540.720	542.949
R M08	550.710	560.092	562.195
R M07	561.378	571.150	573.129
R M06	604.500	614.658	616.429
R M05	618.831	629.455	630.888
R M04	622.890	633.994	635.037
R M03	594.300	605.778	606.451
R M02	577.243	588.970	589.267
R M01	561.940	573.752	573.695
RS01	632.382	644.347	645.741
RS02	612.380	624.276	625.473
RS03	620.304	631.894	632.768
RS04	638.690	649.854	650.320
RS05	623.704	634.401	634.810
RS06	609.699	619.926	620.409
RS07	571.069	580.713	581.376
RS08	556.492	565.401	566.267
RS09	537.182	545.203	546.255
RS10	518.431	525.413	526.592
RS11	502.271	508.202	509.625
RS12	497.861	502.739	504.651
RS13	542.558	546.820	548.976
RS14	551.902	556.528	558.785
RS15	561.023	566.429	569.112
RS16	512.675	518.999	522.110
RS17	532.747	539.767	543.203
RS18	507.693	515.405	519.154
Maximum Stress		650.8355963	651.2835963
Minimum Stress		498.0842426	499.5844756
Median Stress		556.45379	558.64479
Mode Stress		650.8355963	651.2835963
Mean Stress		565.3878409	566.8898858

APPENDIX B
MAXIMUM STRESS RANGES AND RANGE OF APPLIED FORCE IN STAY CABLES

Table B.1: Maximum stress ranges and range of applied force in stay cables LS18-LM18 due to traffic loads in Single Lorry and Convoy Lorry configurations.

Stay No	Convoy Lorry Configuration		Single Lorry Configuration	
	Range of Applied Force (N)	Stress Range (N/mm²)	Range of Applied Force (N)	Stress Range (N/mm²)
LS18	85618.224	7.81901589	98707.972	9.014426667
LS17	72230.289	6.978771884	85823.142	8.292091014
LS16	60780.048	6.139398788	74686.64	7.544105051
LS15	46733.775	4.945373016	61853.457	6.545339365
LS14	34267.9143	3.745127246	50834.884	5.555725027
LS13	26279.3859	2.969422136	53404.981	6.03446113
LS12	27549.6588	3.222182316	30128.6869	3.523823029
LS11	33213.5938	4.025890158	31756.3444	3.849253867
LS10	39206.1059	4.931585648	37860.6525	4.762346226
LS09	43565.0619	5.694779333	41948.6686	5.483486092
LS08	46349.1101	6.306001374	44071.0516	5.996061442
LS07	50320.775	7.137698582	44642.861	6.332320709
LS06	54572.887	8.084872148	46143.388	6.836057481
LS05	56833.213	8.811350853	47001.912	7.28711814
LS04	58893.527	9.576183252	47006.9592	7.643408
LS03	60502.78	10.34235556	46127.3963	7.885025009
LS02	61269.153	11.03948703	44602.7092	8.03652418
LS01	95463.459	11.57132836	66735.2483	8.089121006
LM01	93147.123	11.29056036	79764.758	9.668455515
LM02	58249.572	10.49541838	52693.675	9.494355856
LM03	57415.993	9.814699658	55639.42	9.511011966
LM04	57197.256	9.300366829	56663.489	9.213575447
LM05	54713.599	8.482728527	56755.703	8.799333798
LM06	53892.103	7.984015259	55994.4682	8.29547677
LM07	52966.173	7.51293234	56183.6952	7.969318468
LM08	51922.092	7.064230204	56024.4507	7.622374245
LM09	50164.4884	6.557449464	55637.1772	7.272833621
LM10	47606.6961	5.98826366	54819.9537	6.89559166
LM11	47472.088	5.754192485	58249.973	7.060602788
LM12	47739.346	5.58354924	56983.688	6.66475883
LM13	47715.165	5.391544068	55219.057	6.239441469
LM14	46892.963	5.124913989	53095.268	5.80276153
LM15	46742.019	4.946245397	50335.972	5.326557884
LM16	48708.411	4.920041515	47915.255	4.839924747
LM17	50537.236	4.882824734	45709.783	4.416404155
LM18	52313.776	4.77751379	44501.532	4.064066849

Table B.2: Maximum stress ranges and range of applied force in stay cables LM18-RS18 due to traffic loads in Single Lorry and Convoy Lorry configurations.

Stay No	Convoy Lorry Configuration		Single Lorry Configuration	
	Range of Applied Force (N)	Stress Range (N/mm²)	Range of Applied Force (N)	Stress Range (N/mm²)
R M18	51697.664	4.721247854	33538.1642	3.062846046
R M17	45438.727	4.390215169	33699.9527	3.256034077
R M16	41866.483	4.228937677	33605.3753	3.394482354
R M15	44115.912	4.668350476	61287.344	6.485433228
R M14	40485.6715	4.424663552	65033.032	7.107435191
R M13	42247.1655	4.773691017	67051.113	7.576396949
R M12	44011.7983	5.147578749	67985.293	7.951496257
R M11	45662.6901	5.534871527	68471.607	8.299588727
R M10	47525.1577	5.978007258	68646.928	8.634833711
R M09	49650.339	6.490240392	68050.635	8.895507843
R M08	51249.857	6.97276966	66743.707	9.080776463
R M07	52219.351	7.407000142	64789.1606	9.189951858
R M06	53325.363	7.900053778	62352.3605	9.237386741
R M05	54929.784	8.516245581	59557.7938	9.233766481
R M04	56633.101	9.208634309	56425.8858	9.17494078
R M03	57946.826	9.905440342	44382.6814	7.586783145
R M02	58876.66	10.60840721	43760.2449	7.884728811
R M01	93199.959	11.29696473	66956.7688	8.115971976
RS01	94032.322	11.39785721	80916.391	9.808047394
RS02	59805.833	10.77582577	54075.715	9.743372072
RS03	58802.765	10.0517547	58477.043	9.996075726
RS04	57325.045	9.321145528	59981.496	9.75308878
RS05	55775.936	8.647431938	59802.773	9.271747752
RS06	53998.367	7.999758074	58089.335	8.605827407
RS07	51616.126	7.321436312	54514.6578	7.732575574
RS08	49062.151	6.675122585	49576.3786	6.745085524
RS09	45861.612	5.994981961	44209.1091	5.77896851
RS10	41275.0992	5.191836377	39546.1338	4.974356453
RS11	35328.3391	4.282222921	33055.2652	4.006698812
RS12	28023.6266	3.277617146	32253.4538	3.772333778
RS13	25182.7643	2.84551009	41263.0402	4.662490418
RS14	33672.1378	3.68001506	51243.4115	5.600372842
RS15	44662.207	4.726159471	62122.6146	6.573821651
RS16	60272.034	6.088084242	81799.48	8.262573737
RS17	73813.87	7.131774879	98018.207	9.470358164
RS18	89461.76	8.170023744	117818.311	10.75966311

APPENDIX C
MAXIMUM STRESS RANGES IN STAY CABLES

Table C.1: Maximum stress ranges in stay cables LS18-LM18 due to Kocaeli Bornova ground motions scaled to 0.04g and 0.109g.

Stay No	Stress Range 0.109g (N/mm²)	Stress Range 0.04g (N/mm²)
LS18	2.009251121	0.737223161
LS17	1.830190618	0.671523285
LS16	1.658405528	0.608492862
LS15	1.422532059	0.521947491
LS14	1.467088383	0.538295848
LS13	1.679542838	0.616248446
LS12	1.909245306	0.700529588
LS11	2.477776414	0.909131836
LS10	3.028520439	1.111207747
LS09	3.529986309	1.295202794
LS08	3.982248643	1.461144355
LS07	4.392644995	1.611724684
LS06	4.753613543	1.744169241
LS05	5.082476034	1.864833623
LS04	5.394627759	1.979366585
LS03	5.709188951	2.094783615
LS02	6.045089307	2.218030291
LS01	6.384831307	2.342686521
LM01	6.473252758	2.375129625
LM02	6.072940474	2.228249285
LM03	5.740799529	2.106381991
LM04	5.532712713	2.030031942
LM05	5.315159151	1.950208409
LM06	5.070089502	1.860288826
LM07	4.800365763	1.761323304
LM08	4.486459813	1.646146691
LM09	4.118429967	1.511111243
LM10	3.705512441	1.359605858
LM11	3.246544139	1.191203781
LM12	2.740698997	1.005601917
LM13	2.220370019	0.814685724
LM14	1.795289474	0.658717553
LM15	1.561344876	0.572879912
LM16	1.515779159	0.556161194
LM17	1.720808254	0.631389321
LM18	2.02774256	0.744007936

Table C.2: Maximum stress ranges in stay cables RM18-RS18 due to Kocaeli Bornova
ground motions scaled to 0.04g and 0.109g.

Stay No	Stress Range 0.109g (N/mm²)	Stress Range 0.04g (N/mm²)
RM18	2.042260426	0.74933475
RM17	1.787872381	0.655996115
RM16	1.441476382	0.528898436
RM15	1.249043815	0.458292157
RM14	1.565205072	0.574296273
RM13	1.860864964	0.682778144
RM12	2.187072246	0.802468292
RM11	2.604894512	0.955773296
RM10	2.98978521	1.096995234
RM09	3.347130865	1.228110499
RM08	3.732333189	1.369446777
RM07	4.075041694	1.495191461
RM06	4.382462604	1.607988618
RM05	4.664713534	1.711550548
RM04	4.938448844	1.811987974
RM03	5.235490465	1.920976821
RM02	5.570015643	2.043718924
RM01	5.910748102	2.168738569
RS01	6.054398992	2.221446148
RS02	5.667225625	2.079386666
RS03	5.656224407	2.075350161
RS04	5.455385283	2.001659395
RS05	5.243290751	1.923838858
RS06	5.005135445	1.836456248
RS07	4.734051197	1.736991535
RS08	4.403688951	1.615776871
RS09	4.016330177	1.47364936
RS10	3.569829076	1.309821679
RS11	3.068735519	1.125963239
RS12	2.52168731	0.925243376
RS13	1.941149626	0.712235742
RS14	1.423328243	0.522239622
RS15	1.195607806	0.438685716
RS16	1.464477236	0.53733778
RS17	1.583130191	0.580873257
RS18	1.71187806	0.628112704

Table C.3: Maximum stress ranges in stay cables LS18-LM18 due to Denali ground motions scaled to 0.04g and 0.109g.

Stay No	Stress Range 0.109g (N/mm²)	Stress Range 0.04g (N/mm²)
LS18	4.415506906	1.620369507
LS17	3.964374337	1.454816271
LS16	3.52719139	1.294382162
LS15	2.954982012	1.084397069
LS14	2.641719711	0.969438426
LS13	2.74224731	1.006329288
LS12	3.315424603	1.216669579
LS11	3.892517926	1.428446945
LS10	4.626501607	1.697798755
LS09	5.355927265	1.965477895
LS08	6.010323843	2.205623429
LS07	6.591836457	2.419022553
LS06	7.096506807	2.604222681
LS05	7.546328643	2.769294915
LS04	7.95998753	2.921096341
LS03	8.360825156	3.068192718
LS02	8.770369784	3.218484324
LS01	9.141339533	3.354620012
LM01	8.983167057	3.296575067
LM02	8.35803933	3.067170396
LM03	7.746234759	2.842654957
LM04	7.180425557	2.635018553
LM05	6.48208999	2.37874862
LM06	6.0792505	2.230917615
LM07	5.623409337	2.063636454
LM08	5.184893277	1.902713129
LM09	4.690668099	1.721346092
LM10	3.978748266	1.460091107
LM11	3.492571262	1.281677527
LM12	2.871281187	1.05368117
LM13	2.604348362	0.955724169
LM14	2.495923188	0.915935115
LM15	3.12037348	1.145091185
LM16	3.789991959	1.390822737
LM17	4.465475535	1.638706618
LM18	5.088274516	1.867256703

Table C.4: Maximum stress ranges in stay cables RM18-RS18 due to Denali ground motions scaled to 0.04g and 0.109g.

Stay No	Stress Range 0.109g (N/mm²)	Stress Range 0.04g (N/mm²)
R M18	4.687754837	1.720277005
R M17	4.080423767	1.497403217
R M16	3.559138299	1.306105798
R M15	3.0411981	1.116036
R M14	2.755749079	1.011284066
R M13	2.928769865	1.074777932
R M12	3.403776879	1.249092433
R M11	4.023946691	1.476677685
R M10	4.585989666	1.682931987
R M09	5.066470819	1.859255346
R M08	5.469159827	2.007031129
R M07	5.527156771	2.028314411
R M06	5.978072098	2.193787926
R M05	6.378533061	2.340746078
R M04	6.75670485	2.479524715
R M03	7.115264129	2.611106103
R M02	7.469667236	2.741162288
R M01	7.776733488	2.853847152
RS01	7.412159702	2.720058606
RS02	7.157905386	2.62675427
RS03	6.9631707	2.555292
RS04	6.66450587	2.445690228
RS05	6.476549326	2.376715349
RS06	6.14756839	2.2559884
RS07	5.748336054	2.109481121
RS08	5.269739285	1.933849279
RS09	4.727544509	1.734878719
RS10	4.155015286	1.524776252
RS11	3.522885846	1.292802145
RS12	2.834509846	1.040187099
RS13	2.427247502	0.890733028
RS14	2.439878157	0.895368131
RS15	2.955544602	1.084603524
RS16	3.720777372	1.365422889
RS17	4.35625793	1.598626763
RS18	4.992334284	1.832049279

Table C.5: Maximum stress ranges in stay cables LS18-LM18 due to San Simeon
ground motions scaled to 0.04g and 0.109g.

Stay No	Stress Range 0.109g (N/mm²)	Stress Range 0.04g (N/mm²)
LS18	1.687852557	0.619395434
LS17	1.491804541	0.547451208
LS16	1.295376919	0.475367677
LS15	1.042305291	0.382497354
LS14	1.338406831	0.49115847
LS13	1.851066328	0.679290395
LS12	2.340287368	0.858821053
LS11	2.795704667	1.025946667
LS10	3.203043836	1.175428931
LS09	3.551576209	1.303330719
LS08	3.839973605	1.409164626
LS07	4.056129645	1.488487943
LS06	4.189879259	1.53757037
LS05	4.272385969	1.567848062
LS04	4.30282374	1.579017886
LS03	4.274393077	1.568584615
LS02	5.959354054	2.186918919
LS01	3.604544121	1.322768485
LM01	2.374211576	0.871270303
LM02	3.58500018	1.315596396
LM03	3.411178291	1.251808547
LM04	3.206966098	1.176868293
LM05	2.991965504	1.097968992
LM06	2.741664889	1.006115556
LM07	2.460678865	0.903001418
LM08	2.143362653	0.786555102
LM09	1.997549673	0.733045752
LM10	2.102054717	0.771396226
LM11	2.170229636	0.796414545
LM12	2.203737778	0.808711111
LM13	2.207847345	0.810219209
LM14	2.328585464	0.854526776
LM15	2.474513386	0.908078307
LM16	2.518445	0.9242
LM17	2.52996372	0.928427053
LM18	2.221678813	0.815294977

Table C.6: Maximum stress ranges in stay cables RM18-RS18 due to San Simeon
ground motions scaled to 0.04g and 0.109g.

Stay No	Stress Range 0.109g (N/mm²)	Stress Range 0.04g (N/mm²)
RM18	2.088096575	0.766273973
RM17	2.073432754	0.760892754
RM16	2.001151919	0.734367677
RM15	2.002739471	0.734950265
RM14	2.061886885	0.756655738
RM13	2.079658418	0.763177401
RM12	2.055982222	0.754488889
RM11	1.99139697	0.730787879
RM10	1.901247925	0.69770566
RM09	1.924455556	0.706222222
RM08	2.221182721	0.815112925
RM07	2.511251773	0.921560284
RM06	2.790480741	1.02402963
RM05	3.046600698	1.118018605
RM04	3.285401789	1.205652033
RM03	3.511299915	1.288550427
RM02	5.486362793	2.013344144
RM01	4.53262297	1.663347879
RS01	3.222053212	1.182404848
RS02	5.211672973	1.912540541
RS03	5.276000598	1.936147009
RS04	5.247038455	1.925518699
RS05	5.123540775	1.88019845
RS06	4.905056519	1.800020741
RS07	4.585916028	1.682904965
RS08	4.180513333	1.534133333
RS09	3.697458105	1.356865359
RS10	3.141811887	1.152958491
RS11	2.552476121	0.936688485
RS12	2.031855614	0.745635088
RS13	1.50658322	0.552874576
RS14	1.359432514	0.498874317
RS15	1.479043492	0.542768254
RS16	1.758836111	0.645444444
RS17	2.072885121	0.760691787
RS18	2.121224612	0.77843105

Table C.7: Comparison of maximum stress ranges in stay cables LS18-LM18 due to Kocaeli Bornova, Denali and San Simeon ground motions scaled to 0.109g.

| Stay No | Earthquake Event (Scaled to 0.109g) | | |
| | Kocaeli | Denali | San Simeon |
	Stress Range (N/mm²)	Stress Range (N/mm²)	Stress Range (N/mm²)
LS18	2.009251121	4.415506906	1.687852557
LS17	1.830190618	3.964374337	1.491804541
LS16	1.658405528	3.52719139	1.295376919
LS15	1.422532059	2.954982012	1.042305291
LS14	1.467088383	2.641719711	1.338406831
LS13	1.679542838	2.74224731	1.851066328
LS12	1.909245306	3.315424603	2.340287368
LS11	2.477776414	3.892517926	2.795704667
LS10	3.028520439	4.626501607	3.203043836
LS09	3.529986309	5.355927265	3.551576209
LS08	3.982248643	6.010323843	3.839973605
LS07	4.392644995	6.591836457	4.056129645
LS06	4.753613543	7.096506807	4.189879259
LS05	5.082476034	7.546328643	4.272385969
LS04	5.394627759	7.95998753	4.30282374
LS03	5.709188951	8.360825156	4.274393077
LS02	6.045089307	8.770369784	5.959354054
LS01	6.384831307	9.141339533	3.604544121
LM01	6.473252758	8.983167057	2.374211576
LM02	6.072940474	8.35803933	3.58500018
LM03	5.740799529	7.746234759	3.411178291
LM04	5.532712713	7.180425557	3.206966098
LM05	5.315159151	6.48208999	2.991965504
LM06	5.070089502	6.0792505	2.741664889
LM07	4.800365763	5.623409337	2.460678865
LM08	4.486459813	5.184893277	2.143362653
LM09	4.118429967	4.690668099	1.997549673
LM10	3.705512441	3.978748266	2.102054717
LM11	3.246544139	3.492571262	2.170229636
LM12	2.740698997	2.871281187	2.203737778
LM13	2.220370019	2.604348362	2.207847345
LM14	1.795289474	2.495923188	2.328585464
LM15	1.561344876	3.12037348	2.474513386
LM16	1.515779159	3.789991959	2.518445
LM17	1.720808254	4.465475535	2.52996372
LM18	2.02774256	5.088274516	2.221678813

Table C.8: Comparison of maximum stress ranges in stay cables RM18-RS18 due to Kocaeli Bornova, Denali and San Simeon ground motions scaled to 0.109g.

Stay No	Earthquake Event (Scaled to 0.109g)		
	Kocaeli	Denali	San Simeon
	Stress Range (N/mm²)	Stress Range (N/mm²)	Stress Range (N/mm²)
R M18	2.042260426	4.687754837	2.088096575
R M17	1.787872381	4.080423767	2.073432754
R M16	1.441476382	3.559138299	2.001151919
R M15	1.249043815	3.0411981	2.002739471
R M14	1.565205072	2.755749079	2.061886885
R M13	1.860864964	2.928769865	2.079658418
R M12	2.187072246	3.403776879	2.055982222
R M11	2.604894512	4.023946691	1.99139697
R M10	2.98978521	4.585989666	1.901247925
R M09	3.347130865	5.066470819	1.924455556
R M08	3.732333189	5.469159827	2.221182721
R M07	4.075041694	5.527156771	2.511251773
R M06	4.382462604	5.978072098	2.790480741
R M05	4.664713534	6.378533061	3.046600698
R M04	4.938448844	6.75670485	3.285401789
R M03	5.235490465	7.115264129	3.511299915
R M02	5.570015643	7.469667236	5.486362793
R M01	5.910748102	7.776733488	4.53262297
RS01	6.054398992	7.412159702	3.222053212
RS02	5.667225625	7.157905386	5.211672973
RS03	5.656224407	6.9631707	5.276000598
RS04	5.455385283	6.66450587	5.247038455
RS05	5.243290751	6.476549326	5.123540775
RS06	5.005135445	6.14756839	4.905056519
RS07	4.734051197	5.748336054	4.585916028
RS08	4.403688951	5.269739285	4.180513333
RS09	4.016330177	4.727544509	3.697458105
RS10	3.569829076	4.155015286	3.141811887
RS11	3.068735519	3.522885846	2.552476121
RS12	2.52168731	2.834509846	2.031855614
RS13	1.941149626	2.427247502	1.50658322
RS14	1.423328243	2.439878157	1.359432514
RS15	1.195607806	2.955544602	1.479043492
RS16	1.464477236	3.720777372	1.758836111
RS17	1.583130191	4.35625793	2.072885121
RS18	1.71187806	4.992334284	2.121224612
Maximum	6.473252758	9.141339533	5.959354054
Minimum	1.195607806	2.427247502	1.042305291
Mean	3.544471847	5.135076611	2.886183228

Table C.9: Comparison of maximum stress ranges in stay cables LS18-LM18 due to Kocaeli Bornova, Denali and San Simeon ground motions that are unscaled.

| Stay No | Earthquake Event (unscaled) | | |
| | Kocaeli | Denali | San Simeon |
	Stress Range (N/mm²)	Stress Range (N/mm²)	Stress Range (N/mm²)
LS18	0.553055635	1.620369507	0.309697717
LS17	0.503768406	1.454816271	0.273725604
LS16	0.456483768	1.294382162	0.237683838
LS15	0.391558508	1.084397069	0.191248677
LS14	0.403822842	0.969438426	0.245579235
LS13	0.46230191	1.006329288	0.339645198
LS12	0.525528573	1.216669579	0.429410526
LS11	0.682019382	1.428446945	0.512973333
LS10	0.833614214	1.697798755	0.587714465
LS09	0.971645007	1.965477895	0.651665359
LS08	1.096132299	2.205623429	0.704582313
LS07	1.209095787	2.419022553	0.744243972
LS06	1.308454044	2.604222681	0.768785185
LS05	1.398974961	2.769294915	0.783924031
LS04	1.484896163	2.921096341	0.789508943
LS03	1.571480581	3.068192718	0.784292308
LS02	1.663938703	3.218484324	1.093459459
LS01	1.757454255	3.354620012	0.661384242
LM01	1.781792667	3.296575067	0.435635152
LM02	1.671604865	3.067170396	0.657798198
LM03	1.580181538	2.842654957	0.625904274
LM04	1.522904683	2.635018553	0.588434146
LM05	1.463022062	2.37874862	0.548984496
LM06	1.395565511	2.230917615	0.503057778
LM07	1.321322809	2.063636454	0.451500709
LM08	1.234918748	1.902713129	0.393277551
LM09	1.133616837	1.721346092	0.366522876
LM10	1.019959384	1.460091107	0.385698113
LM11	0.893626242	1.281677527	0.398207273
LM12	0.754390035	1.05368117	0.404355556
LM13	0.611167085	0.955724169	0.405109605
LM14	0.494161705	0.915935115	0.427263388
LM15	0.429767376	1.145091185	0.454039153
LM16	0.417225202	1.390822737	0.4621
LM17	0.473660406	1.638706618	0.464213527
LM18	0.558145489	1.867256703	0.407647489

Table C.10: Comparison of maximum stress ranges in stay cables RM18-RS18 due to Kocaeli Bornova, Denali and San Simeon ground motions that are unscaled.

Stay No	Earthquake Event (unscaled)		
	Kocaeli	Denali	San Simeon
	Stress Range (N/mm²)	Stress Range (N/mm²)	Stress Range (N/mm²)
RM18	0.562141598	1.720277005	0.383136986
RM17	0.492120116	1.497403217	0.380446377
RM16	0.39677302	1.306105798	0.367183838
RM15	0.343805069	1.116036	0.367475132
RM14	0.430829913	1.011284066	0.378327869
RM13	0.512211661	1.074777932	0.381588701
RM12	0.602001719	1.249092433	0.377244444
RM11	0.717009224	1.476677685	0.365393939
RM10	0.822952164	1.682931987	0.34885283
RM09	0.921313203	1.859255346	0.353111111
RM08	1.027341918	2.007031129	0.407556463
RM07	1.121674014	2.028314411	0.460780142
RM06	1.206293037	2.193787926	0.512014815
RM05	1.283983907	2.340746078	0.559009302
RM04	1.359330813	2.479524715	0.602826016
RM03	1.441092889	2.611106103	0.644275214
RM02	1.533172486	2.741162288	1.006672072
RM01	1.626960667	2.853847152	0.831673939
RS01	1.666501236	2.720058606	0.591202424
RS02	1.559929982	2.62675427	0.95627027
RS03	1.556901846	2.555292	0.968073504
RS04	1.501619951	2.445690228	0.96275935
RS05	1.443239953	2.376715349	0.940099225
RS06	1.377686607	2.2559884	0.90001037
RS07	1.303069418	2.109481121	0.841452482
RS08	1.212135687	1.933849279	0.767066667
RS09	1.105513399	1.734878719	0.67843268
RS10	0.982611912	1.524776252	0.576479245
RS11	0.8446836	1.292802145	0.468344242
RS12	0.694106058	1.040187099	0.372817544
RS13	0.534310384	0.890733028	0.276437288
RS14	0.391777661	0.895368131	0.249437158
RS15	0.329096561	1.084603524	0.271384127
RS16	0.403104111	1.365422889	0.322722222
RS17	0.435763884	1.598626763	0.380345894
RS18	0.471202329	1.832049279	0.389215525
Maximum	1.781792667	3.354620012	1.093459459
Minimum	0.329096561	0.890733028	0.191248677
Mean	0.975632218	1.884431784	0.529574904

131

Table C.11: Comparison of maximum stress ranges in stay cables LS18-LM18 due to combination of traffic in Convoy Lorry configuration only, traffic in Convoy Lorry configuration and Denali ground motions scaled to 0.04g, and traffic in Convoy Lorry configuration and Denali ground motions scaled to 0.109g.

Stay No	Stress Range Convoy Only (N/mm²)	Stress Range Convoy+Denali(0.04g) (N/mm²)	Stress Range Convoy+Denali(0.109g) (N/mm²)
LS18	5.14745516	5.988104475	7.438224543
LS17	7.514801256	8.261341063	9.549122229
LS16	6.845759091	7.504448081	8.640686588
LS15	5.949583598	6.495152804	7.436259685
LS14	5.286655191	5.767931803	6.598133959
LS13	5.617410395	6.160465311	7.09723504
LS12	5.96724807	6.673408655	7.891535664
LS11	6.239617455	7.099557818	8.582954945
LS10	6.392415472	7.393791824	9.121166031
LS09	6.382407712	7.510866536	9.457458007
LS08	6.864485714	8.104632789	10.24388649
LS07	7.312079149	8.64902383	10.9552534
LS06	7.63599837	9.053745037	11.49935804
LS05	8.132320775	9.618457054	12.18204214
LS04	8.383702764	9.928139675	12.59229335
LS03	8.357483077	9.952910427	12.70502261
LS02	8.057208829	9.158661622	11.05866769
LS01	7.617323758	9.300463152	12.20387861
LM01	9.42255297	11.15129842	14.13338433
LM02	9.237250631	10.86305586	13.66756987
LM03	8.936218462	10.46124256	13.09190914
LM04	8.632216911	10.06365593	12.53288825
LM05	8.346404031	9.685847287	11.9963869
LM06	8.072901778	9.316070519	11.4605366
LM07	7.941619716	9.079677872	11.04282819
LM08	8.097901224	9.129421497	10.90879397
LM09	8.111200392	9.031657124	10.61944499
LM10	7.995834969	8.789328176	10.15810396
LM11	7.795706788	8.481210424	9.663704197
LM12	7.546191111	8.221188421	9.385558781
LM13	7.236141243	7.895535367	9.032990232
LM14	6.847341967	7.487623934	8.592110328
LM15	6.325745503	6.952550476	8.033789056
LM16	5.70995303	6.389701818	7.562268477
LM17	5.112838551	5.936807053	7.35815272
LM18	4.532976804	5.490707397	7.142792671

Table C.12: Comparison of maximum stress ranges in stay cables RM18-RS18 due to combination of traffic in Convoy Lorry configuration only, traffic in Convoy Lorry configuration and Denali ground motions scaled to 0.04g, and traffic in Convoy Lorry configuration and Denali ground motions scaled to 0.109g.

Stay No	Stress Range Convoy Only (N/mm²)	Stress Range Convoy+Denali(0.04g) (N/mm²)	Stress Range Convoy+Denali(0.109g) (N/mm²)
RM18	4.117377626	5.013335708	6.5588634
RM17	4.759369469	5.491526763	6.754498097
RM16	5.406392525	5.990602424	6.9983645
RM15	6.085289947	6.622993757	7.550532828
RM14	6.683855847	7.226017158	8.161245421
RM13	7.134826102	7.759259774	8.836407859
RM12	7.501116257	8.218902105	9.457082693
RM11	7.850426788	8.660257576	10.05721568
RM10	8.184758742	9.083456981	10.63371144
RM09	8.452251373	9.428383268	11.11221079
RM08	8.641166803	9.683490204	11.48149807
RM07	8.74930922	9.848259007	11.74394739
RM06	8.788460889	9.937139852	11.91861106
RM05	8.763802326	9.972711628	12.04773017
RM04	8.696073496	9.960920813	12.14278243
RM03	8.535570085	9.861956068	12.14997189
RM02	8.229856577	9.621773153	12.02282925
RM01	7.784295515	9.240392485	11.75215976
RS01	9.212105212	10.73349673	13.35789709
RS02	9.151822162	10.59761189	13.09159918
RS03	8.734942393	10.10316034	12.4633363
RS04	8.106253821	9.399138211	11.62936378
RS05	7.589575504	8.945572713	11.2846679
RS06	7.553973481	8.711186815	10.70737981
RS07	7.348522695	8.432824681	10.30324561
RS08	7.050267075	8.046862313	9.765989099
RS09	6.615548627	7.513916732	9.063601712
RS10	6.013290818	6.798531572	8.153071874
RS11	5.439582182	6.141858424	7.353284942
RS12	5.021291228	5.669975088	6.788954746
RS13	4.795795706	5.390400226	6.416093023
RS14	5.407211803	5.947434317	6.879318153
RS15	6.361435344	6.993993228	8.085155577
RS16	7.316205859	8.092588889	9.431849616
RS17	8.028200483	8.917954493	10.45278016
RS18	8.716726941	9.722646575	11.45785795

APPENDIX D
CRITICAL STAY CABLES BASED ON MAXIMUM STRESS RANGES IN THE 85TH PERCENTILE

Table D.1: Critical stay cables in the 85th percentile of the maximum stress range due to different load applications.

Stay No	Single Lorry Stress Range (N/mm²)	Condition	Stay No	Convoy Lorry Stress Range (N/mm²)	Condition	Stay No	Kocaeli Bornova(0.109g) Stress Range (N/mm²)	Condition	Stay No	Denali (0.109g) Stress Range (N/mm²)	Condition	Stay No	San Simeon(0.109g) Stress Range (N/mm²)	Condition
LS01	11.57132836	Critical	RS18	10.75966311	Critical	LM01	6.473252758	Critical	LS01	9.141339533	Critical	LS02	5.959354054	Critical
RS01	11.39785721	Critical	RS03	9.996075726	Critical	LS01	6.384831307	Critical	LM01	8.983167057	Critical	RM02	5.486362793	Critical
RM01	11.29696473	Critical	RS01	9.808047394	Critical	LM02	6.072940474	Critical	LS02	8.770369784	Critical	RS03	5.276000598	Critical
LM01	11.29056036	Critical	RS04	9.75308878	Critical	RS01	6.054398992	Critical	LS03	8.360825156	Critical	RS04	5.247038455	Critical
LS02	11.03948703	Critical	RS02	9.743372072	Critical	LS02	6.045089307	Critical	LM02	8.35803933	Critical	RS02	5.211672973	Critical
RS02	10.77582577	Critical	LM01	9.668455515	Critical	RM01	5.910748102	Critical	LS04	7.95998753	Critical	RS05	5.123540775	Critical
RM02	10.60840721	Critical	LM03	9.511011966	Critical	LM03	5.740799529	Critical	RM01	7.776733488	Critical	RS06	4.905056519	Critical
LM02	10.49541838	Critical	LM02	9.494355856	Critical	LS03	5.709188951	Critical	LM03	7.746234759	Critical	RS07	4.585916028	Critical
LS03	10.34235556	Critical	RS17	9.470358164	Critical	RS02	5.667225625	Critical	LS05	7.546328643	Critical	RM01	4.53262297	Critical
RS03	10.0517547	Critical	RS05	9.271747752	Critical	RS03	5.656224407	Critical	RM02	7.469667236	Critical	LS04	4.30282374	Critical
RM03	9.905440342	Critical	RM06	9.237386741	Critical	RM02	5.570015643	Critical	RS01	7.412159702	Critical	LS03	4.274393077	Critical
M03	9.814699658		RM05	9.233766481	Critical	LM04	5.532712713		LM04	7.180425557		LS05	4.272385969	
LS04	9.576183252		LM04	9.213575447		RS04	5.455385283		RS02	7.157905386		LS06	4.189879259	
RS04	9.321145528		RM07	9.189951858		LS04	5.394627759		RM03	7.115264129		RS08	4.180513333	
LM04	9.300366829		RM04	9.17494078		LM05	5.315159151		LS06	7.096506807		LS07	4.056129645	
RM04	9.208634309		RM08	9.080776463		RS05	5.243290751		RS03	6.9631707		LS08	3.839973605	
LS05	8.811350853		LS18	9.014426667		RM03	5.235490465		RM04	6.75670485		RS09	3.697458105	
RS05	8.647431938		RM09	8.895507843		LS05	5.082476034		RS04	6.66450587		LS01	3.604544121	
RM05	8.516245581		LM05	8.799333798		LM06	5.070089502		LS07	6.591836457		LM02	3.58500018	
LM05	8.482728527		RM10	8.634833711		RS06	5.005135445		LM05	6.48208999		LS09	3.551576209	
RS18	8.170023744		RS06	8.605827407		RM04	4.938448844		RS05	6.476549326		RM03	3.511299915	
LS06	8.084872148		RM11	8.299588727		LM07	4.800365763		RM05	6.378533061		LM03	3.411178291	
RS06	7.999758074		LM06	8.29547677		LS06	4.753613543		RS06	6.14756839		RM04	3.285401789	
LM06	7.984015259		LS17	8.292091014		RS07	4.734051197		LM06	6.0792505		RS01	3.222053212	
RM06	7.900053778		RS16	8.262573737		RM05	4.664713534		LS08	6.010323843		LM04	3.206966098	
LS18	7.81901589		RM01	8.115971976		LM08	4.486459813		RM06	5.978072098		LS10	3.203043836	
LM07	7.51293234		LS01	8.089121006		RS08	4.403688951		RS07	5.748336054		RS10	3.141811887	
RM07	7.407000142		LS02	8.03652418		LS07	4.392644995		LM07	5.623409337		RM05	3.046600698	
RS07	7.321436312		M07	7.969318468		RM06	4.382462604		RM07	5.527156771		LM05	2.991965504	
LS07	7.137698582		RM12	7.951496257		LM09	4.118429967		RM08	5.469159827		LS11	2.795704667	
RS17	7.131774879		LS03	7.885025009		RM07	4.075041694		LS09	5.355927265		RM06	2.790480741	
LM08	7.064230204		RM02	7.884728811		RS09	4.016330177		RS08	5.269739285		LM06	2.741664889	
LS14	7.02381577		RS07	7.732575574		LS08	3.982248643		LM08	5.184893277		RS11	2.552476121	
LS17	6.978771884		LS04	7.643408		RM08	3.732333189		LM18	5.088274516		LM17	2.52996372	
RM08	6.97276966		LM08	7.622374245		LM10	3.705512441		RM09	5.066470819		LM16	2.518445	
RS08	6.675122585		RM03	7.586783145		RS10	3.569829076		RS18	4.992334284		RM07	2.511251773	

cont' Table D.1: Critical stay cables in the 85th percentile of the maximum stress range due to different load applications.

Stay No	Single Lorry Stress Range (N/mm³)	Condition	Stay No	Convoy Lorry Stress Range (N/mm³)	Condition	Stay No	Kocaeli Bornova(0.109g) Stress Range (N/mm³)	Condition	Stay No	Denali (0.109g) Stress Range (N/mm³)	Condition	Stay No	San Simeon(0.109g) Stress Range (N/mm³)	Condition
LM09	6.557449464		R M13	7.576396949		LS09	3.529986309		RS09	4.727544509		LM15	2.474513386	
R M09	6.490240392		LS16	7.544105051		R M09	3.347130865		LM09	4.690668099		LM07	2.460678865	
RS10	6.449698013		LS11	7.485617503		LM11	3.246544139		R M18	4.687754837		LM01	2.374211576	
LS08	6.306001374		LS05	7.28711814		RS11	3.068735519		LS10	4.626501607		LS12	2.340287368	
LS16	6.139398788		M09	7.272833621		LS10	3.028520439		R M10	4.585989666		LM14	2.328585464	
RS16	6.088084242		R M14	7.107435191		R M10	2.98978521		LM17	4.465475535		LM18	2.221678813	
RS09	5.994981961		LM11	7.060602788		LM12	2.740698997		LS18	4.415506906		R M08	2.221182721	
LM10	5.98826366		LM10	6.89559166		R M11	2.604894512		RS17	4.35625793		LM13	2.207847345	
R M10	5.978007258		S06	6.836057481		RS12	2.52168731		RS10	4.155015286		LM12	2.203737778	
M11	5.754192485		RS08	6.745085524		LS11	2.477776414		R M17	4.080423767		LM11	2.170229636	
LS09	5.694779333		LM12	6.66475883		LM13	2.220370019		R M11	4.023946691		LM08	2.143362653	
LM12	5.58354924		RS15	6.573821651		R M12	2.187072246		LM10	3.978748266		RS18	2.121224612	
R M11	5.534871527		LS15	6.545339365		R M18	2.042260426		LS17	3.964374337		LM10	2.102054717	
LM13	5.391544068		R M15	6.485433228		LM18	2.02774256		LS11	3.892517926		R M18	2.088096575	
R M12	5.147578749		LS07	6.332320709		LS18	2.009251121		LM16	3.789991959		R M13	2.079658418	
LM14	5.124913989		M13	6.239441469		RS13	1.941149626		RS16	3.720777372		R M17	2.073432754	
LM15	4.946245397		LS13	6.03446113		LS12	1.909245306		R M16	3.559138299		RS17	2.072885121	
LS15	4.945373016		S08	5.996061442		R M13	1.860864964		LS16	3.52719139		R M14	2.061886885	
LS10	4.931585648		LM14	5.80276153		LS17	1.830190618		RS11	3.522885846		R M12	2.055982222	
LM16	4.920041515		RS09	5.77896851		LM14	1.795289474		LM11	3.492571262		RS12	2.031855614	
LM17	4.882824734		RS14	5.600372842		R M17	1.787872381		R M12	3.403776879		R M15	2.002739471	
LM18	4.77751379		LS14	5.555725027		LM17	1.720808254		LS12	3.315424603		R M16	2.001151919	
R M13	4.773691017		S09	5.483486092		RS18	1.71187806		LM15	3.12037348		LM09	1.997549673	
RS15	4.726159471		LM15	5.326557884		LS13	1.679542838		R M15	3.0411981		R M11	1.99139697	
R M18	4.721247854		RS10	4.974356453		LS16	1.658405528		RS15	2.955544602		R M09	1.924455556	
R M15	4.668350476		LM16	4.839924747		RS17	1.583130191		LS15	2.954982012		R M10	1.901247925	
R M14	4.424663552		LS10	4.762346226		R M14	1.565205072		R M13	2.928769865		LS13	1.851066328	
R M17	4.390215169		RS13	4.662490418		LM15	1.561344876		LM12	2.871281187		RS16	1.758836111	
RS11	4.282222921		LM17	4.416404155		LM16	1.515779159		RS12	2.834509846		LS18	1.687852557	
R M16	4.228937677		LM18	4.064066849		LS14	1.467088383		R M14	2.755749079		RS13	1.50658322	
LS11	4.025890158		RS11	4.006698812		RS16	1.464477236		LS13	2.74224731		LS17	1.491804541	
RS14	3.68001506		RS12	3.772333778		R M16	1.441476382		LS14	2.641719711		RS15	1.479043492	
RS12	3.277617146		LS12	3.523823029		RS14	1.423328243		LM13	2.604348362		RS14	1.359432514	
LS12	3.222182316		R M16	3.394482354		LS15	1.422532059		LM14	2.495923188		LS14	1.338406831	
LS13	2.969422136		R M17	3.256034077		R M15	1.249043815		RS14	2.439878157		LS16	1.295376919	
RS13	2.84551009		R M18	3.062846046		RS15	1.195607806		RS13	2.427247502		LS15	1.042305291	
85th Percentile	9.846458897		85th Percentile	9.235033572		85th Percentile	5.545768739		85th Percentile	7.261532507		85th Percentile	4.273088457	